

**THE UNIVERSITY OF CALGARY**

**The Shallow Contact System**

**Binary TY Bootis**

**BY**

**Gaston Groisman**

**A THESIS**

**SUBMITTED TO THE FACULTY OF GRADUATE STUDIES  
IN PARTIAL FULFILLMENT OF THE REQUIREMENTS FOR THE  
DEGREE OF Master of Science**

**DEPARTMENT OF Physics**

**CALGARY, ALBERTA**

**January, 1989**

**© Gaston Groisman 1989**



National Library  
of Canada

Bibliothèque nationale  
du Canada

Canadian Theses Service    Service des thèses canadiennes

Ottawa, Canada  
K1A 0N4

The author has granted an irrevocable non-exclusive licence allowing the National Library of Canada to reproduce, loan, distribute or sell copies of his/her thesis by any means and in any form or format, making this thesis available to interested persons.

The author retains ownership of the copyright in his/her thesis. Neither the thesis nor substantial extracts from it may be printed or otherwise reproduced without his/her permission.

L'auteur a accordé une licence irrévocable et non exclusive permettant à la Bibliothèque nationale du Canada de reproduire, prêter, distribuer ou vendre des copies de sa thèse de quelque manière et sous quelque forme que ce soit pour mettre des exemplaires de cette thèse à la disposition des personnes intéressées.

L'auteur conserve la propriété du droit d'auteur qui protège sa thèse. Ni la thèse ni des extraits substantiels de celle-ci ne doivent être imprimés ou autrement reproduits sans son autorisation.

ISBN 0-315-50317-3

April 18, 1989

To Whom it May Concern:

This is to inform you that Mr. Gaston Groisman has been informed that Page 123 of his Thesis may not be acceptable to you. He has stated that he would prefer to leave the page the way it is, as the numbers "are not meant to be read."

Yours sincerely,

*E. Mansfield*

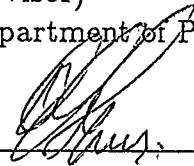
E. Mansfield  
Faculty of Graduate Studies  
University of Calgary

**THE UNIVERSITY OF CALGARY**  
**FACULTY OF GRADUATE STUDIES**

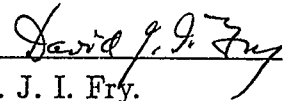
The undersigned certify that they have read, and recommend to the Faculty of Graduate Studies for acceptance, a thesis entitled, "The Shallow Contact System Binary TY Bootis," submitted by Gaston Groisman in partial fulfillment of the requirements for the degree of Master in Science.



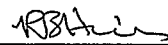
Dr. E. F. Milone (supervisor)  
Department of Physics



Dr. E. G. Enns.  
Department of Mathematics and Statistics



Dr. J. I. Fry.  
Department of Physics



Dr. R. B. Hicks.  
Department of Physics

Date 89/04/07

## Abstract

Modeling of the W UMa binary star system TY Boo has been carried out with the Wilson-Devinney program, to obtain solutions to the elements of the system. BVI light curves obtained at the Rothney Astrophysical Observatory, together with BVRI light curves obtained by D.H. Bradstreet at Kitt Peak National Observatory, and radial velocity data from the Dominion Astrophysical Observatory were used. The program was run in the Cyber 205 supercomputer of the University of Calgary.

The O'Connell effect was observed in all light curves, together with other distortions, and studied by Fourier analysis. New elements were computed from the above mentioned observations together with all other previously published data. The asymmetries were successfully modeled with the use of homogeneous spots, one cool and one warm, near the equator of star 2.

The results indicate that TY Boo is a shallow contact system, as confirmed by runs of the Wilson Devinney program in the semi-detached mode, with  $f=0.087(7)$ . The mass ratio  $m_2/m_1 = 2.084(3)$ , where  $m_1$  is the mass of the star eclipsed during primary minimum, shows the hotter star to be the less massive one, making this a W-type W UMa system. The temperature of the hotter component was assumed to be 5623 K, appropriate for a G3V star; the temperature difference was found to be 395(5) K, satisfactorily consistent with the observed spectral type at primary minimum -  $G8 \pm 1/10$  spectral class.

Dedicated to Susana and Goyo who made it all possible,  
and to Andrea who made it all worthwhile.

## Acknowledgements

I would like to thank my supervisor, Dr. E.F. Milone, for his help and guidance. I would also like to thank Dr. D.H. Bradstreet for allowing me to use his observations and preliminary results, which made this thesis more valuable.

Finally I would like to thank Jim, Steve and all those who made my stay at Science B an enjoyable one.

# Contents

Abstract	iii
Acknowledgements	v
<b>1 Introduction</b>	<b>1</b>
1.1 W UMa Stars . . . . .	3
1.2 TY Bootis . . . . .	5
1.3 Analysis History . . . . .	6
1.4 Aims . . . . .	7
<b>2 Photometric Observations and Reduction</b>	<b>9</b>
2.1 Observations . . . . .	9
2.2 Light Curve Analysis . . . . .	11
2.3 Period Analysis . . . . .	19
2.4 Fourier Analysis . . . . .	22
<b>3 Spectroscopic Observations and Reduction</b>	<b>35</b>
3.1 Background . . . . .	35
3.2 Spectral Type Determination . . . . .	36
3.3 Data Reduction . . . . .	41
3.4 Radial Velocity of Comparison Stars . . . . .	48
3.5 The Cross-Correlation Technique . . . . .	49
3.6 TY Boo Radial Velocities . . . . .	54
<b>4 Light Curve and Radial Velocity Curve Analysis</b>	<b>61</b>
4.1 Light Curve Synthesis . . . . .	61
4.2 Roche Model . . . . .	63
4.3 Differential Corrections . . . . .	68
4.4 Spots . . . . .	69
4.5 Graphical Representation of the Model . . . . .	80
4.6 Tests of the Model . . . . .	83
4.7 Contact Parameter and Fill-Out Factor . . . . .	88
4.8 Conclusions . . . . .	94
Bibliography	
<b>A Spectroscopic and photometric data</b>	<b>105</b>

B	Hardware and software	118
B.1	The RADS System . . . . .	118
B.2	Data Reduction . . . . .	120
B.3	Use of Mainframe Computers . . . . .	121

## List of Tables

2.1	Light curve sets. . . . .	10
2.2	Mean differential magnitudes at Maximum Light of TY Boo . . . . .	17
2.3	Phases of Minima . . . . .	18
2.4	Average Phase Shift . . . . .	18
2.5	$O - C$ Phases of minima for two sets of elements. . . . .	21
2.6	9 Term Fourier Representation (Fit to Minima Only) . . . . .	30
2.7	9 Term Fourier Representation (Fit to Maxima Only) . . . . .	31
2.8	9 Term Fourier Representation (Fit to Full Light Curve) . . . . .	32
3.1	Comparison Stars Radial Velocities . . . . .	50
3.2	Computed Comparison Stars Radial Velocities . . . . .	50
3.3	Radial Velocities for TY Boo. . . . .	55
3.4	Photometric elements. . . . .	60
4.1	Synthetic Light Curve Parameters. . . . .	62
4.2	Spot 1, $\rho$ and $\Sigma wr^2$ . . . . .	72
4.3	Spot 1, $t_f$ and $\Sigma wr^2$ . . . . .	73
4.4	Spot 2, longitude and $\Sigma wr^2$ . . . . .	77
4.5	Spot 2, $\rho$ and $\Sigma wr^2$ . . . . .	78
4.6	Spot 2, $t_f$ and $\Sigma wr^2$ . . . . .	79
4.7	TY Boo, Solutions to Radial Velocity and Light Curves . . . . .	89
4.8	TY Boo, Absolute Parameters . . . . .	97
A.1	Cross-correlation results (all velocities in km/sec) . . . . .	106
A.2	RAO 1985 light curves. . . . .	107
A.3	RAO 1986 V light curve. Normal points. . . . .	108
A.4	RAO 1986 B light curve. Normal points. . . . .	109
A.5	RAO 1986 I light curve. Normal points. . . . .	110
A.6	RAO 1987 V light curve. Normal points. . . . .	111
A.7	RAO 1987 B light curve. Normal points. . . . .	112
A.8	RAO 1987 I light curve. Normal points. . . . .	113
A.9	Bradstreet Normal points. B bandpass. . . . .	114
A.10	Bradstreet Normal points. V bandpass. . . . .	115
A.11	Bradstreet Normal points. R bandpass. . . . .	116
A.12	Bradstreet Normal points. R bandpass. . . . .	117

## List of Figures

1.1	Detached system light curve . . . . .	2
1.2	Semi-Detached system light curve . . . . .	3
1.3	Contact system light curve . . . . .	4
2.1	Finding chart for TY Boo . . . . .	10
2.2	B, V and I Light Curves for 1985 (LC 1) . . . . .	12
2.3	B, V, R and I Light Curves for 1985 (LC 2) . . . . .	13
2.4	B, V and I Light Curves for 1986 (LC 3) . . . . .	14
2.5	B, V and I Light Curves for 1987 (LC 4) . . . . .	15
2.6	Phases of minima for Bradstreet's elements . . . . .	19
2.7	$O - C$ phases of minima from the new elements . . . . .	22
2.8	LC 1 with Fourier fit to the full light curve. . . . .	24
2.9	LC 2 with Fourier fit to the full light curve. . . . .	25
2.10	LC 3 with Fourier fit to the full light curve. . . . .	26
2.11	LC 4 with Fourier fit to the full light curve. . . . .	27
2.12	LC 2 with Fourier fit to the minima. . . . .	28
2.13	LC 2 with Fourier fit to the maxima. . . . .	29
3.1	TY Boo Spectrum . . . . .	37
3.2	TY Boo spectrum, exposure No 0446, phase 0.06 . . . . .	39
3.3	Comparison Spectrum HD144579 (G8) . . . . .	39
3.4	TY Boo spectrum, exposure No 0209, phase 0.49 . . . . .	40
3.5	Comparison Spectrum HD154417 (G3) . . . . .	40
3.6	Fe arc Spectrum . . . . .	42
3.7	Arc line determination . . . . .	44
3.8	TY Boo spectrum with continuum fit . . . . .	45
3.9	Cross-Correlation Curve . . . . .	47
3.10	Vector diagram of cross-correlation results and their differences . . . . .	49
3.11	TY Boo Radial Velocity Curves . . . . .	56
3.12	$u$ and $v$ vs $\sin(\phi)$ and best fits. . . . .	57
3.13	$v$ vs $u$ plot of TY Boo Radial Velocities . . . . .	58
4.1	Coordinate system for Roche lobe computation . . . . .	64
4.2	Roche Potential: Surface Plot . . . . .	66
4.3	Roche Potential: Contour Plot . . . . .	67
4.4	Data from Bradstreet compared to initial parameters. . . . .	68
4.5	Spot 1, first attempt . . . . .	71
4.6	Spot 1, $\Sigma wr^2$ for $\rho$ determination . . . . .	72

4.7	Spot 1, $\Sigma wr^2$ for $t_f$ determination . . . . .	73
4.8	B light curve. 1 spot fit . . . . .	74
4.9	V light curve. 1 spot fit . . . . .	75
4.10	R light curve. 1 spot fit . . . . .	75
4.11	I light curve. 1 spot fit . . . . .	76
4.12	Spot 2, $\Sigma wr^2$ for longitude determination . . . . .	77
4.13	Spot 2, $\Sigma wr^2$ for $\rho$ determination . . . . .	78
4.14	Spot 2, $\Sigma wr^2$ for $t_f$ determination . . . . .	79
4.15	B light curve, 2 spot fit . . . . .	80
4.16	V light curve, 2 spot fit . . . . .	81
4.17	R light curve, 2 spot fit . . . . .	81
4.18	I light curve, 2 spot fit . . . . .	82
4.19	Model of TY Boo facing earth at phase 0.0 . . . . .	84
4.20	Model of TY Boo facing earth at phase 0.1 . . . . .	84
4.21	Model of TY Boo facing earth at phase 0.2 . . . . .	85
4.22	Model of TY Boo facing earth at phase 0.5 . . . . .	85
4.23	Model of TY Boo facing earth at phase 0.6 . . . . .	86
4.24	Model of TY Boo facing earth at phase 0.7 . . . . .	86
4.25	$f'$ determination . . . . .	92
4.26	Comparison of TY Boo with other stars . . . . .	93
4.27	Mass-luminosity plot. Main-sequence stars, and TY Boo 1 and 2 . . . . .	95
4.28	Flare observed in the spectrum of TY Boo. June 1985 . . . . .	96
4.29	Plot of $B - V$ from LC 2 . . . . .	98
B.1	RADS system . . . . .	119
B.2	Sample graph from the LC mode output . . . . .	123

# Chapter 1

## Introduction

It has been shown that a large fraction of the stars we observe are not single stars. Over 50 % of the stars within 5 pcs of the sun are double or multiple stars (Mihalas and Binney 1981) moving around a common center of mass. These stars are called binary stars. There is more that one can learn from such a pair as opposed to a single star, by studying the interaction that takes place between them.

The most obvious effect is the eclipse phenomenon that occurs if the plane of the orbit of the stars is close to the line of sight of the observer. Here one star moves in front of the other blocking some of its light. If the observer records the brightness of the system at consecutive times, he can then obtain a light curve as shown in Figure 1.1.

There are three types of light curves. The diagram shows the light curve of a detached system in which the light remains constant most of the time except when one of the stars moves in front of the other, eclipsing it. At this point we see a rapid reduction in the amount of light until one star is in front of the other, then the light increases again as the eclipse ends. A second eclipse takes place half a period later, when the positions of the two stars reverse.

The difference between the shapes and depths of the two eclipses depends on the sizes and temperatures of the stars. The deeper minimum is called the primary minimum, and occurs when the star with the higher surface brightness is eclipsed

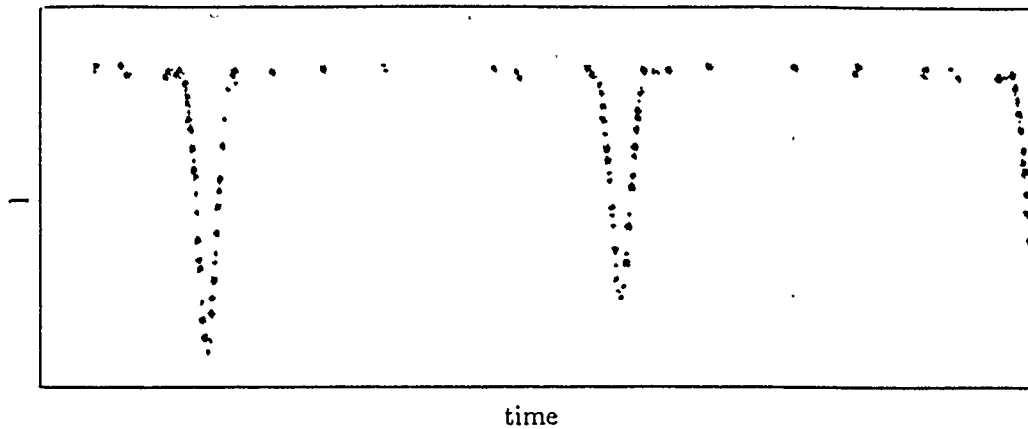


Figure 1.1: Detached system light curve

by the other. The shallow minimum is called the secondary minimum. The fact that the light remains constant outside eclipse shows that the two stars are essentially undistorted spheres, and that the light variation come only from the eclipses themselves. Light curves of this sort are often designated “Algol” light curves after the prototype.

If the two stars are closer together then the tidal forces can distort the surfaces of the stars into oblate spheroids. This distortion will manifest itself in the light curve since now there will be a continuous change of light as the exposed surface of the spheroid changes with respect to its position. The observer would see a change in the light of the system even outside the eclipses as the spheroids turn and expose different surface areas and brightnesses. The peak brightness occurs at phases 0.25 and 0.75 when no eclipses take place, and the surface exposed is maximum. Such

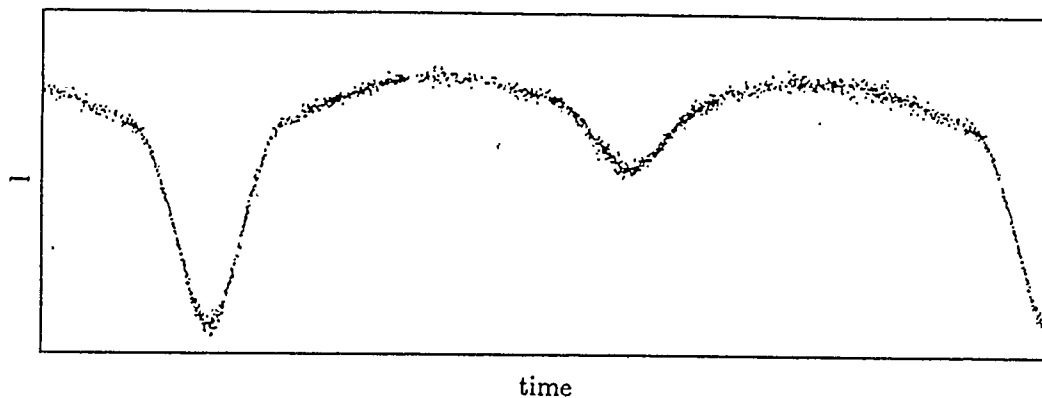


Figure 1.2: Semi-Detached system light curve

light curves are referred to as “ $\beta$  Lyrae” light curves after this archetype star. The light curve of such a system will now look like that in Figure 1.2.

These systems are known as close binaries, since the distortion is only possible when the stars are close to each other.

### 1.1 W UMa Stars

In an extreme case, the surfaces of the stars can be so close together that exchange of material can take place through a bridge of matter running from one star to the other. This is a contact type binary. The “contact” designation refers to the physical circumstances of the system. The term “W UMa” refers to the light curves of the archetype system W Ursae Majoris, in which the light continuously varies

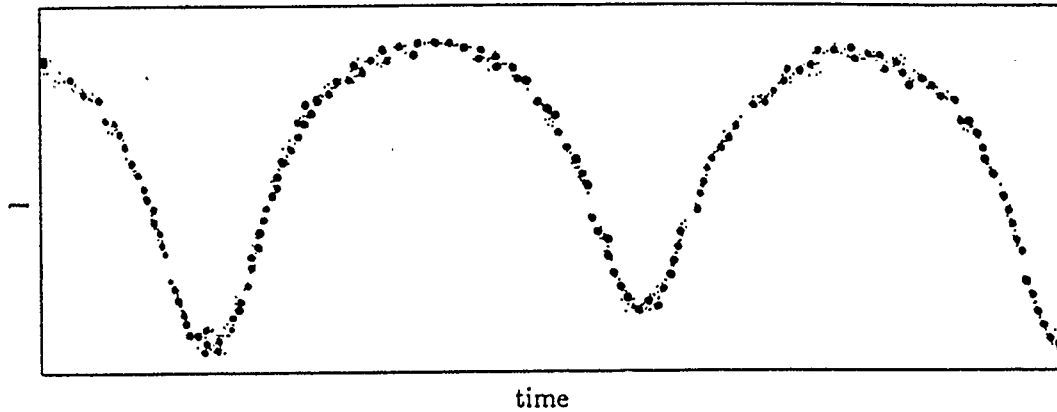


Figure 1.3: Contact system light curve

and the eclipse depths are approximately equal. About 400 contact systems are known to date, and only about one-tenth have been reasonably studied.

Because of the interaction that takes place certain parameters of the component stars in contact systems have the same value. Since the outer envelope is shaped by both stars, the potential, the gravity darkening, albedo, and for many cases the limb-darkening (at a particular wavelength) are taken as equal.

The components of a W UMa system are not identical. Usually sizes and temperatures will differ, although the contact between the stars will tend to force the temperatures to equilibrium through the exchange of material. If the larger star is the hotter, primary minimum occurs when this component is eclipsed by the smaller star. In such a case, the system is known as an A type W UMa system. If the situation is such that primary minimum happens when the smaller

star is eclipsed by the larger and cooler component, the system is called a W type W UMa system. Another way to express this condition is that a transit during primary minimum would characterize an A type system, while an occultation at this minimum will correspond to a W type. If the inclination of the system is large enough for the eclipses to be total, then identification of subtype can be made by inspection of the light curve. If the eclipses are partial, or if no total eclipses take place, then spectroscopy is essential to determine the motion and relative masses of the components.

## 1.2 TY Bootis

The binary system known as TY Bootis seemed a suitable candidate for further study because of its variable light curve, its solar type spectrum, and because of the observed flares seen in Ca II by Milone (1986). A study of it would almost certainly result in a useful contribution to our knowledge of W UMa stars. TY Boo had been chosen earlier as a program star at the Rothney Astrophysical Observatory for displaying some asymmetry in its light curve.

TY Boo was discovered by Guthnick and Prager (1926) and was originally cataloged as a  $\beta$  Lyrae system. The latter systems are characterized, however, by larger differences between the depths of the minima than are seen here (see Figure 1.2 for an example of a  $\beta$  Lyr type curve). The change in brightness was reported as being in the range  $11.5^m - 12.0^m$ .

TY Boo was extensively observed by R. Szafraniec (1948, 1949, 1959, 1951, 1953, 1955, 1956, 1957, 1958, 1959, 1960, 1963, 1966) who recorded several times

of minima. UVB light curves obtained in May 1969, with “nonrectifiable distortions” were published by Carr (1972). The term “nonrectifiable distortions” refers to features in the light curve which indicate variability above and beyond the causes of light variation already discussed, and which can not be removed by following the technique described by Russell and Merrill (1952). The Russell-Merrill light curve analysis method calls for the removal of the sine terms in the Fourier representation of the light curve. Niarchos (1978) later analyzed these light curves with the “frequency domain” method. Samec and Bookmyer (1987) observed TY Boo on five nights beginning on 1986 June 5 U.T. with the 0.79 m reflector at Lowell Observatory. Independently of the previous work Bradstreet (private communication 1985) made high quality observations of TY Boo in 1985 with a 36-inch telescope at KPNO and carried out a preliminary solution. At the Rothney Astrophysical Observatory (hereafter referred to as RAO) of the University of Calgary, TY Boo has been part of the ongoing observing program since 1985.

### **1.3 Analysis History**

In her study of a large set of observations, Szafraniec (1952) analyzed the basic characteristics of TY Boo. She described the asymmetry of the light curve, indicating that the descending branch of both the primary and secondary minima had a smaller slope than the ascending branch. The difference in the maxima was also evident from the light curve published. To minimize systematic error, she also reworked all observations with the tracing paper method she had used on her own observations.

In a later study, Samec and Bookmyer (1987) obtained a least-squares solution to the  $O - C$  (observed minus computed data points) of Szafraniec's study together with new observations, and recomputed the elements:  $P_o = 0.31714964(3)$  day and  $E_o = 2446589.7906(t)$ . However the  $O - C$  curve is far from being smooth, and from the early visual observations they concluded that "two period changes have taken place in a 19-year interval".

Carr (1972) attempted a light curve solution based on his observations. However he asserted that nonrectifiable distortions in the light curves limited the accuracy of his results. He found an orbital inclination of  $73.7^\circ$ , and suggested the components to be of spectral type G3 and G7.

#### 1.4 Aims

It is the purpose of binary star research to shed light on the nature of these stars, especially the poorly understood ones, such as the W-type W UMa systems. With all the available data, a complete solution of one of these — TY Boo — was now possible. The four recent light curves together with the radial velocity observations (some of which were reported by Milone, Fry and Grillmair 1987) would be combined and studied using the Wilson-Devinney program.

From the radial velocity data the mass ratio and other spectroscopic parameters are determinable. The inclination, relative brightnesses, sizes and other photometric elements would be obtained from the light curves. Preliminary values could then be improved by using the Wilson-Devinney program to compute differential corrections, which would be applied in an iterative fashion.

The anomalies present in both the radial velocity and light curve data made TY Boo an ideal system in which to study the effects of such phenomena on the derived elements of the system, and the results would become an important contribution to the study of close binary stars.

## Chapter 2

# Photometric Observations and Reduction

### 2.1 Observations

Figure 2.1 shows a finding chart for TY Boo; it identifies the comparison and check stars used. The variable is located at  $\alpha = 14^h 58^m 47^s$ ,  $\delta = 35^\circ 19'.8$  (1950 coordinates).

The starting point for this study was a collection of light curves observed in the years 1985, 1986 and 1987 using the RADS system on the 0.4-m telescope at RAO in Priddis. These are referred below as data sets LC 1, 3 and 4 respectively. RADS will be described in depth in a later Appendix. TY Boo was part of the RAO observing program of Milone carried out during this period by student observers J. Van Leeuwen, S.C. Griffiths, C. Rousseau and the author. The light curves were restricted to the B, V and I bandpasses as a compromise between full wavelength coverage and phase-limited integration times for this short-period variable. All the times are converted into phase by subtracting the epoch ( $E_o$ ) and dividing by the period ( $P_o$ ).

Another set of light curves was obtained by Bradstreet in the BVRI filter bands during 1985 (private communication) at Kitt Peak, with 0.9-m telescope. These observations consist of a much larger set of points and are of a higher quality. From these data normal points were computed and used instead of the full set. The normal points light curves constitute data set LC 2.

Table 2.1: Light curve sets.

name	JD +2446000	observer(s)	bandpasses
LC 1	228.3	RAO	BVI
LC 2	229.3	Bradstreet	BVRI
LC 3	560.0	RAO	BVI
LC 4	927.8	RAO	BVI

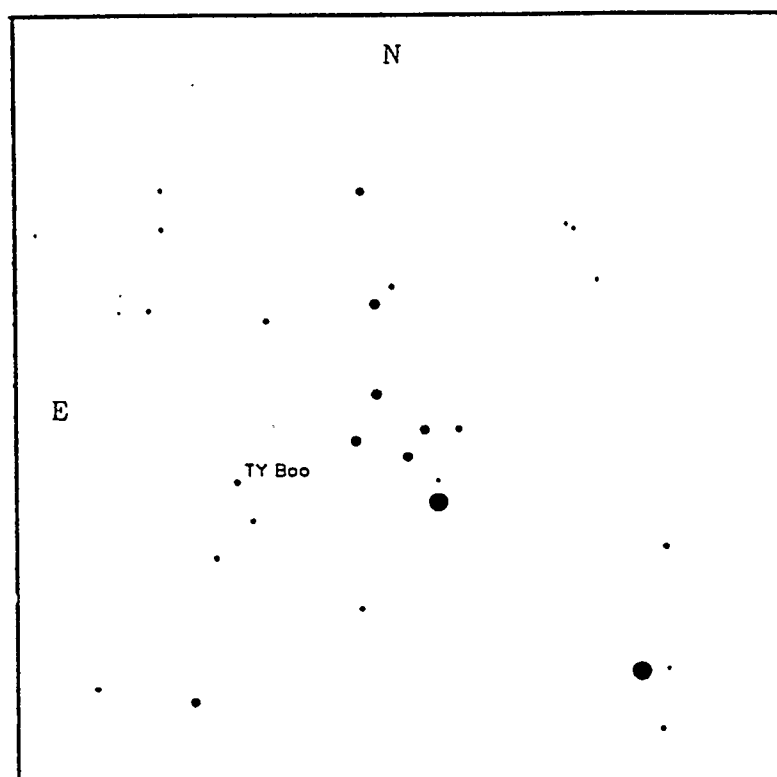


Figure 2.1: Finding chart for TY Boo

The four sets of differential light curves are reproduced in Figures 2.2 through 2.5 in luminosity units normalized to the higher maximum in each case.

## 2.2 Light Curve Analysis

The TY Boo light curves are typical of W UMa systems as the change in the light from the system is continuous. The beginnings and endings of the eclipses can be seen at about 0.2 phase on both sides of each minimum.

Visual inspection of these light curves revealed the secondary minimum at precisely 0.5 phase units following the primary minimum. This, together with the widths of both eclipses being similar in width, indicated that the orbit is circular, a common condition in W UMa systems.

It was also observed that the brightness of the system outside eclipse was different from one maximum to the other. This is known as the O'Connell effect, a name given the phenomenon by Wesselink and Milone (Milone 1968). The most important work on this phenomenon (formerly called the "periastron effect") was done by O'Connell (1951) and, independently, by Mergentaler (1950), who treated a much smaller volume of data. In his paper, O'Connell defined  $\Delta m$  as the magnitude difference  $maximum_{II} - maximum_I$  where the subscripts  $I$  and  $II$  refer to the maximum following primary and secondary minima respectively; in this way  $\Delta m$  would result positive for a system with a brighter maximum following the primary minimum. A subsequent study of this phenomenon was carried out by Davidge and Milone (1984) and by Davidge (1981). A principal result of that study was that the O'Connell effect had more than one origin; i.e. it could not

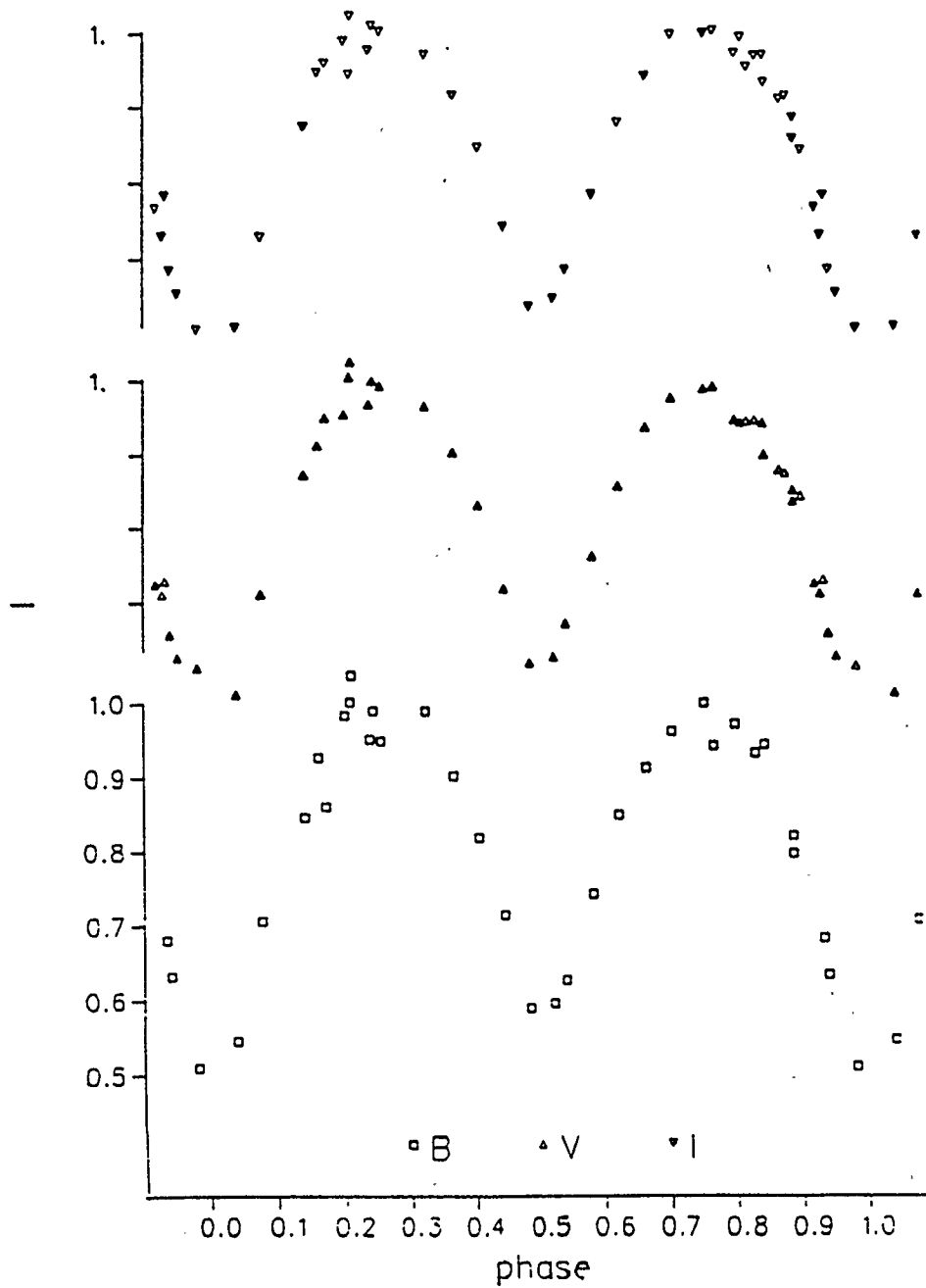


Figure 2.2: B, V and I Light Curves for 1985 (LC 1)

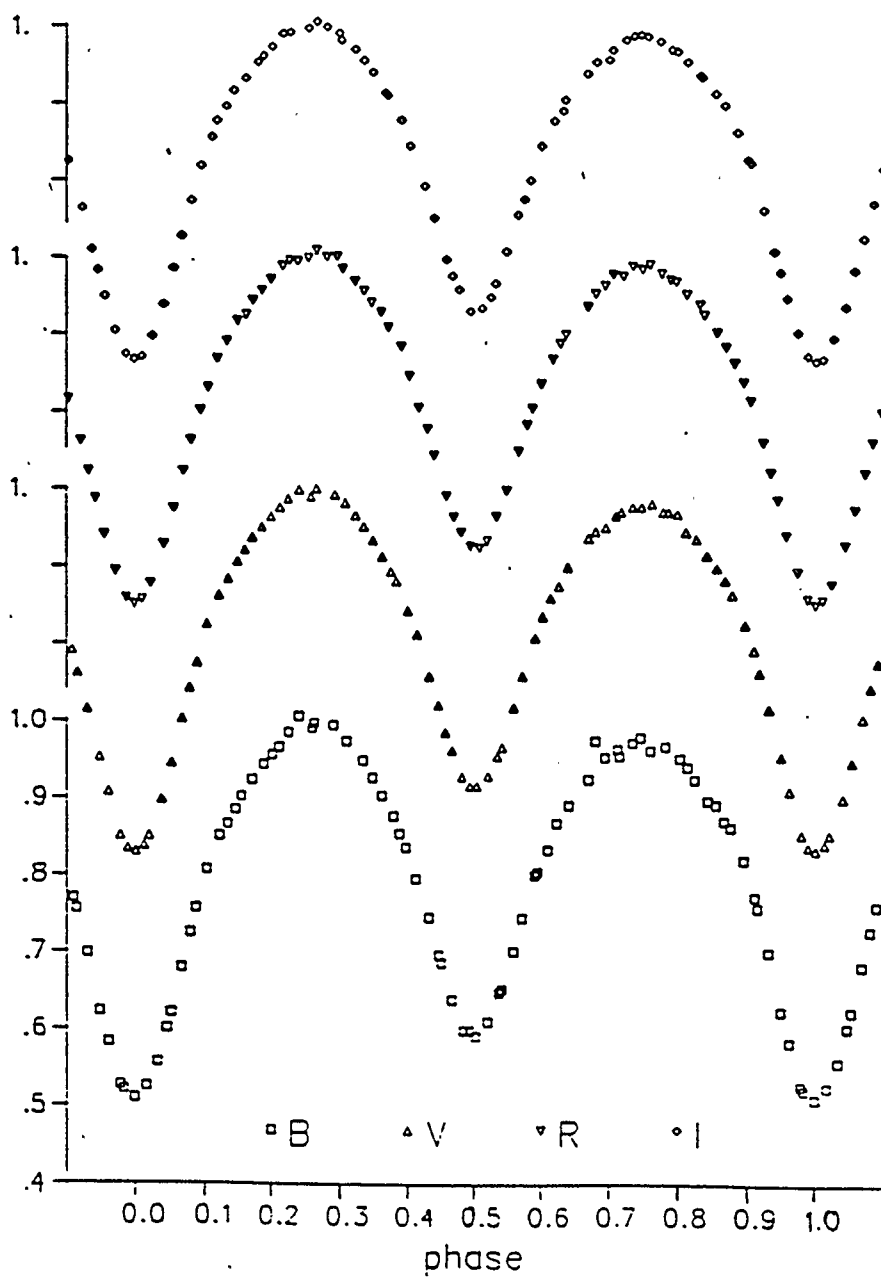


Figure 2.3: B, V, R and I Light Curves for 1985 (LC 2)

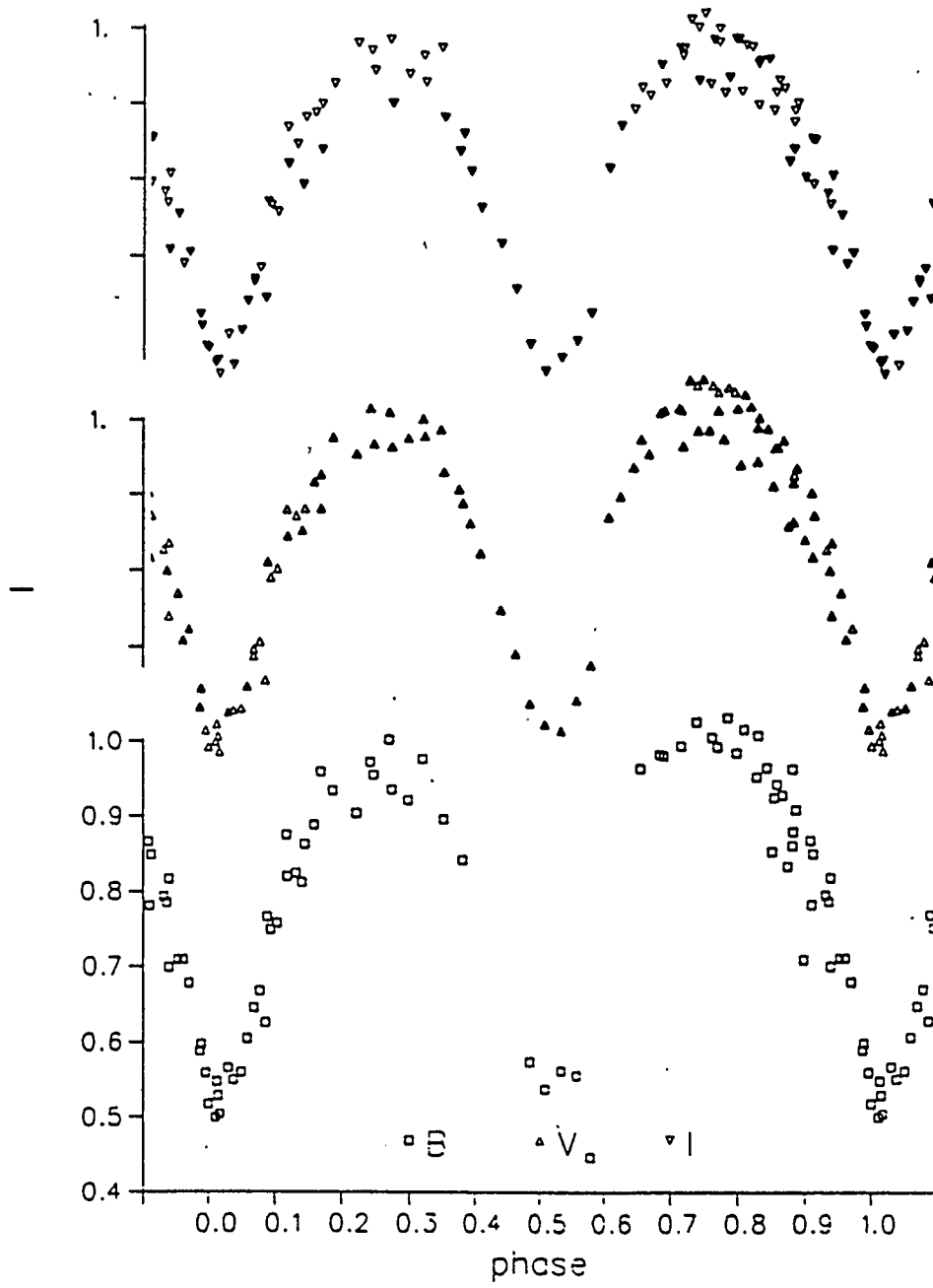


Figure 2.4: B, V and I Light Curves for 1986 (LC 3)

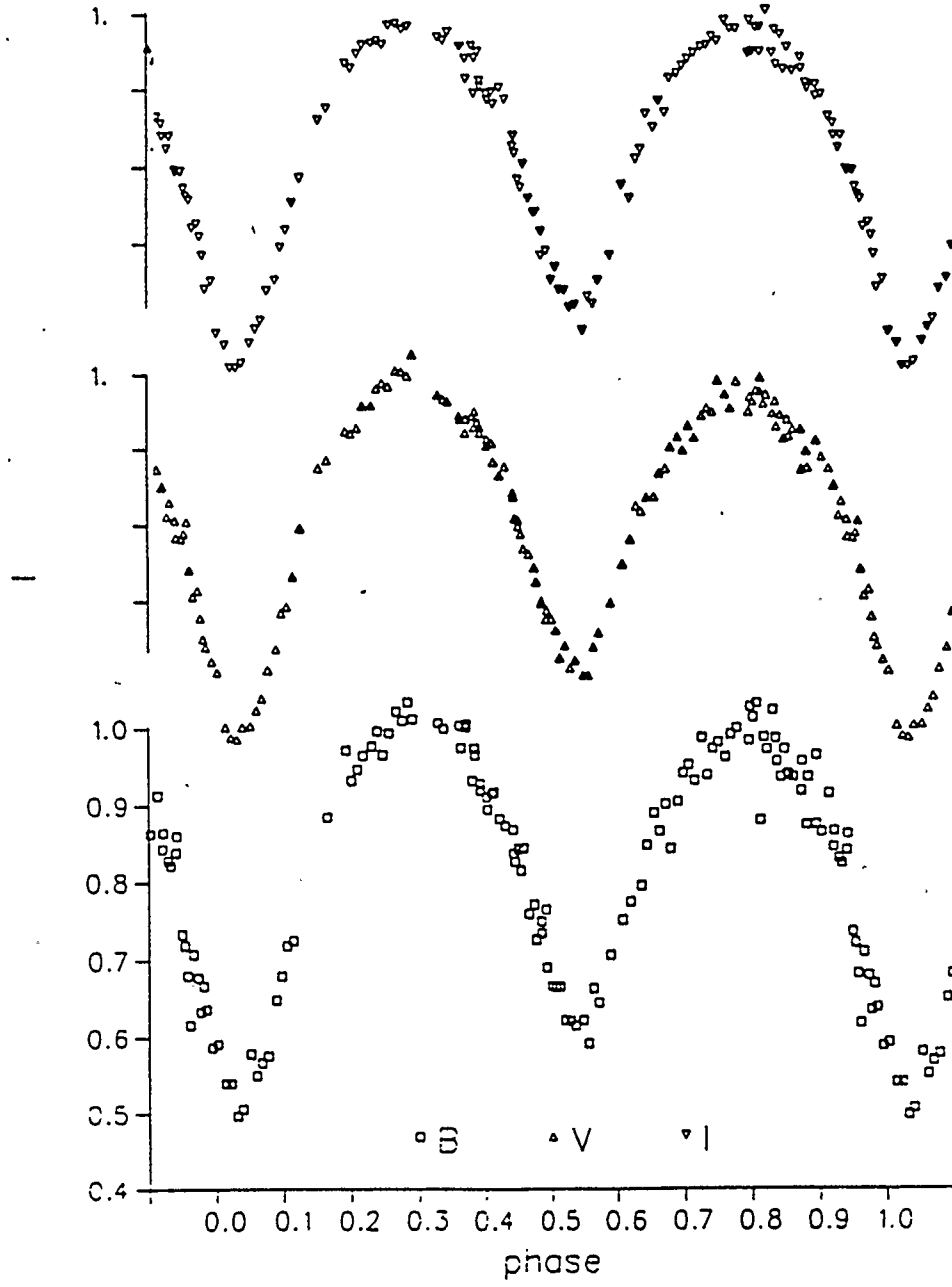


Figure 2.5: B, V and I Light Curves for 1987 (LC 4)

always be attributed, say, to starspots alone. The study did not include contact systems, however. Hence, further work needs to be done.

In the present light curves not only does the magnitude of the effect change from one wavelength to another, but the sign and magnitude vary as well, from one year to the next. In the years 1985 and 1987 (Sets LC 1, 2 and 4) maximum  $I$  is brighter than  $II$ . The opposite is true during 1986. Table 2.2 lists the values of  $\Delta m$  in the RAO light curves for both maxima and each year. The mean magnitude of each maximum is taken as the average of all observations within 0.1 phase around each maximum. As in other tables in this thesis, the standard deviation of the mean appears in the parenthesis in units of the last digit. This error is larger than that of a single observation as computed from the whole light curve. This can be attributed to the fact that the latter is computed from a specific region of the light curve that appears to contain higher scatter than the overall average. Errors computed from the whole set of points include data with less scatter, and are hence smaller.

A more objective way of studying these changes is by Fourier analyzing the data. This process yields a best fit curve expressed as a series of sine and cosine terms; the coefficients of each light curve can then be compared term by term. Before doing this, one must make sure that the center of the primary eclipse falls exactly at phase 0. Variations of the phase of minima of TY Boo had already been observed by Szafraniec (1952). Phases of minima were computed for each light curve observed at the RAO using the University of Calgary PHIMIN program. This program is essentially the method of Hertzsprung as developed by Kwee and Van Woerden (1956). Table 2.3 lists the phases of minima for each light curve. The

Table 2.2: Mean differential magnitudes at Maximum Light of TY Boo

Light Curve	max	B	V	I
LC 1	I	3.356(34)	3.568(19)	3.743(29)
	II	3.372(30)	3.577(02)	3.732(02)
	$\Delta m$	+0.017(45)	+0.009(19)	-0.011(29)
LC 3	I	3.462(37)	3.667(29)	3.799(34)
	II	3.408(32)	3.626(32)	3.780(35)
	$\Delta m$	-0.053(50)	-0.041(43)	-0.018(49)
LC 4	I	3.419(29)	3.620(30)	3.790(15)
	II	3.444(26)	3.647(26)	3.792(15)
	$\Delta m$	+0.025(39)	+0.027(40)	+0.001(21)

elements used were those of Bradstreet (private communication):  $P_o$ : 0.317146(5) day,  $E_o$ : 2446230.7751(4). Here  $P_o$  is the period of the system in days and  $E_o$  the date (in Julian Days) of a primary minimum used as reference. Data Set LC 2 had already been adjusted in phase by Bradstreet.

From these figures an average phase shift can be computed for a run of data. Results are listed in Table 2.4.

Two methods were used to compute the errors. First the weighted average of the values in Tables 2.3 and 2.4 were computed. This led to a very small error for the data set LC 3, since the phase shifts for both minima are almost equal. The root mean square of the error estimates was also computed, and then the larger of the two error estimates was reported.

Even though the changes in phase seem to show a predictable trend from the three values obtained for our light curves, Szafraniec's work (1952), and the work presented here, show that over a longer period of time irregular short term varia-

Table 2.3: Phases of Minima

<b>Phase of Primary Minimum</b>				
<b>Light Curve</b>	<b>V</b>	<b>B</b>	<b>I</b>	<b>mean</b>
LC 1	0.0045 (133)	0.9999 (75)	0.0051 (94)	0.0023 (18)
LC 3	0.0194 (050)	0.0208 (49)	0.0218 (33)	0.0210 (07)
LC 4	0.0358 (042)	0.0347 (41)	0.0344 (31)	0.0348 (04)

<b>Phase of Secondary Minimum</b>				
<b>Light Curve</b>	<b>V</b>	<b>B</b>	<b>I</b>	<b>mean</b>
LC 1	0.5037 (44)	0.5074 (048)	0.5042 (40)	0.5049 (11)
LC 3	0.5210 (15)	0.5212 (034)	0.5207 (47)	0.5210 (01)
LC 4	0.5369 (47)	0.5410 (054)	0.5393 (31)	0.5390 (10)

Table 2.4: Average Phase Shift

<b>Light Curve</b>	<b>Phase Shift</b>
LC 1	0.0042 (15)
LC 3	0.0210 (05)
LC 4	0.0354 (14)



values derived from the Bradstreet elements, and 2 those derived from the new elements, namely:  $O - C_1$ :  $P_0$ : 0.317146  $E_0$ : 2446230.7751;  $O - C_2$ :  $P_0$ : 0.3171482  $E_0$ : 2446230.7666.

As was mentioned in Chapter 1 the significant spread of the data points is in part due to the varying quality of the observations, in particular those around JD 2442000 to 2444000, which were observed by European amateur Roger Diethelm (Diethelm 1972, 1976a, 1976b, 1977, 1980). Mochnacki (1971), however, indicates that even the archetype for TY Boo's classification, W UMa itself has shown considerable variation in period during the several decades it has been observed.

Table 2.5:  $O - C$  Phases of minima for two sets of elements.

JD	$O - C_1$	$O - C_2$	JD	$O - C_1$	$O - C_2$
+2400000			+2400000		
32650.4710	0.354	0.021	34456.4830	0.278	-0.014
32659.5080	0.360	0.026	34457.5950	0.272	-0.020
32676.4860	0.326	-0.007	34480.4250	0.286	-0.006
32682.5080	0.338	0.005	34481.3690	0.310	0.018
32688.5390	0.321	-0.011	34488.3500	0.298	0.006
32688.5450	0.302	-0.030	34604.4420	0.246	-0.044
32717.4100	0.288	-0.044	35217.4980	0.205	-0.070
32987.6110	0.311	-0.015	35240.4780	0.247	-0.028
32996.4900	0.314	-0.011	35603.4400	0.283	0.016
33001.4060	0.314	-0.012	35903.4690	0.255	-0.005
33002.3580	0.312	-0.014	35933.4420	0.247	-0.013
33005.3680	0.321	-0.004	36074.4080	0.264	0.008
33006.4850	0.299	-0.026	36361.4310	0.245	-0.004
33010.4370	0.338	0.013	36727.4100	0.269	0.027
33028.5110	0.348	0.023	36728.3730	0.232	-0.009
33031.3650	0.349	0.024	37015.3800	0.264	0.029
33032.4750	0.349	0.024	37027.4230	0.291	0.057
33040.4110	0.326	0.002	38882.4230	0.250	0.057
33041.3650	0.318	-0.007	38961.4030	0.216	0.026
33053.4210	0.304	-0.020	40367.7910	0.205	0.046
33054.5190	0.342	0.018	40367.9490	0.206	0.047
33056.4250	0.332	0.008	40368.9000	0.206	0.047
33059.4440	0.313	-0.011	40368.7420	0.205	0.046
33063.3990	0.342	0.018	40369.6940	0.204	0.045
33066.4280	0.291	-0.033	40369.8520	0.206	0.047
33068.4780	0.327	0.003	40370.8030	0.206	0.047
33069.4330	0.318	-0.006	41460.3820	0.131	-0.003
33082.4330	0.326	0.002	42887.3830	0.123	0.021
33082.4350	0.319	-0.004	42900.3790	0.145	0.043
33350.4150	0.346	0.028	43360.4000	0.143	0.051
33357.3940	0.340	0.023	44303.4610	0.056	-0.014
33362.4660	0.347	0.030	44342.4380	0.157	0.088
33362.4730	0.325	0.008	45120.4390	0.024	-0.028
33390.3880	0.306	-0.011	46226.8110	-0.001	-0.028
33391.3390	0.307	-0.009	46227.7630	-0.002	-0.029
33410.3620	0.325	0.009	46228.3000	-0.005	-0.028
33440.4980	0.303	-0.013	46228.3000	-0.002	-0.027
33746.3750	0.335	0.027	46230.7750	0.001	-0.026
33762.3970	0.316	0.008	46231.7270	0.000	-0.027
33782.3810	0.304	-0.004	46560.0000	-0.021	-0.027
33798.4070	0.272	-0.035	46560.0000	-0.021	-0.027
33860.4110	0.266	-0.040	46587.7280	-0.016	-0.035
34123.3160	0.295	-0.006	46588.8390	-0.020	-0.038
34131.4080	0.279	-0.020	46589.7910	-0.020	-0.039
34133.4640	0.297	-0.003	46590.7430	-0.022	-0.041
34179.4470	0.307	0.008	46591.8510	-0.016	-0.035
34451.5710	0.266	-0.026	46927.8000	-0.040	-0.040
34452.5050	0.321	0.029	46927.8000	-0.035	-0.035



$$l = \sum_{i=0}^4 a_i \cos(i\theta) + \sum_{i=1}^4 b_i \sin(i\theta)$$

Where  $l$  is the broad-band flux of the system relative to the comparison star. To study the different effects individually one may choose to fit either only the maxima, to study proximity effects, or the minima to look at the eclipses themselves. A full light curve fit is also useful, as will become clear in Chapter 4.

To compute the fit the program FOURIER from the University of Calgary was used. The program computes not only the coefficients but also the standard deviation for a single observation. This value is a good estimate of the error of each fit. Three tables list the results from the fourier fits with the last column,  $e_1$  indicating the error of the fit. The fits have been graphed against the corresponding light curves, and are presented in Figures 2.8 through 2.13. The fit coefficients are listed in Tables 2.6 through 2.8. From the light curves —and specially LC 2— the points of first and last contact were taken to be at phases 0.125 and 0.375 for the primary eclipse and phases 0.625 and 0.875 for the secondary eclipse.

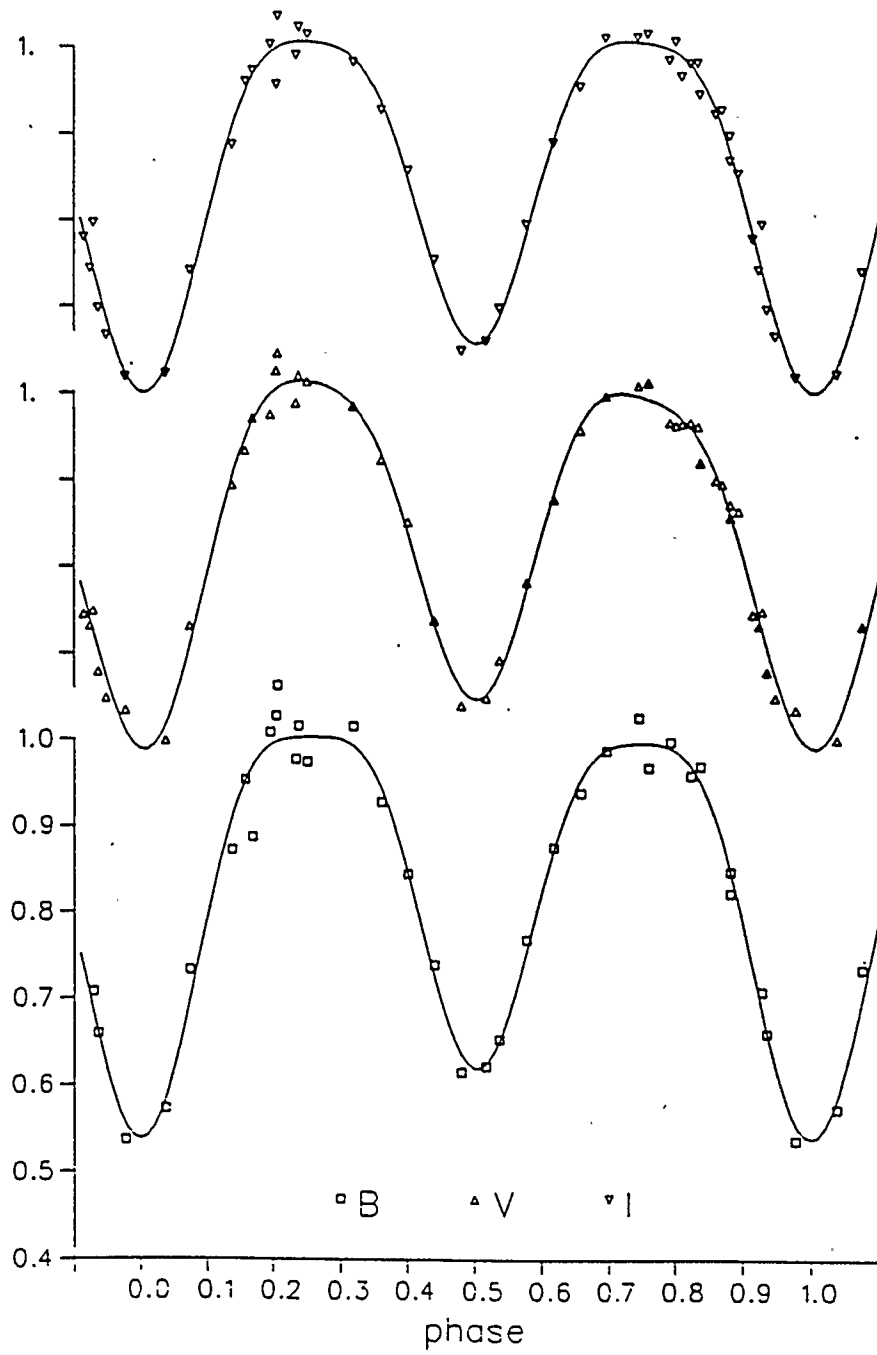


Figure 2.8: LC 1 with Fourier fit to the full light curve.

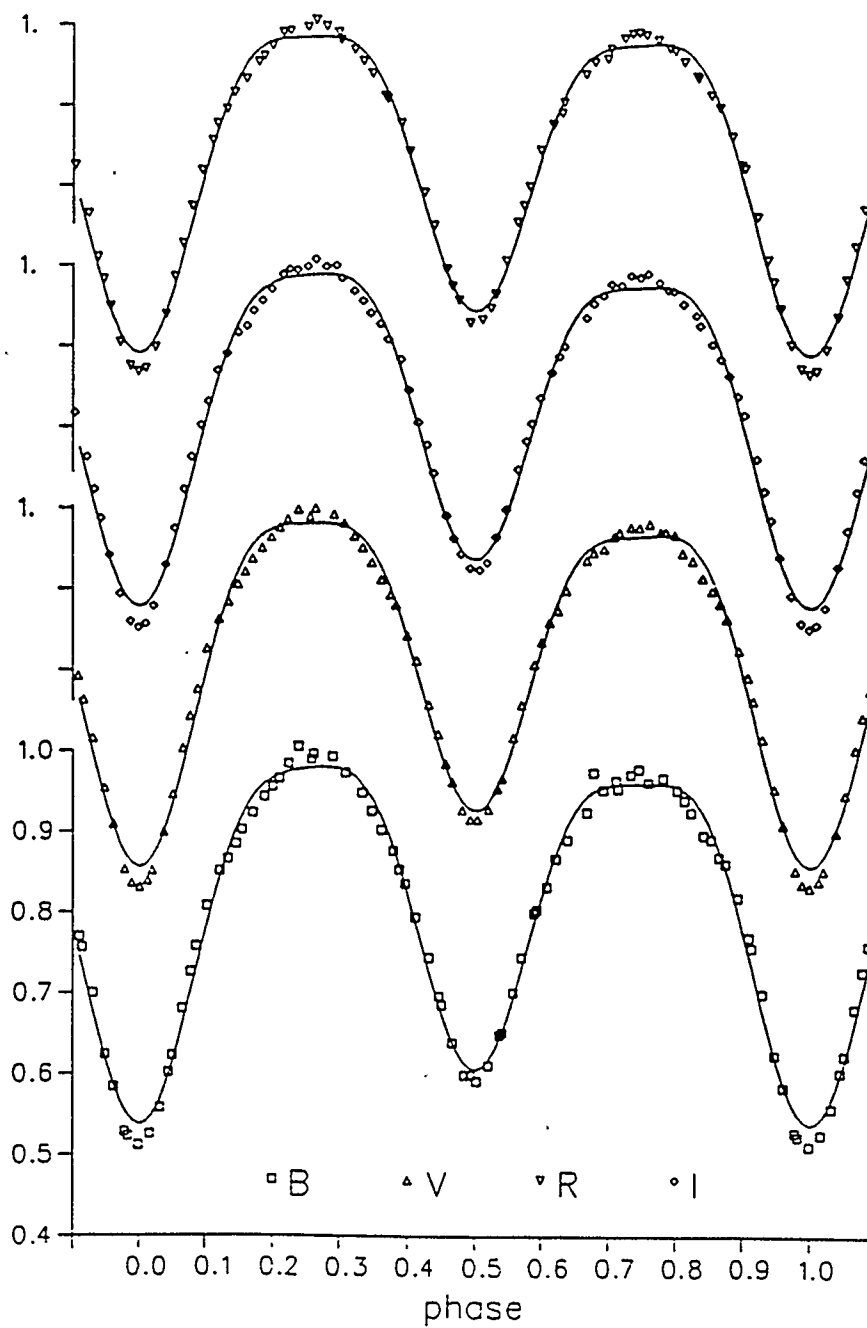


Figure 2.9: LC 2 with Fourier fit to the full light curve.

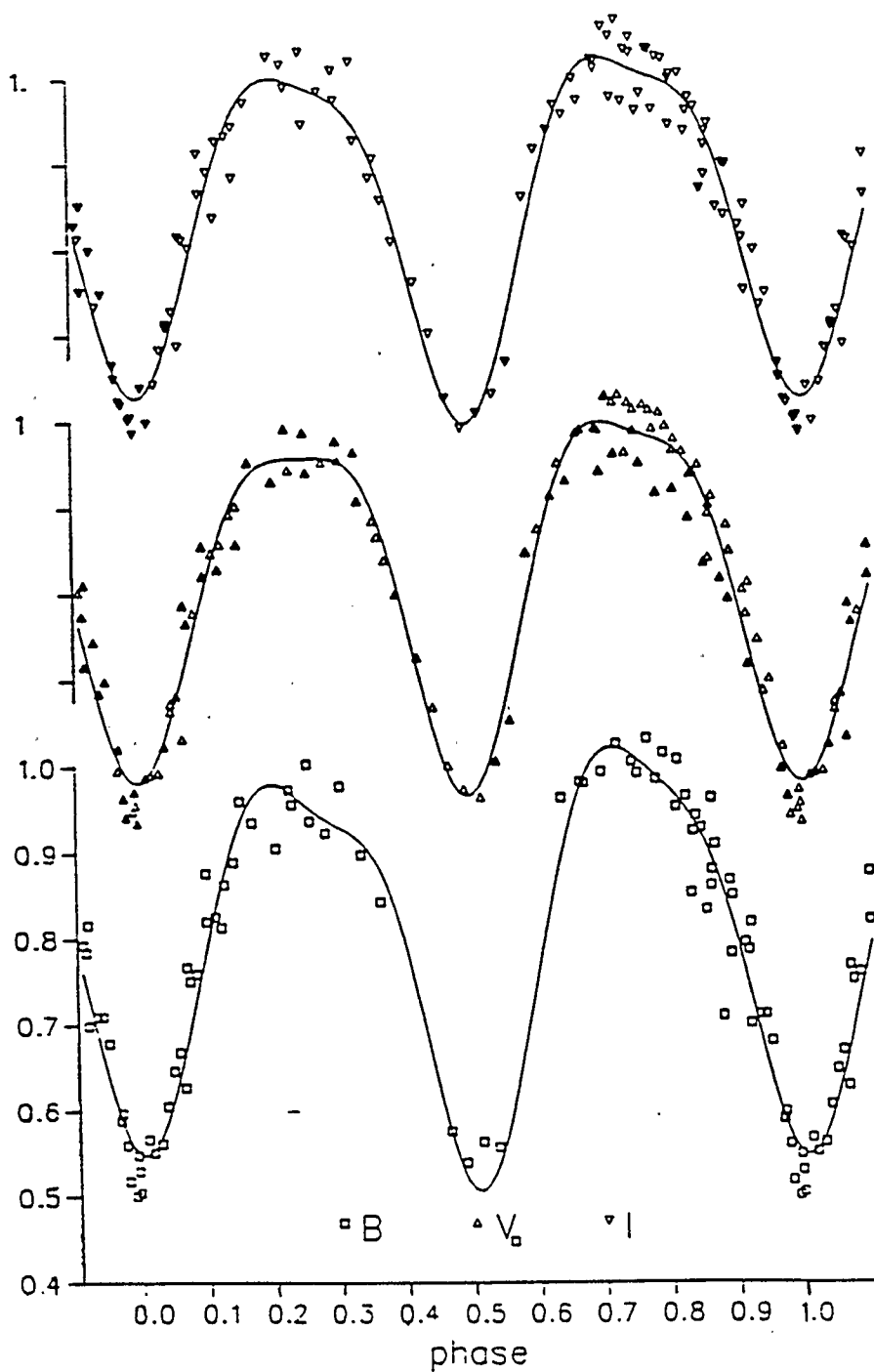


Figure 2.10: LC 3 with Fourier fit to the full light curve.

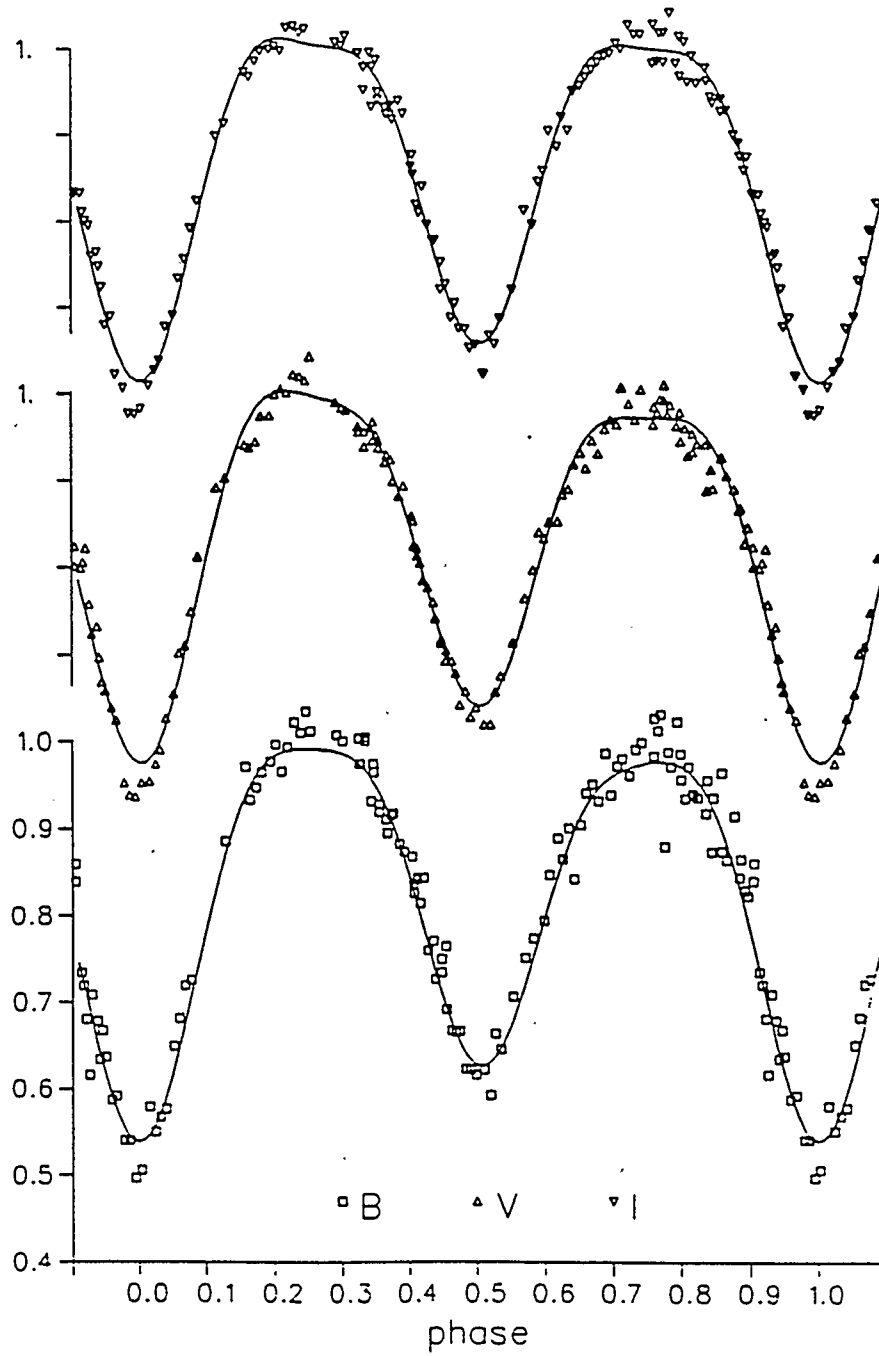


Figure 2.11: LC 4 with Fourier fit to the full light curve.

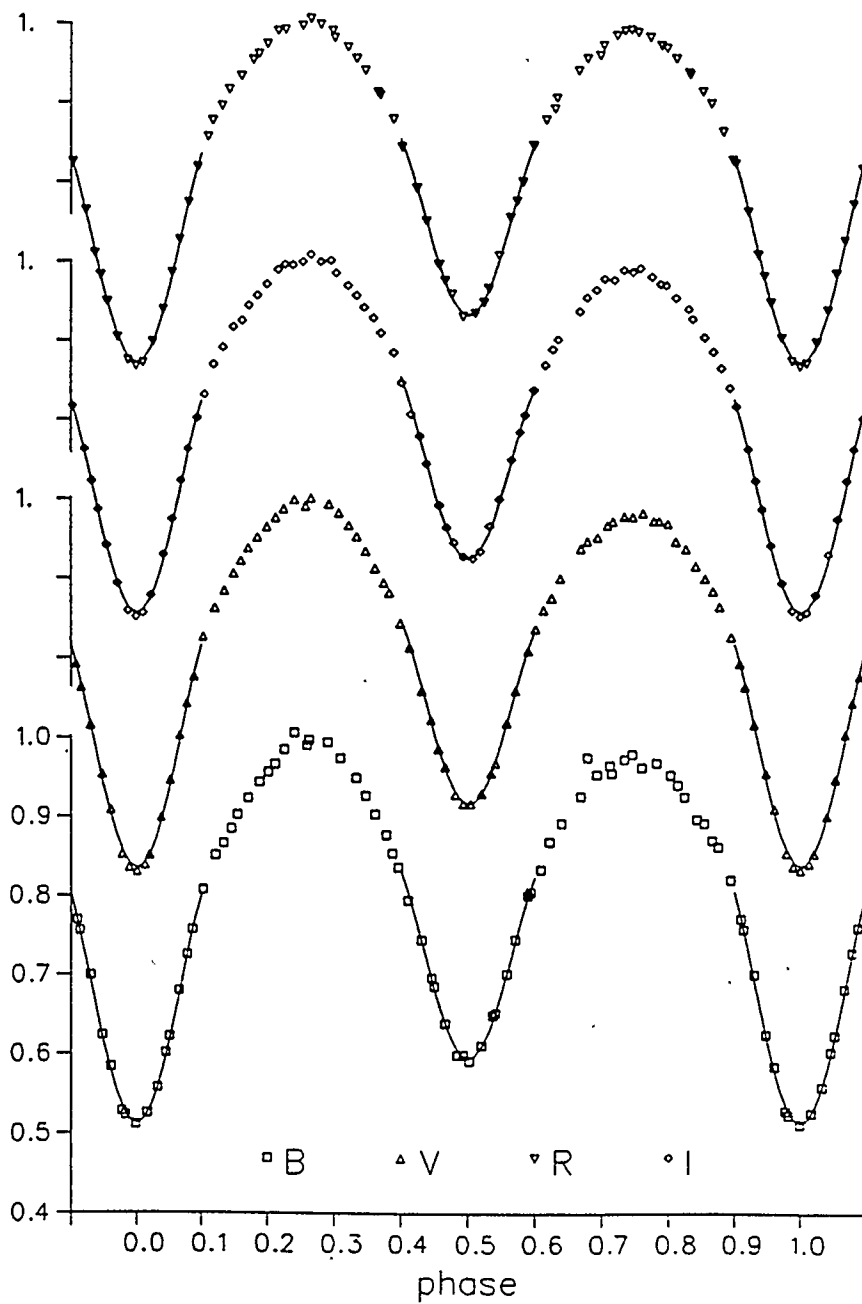


Figure 2.12: LC 2 with Fourier fit to the minima.

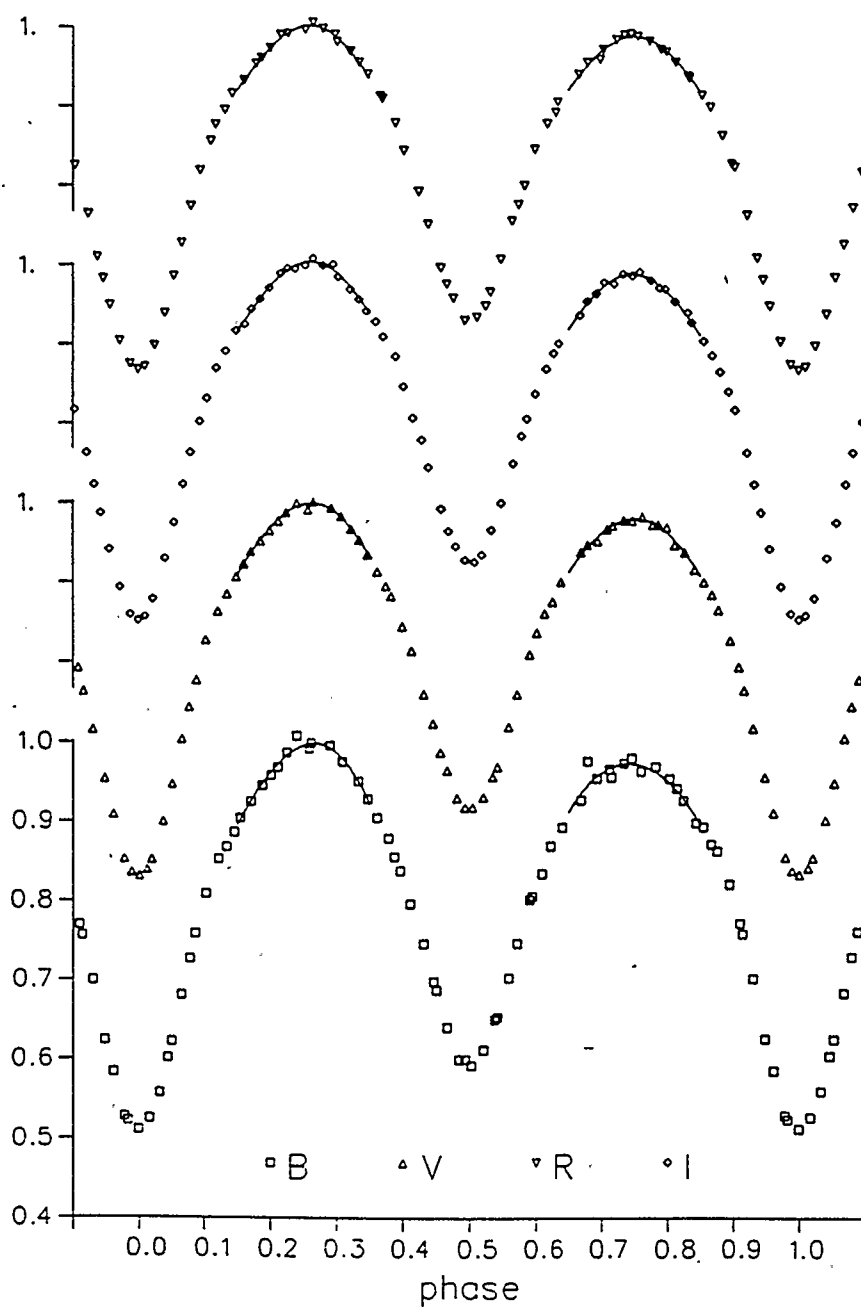


Figure 2.13: LC 2 with Fourier fit to the maxima.

Table 2.6: 9 Term Fourier Representation (Fit to Minima Only)

L.C.	$a_0$	$a_1$	$a_2$	$a_3$	$a_4$
LC 1-B	0.816(058)	-0.021(008)	-0.105(086)	-0.028(012)	-0.112(032)
V	0.922(103)	-0.020(014)	-0.254(154)	-0.009(021)	-0.025(056)
I	0.883(101)	-0.021(014)	-0.145(150)	-0.010(021)	-0.071(055)
LC 2-B	0.750(007)	-0.022(001)	-0.084(011)	-0.019(002)	-0.112(005)
V	0.754(007)	-0.021(001)	-0.063(011)	-0.018(001)	-0.116(005)
R	0.764(008)	-0.019(001)	-0.062(012)	-0.014(002)	-0.112(005)
I	0.771(006)	-0.016(001)	-0.058(010)	-0.014(001)	-0.111(004)
LC 3-B	0.642(063)	0.024(013)	0.040(101)	-0.002(017)	-0.170(046)
V	0.679(038)	0.003(007)	0.036(059)	0.004(010)	-0.165(026)
I	0.710(038)	0.013(007)	0.043(060)	0.004(010)	-0.163(026)
LC 4-B	0.816(046)	-0.027(009)	-0.163(068)	-0.021(012)	-0.078(026)
V	0.766(018)	-0.013(003)	-0.058(027)	-0.027(004)	-0.120(012)
I	0.799(020)	-0.014(003)	-0.066(031)	-0.013(004)	-0.112(013)
	$b_1$	$b_2$	$b_3$	$b_4$	$e_1$
LC 1-B	0.048(062)	0.023(016)	-0.011(028)	-0.018(013)	0.012
V	0.070(113)	-0.005(029)	-0.034(051)	0.002(023)	0.023
I	0.018(110)	-0.006(028)	-0.012(050)	0.001(022)	0.023
LC 2-B	0.000(006)	-0.004(002)	0.002(003)	0.001(002)	0.005
V	0.009(006)	-0.002(002)	-0.002(003)	-0.003(002)	0.004
R	0.013(007)	-0.005(002)	-0.005(004)	0.001(002)	0.005
I	0.004(005)	-0.000(002)	0.000(003)	-0.002(002)	0.004
LC 3-B	-0.081(066)	0.041(022)	0.059(038)	-0.056(022)	0.049
V	-0.068(039)	0.038(013)	0.022(022)	-0.017(013)	0.030
I	-0.077(039)	0.047(013)	0.027(022)	-0.027(013)	0.030
LC 4-B	-0.037(048)	-0.009(019)	0.033(021)	-0.002(015)	0.027
V	0.048(016)	0.000(006)	-0.023(009)	-0.006(005)	0.014
I	0.027(018)	-0.001(006)	-0.010(010)	-0.004(006)	0.016

Table 2.7: 9 Term Fourier Representation (Fit to Maxima Only)

L.C.	$a_0$	$a_1$	$a_2$	$a_3$	$a_4$
LC 1-B	0.795(137)	0.005(146)	-0.333(210)	0.007(072)	-0.088(081)
V	0.866(052)	-0.009(049)	-0.211(081)	0.002(026)	-0.037(032)
I	0.883(056)	0.022(053)	-0.226(087)	0.014(028)	-0.047(034)
LC 2-B	0.848(018)	-0.000(015)	-0.147(028)	0.011(008)	-0.013(012)
V	0.871(005)	-0.007(004)	-0.123(008)	0.003(002)	-0.006(003)
R	0.887(005)	-0.007(005)	-0.109(008)	0.004(003)	0.000(004)
I	0.896(005)	-0.001(005)	-0.098(009)	0.004(003)	0.002(004)
LC 3-B	0.900(069)	0.047(063)	-0.071(109)	0.029(035)	0.012(045)
V	0.843(049)	-0.001(041)	-0.163(077)	0.012(023)	-0.024(033)
I	0.834(051)	0.002(043)	-0.224(081)	0.006(024)	-0.049(034)
LC 4-B	0.867(034)	0.027(031)	-0.149(052)	0.020(017)	-0.011(023)
V	0.944(017)	-0.002(015)	-0.029(026)	0.003(008)	0.036(011)
I	0.899(019)	0.000(017)	-0.137(029)	0.004(009)	-0.016(013)
	$b_1$	$b_2$	$b_3$	$b_4$	$e_1$
LC 1-B	0.007(018)	-0.044(048)	0.002(024)	-0.032(043)	0.040
V	0.004(007)	-0.017(016)	-0.001(010)	-0.022(014)	0.019
I	-0.002(007)	-0.024(017)	0.002(011)	-0.022(015)	0.020
LC 2-B	0.006(002)	-0.001(005)	-0.006(003)	0.003(005)	0.009
V	0.007(001)	-0.003(001)	-0.002(001)	0.003(001)	0.003
R	0.007(001)	-0.004(002)	-0.000(001)	0.001(002)	0.004
I	0.005(001)	-0.003(001)	-0.001(001)	0.002(001)	0.004
LC 3-B	-0.023(009)	0.043(019)	-0.003(013)	0.019(020)	0.038
V	-0.019(006)	0.026(013)	-0.006(009)	0.013(013)	0.031
I	-0.015(007)	0.017(013)	-0.009(009)	0.001(014)	0.032
LC 4-B	0.018(005)	-0.004(010)	0.004(007)	0.006(010)	0.028
V	0.012(002)	-0.011(005)	-0.001(004)	-0.010(005)	0.014
I	0.004(003)	-0.003(005)	0.001(004)	-0.003(005)	0.015

Table 2.8: 9 Term Fourier Representation (Fit to Full Light Curve)

L.C.	$a_0$	$a_1$	$a_2$	$a_3$	$a_4$
LC 1-B	0.878(4)	-0.031(6)	-0.210(6)	-0.010(6)	-0.049(6)
V	0.879(3)	-0.024(5)	-0.194(5)	-0.004(5)	-0.038(5)
I	0.909(4)	-0.022(5)	-0.189(5)	-0.006(6)	-0.041(5)
LC 2-B	0.820(2)	-0.026(3)	-0.198(3)	-0.006(3)	-0.048(3)
V	0.831(2)	-0.025(3)	-0.186(3)	-0.008(3)	-0.045(3)
R	0.841(2)	-0.022(2)	-0.186(2)	-0.006(2)	-0.046(2)
I	0.846(2)	-0.019(2)	-0.181(2)	-0.007(2)	-0.046(2)
LC 3-B	0.808(5)	0.015(8)	-0.225(8)	0.005(8)	-0.055(7)
V	0.824(3)	-0.000(5)	-0.199(5)	0.008(5)	-0.052(4)
I	0.856(4)	0.011(5)	-0.194(5)	0.004(5)	-0.050(5)
LC 4-B	0.827(2)	-0.030(3)	-0.200(3)	-0.014(3)	-0.044(4)
V	0.845(2)	-0.021(3)	-0.189(3)	-0.012(3)	-0.048(3)
I	0.871(2)	-0.016(3)	-0.184(3)	-0.007(2)	-0.050(3)
	$b_1$	$b_2$	$b_3$	$b_4$	$e_1$
LC 1-B	0.008(6)	-0.004(6)	0.004(6)	-0.002(6)	0.023
V	0.003(5)	-0.002(5)	-0.006(5)	-0.007(5)	0.019
I	-0.004(5)	-0.006(5)	-0.004(5)	-0.005(5)	0.020
LC 2-B	0.007(3)	-0.003(3)	-0.003(2)	0.000(2)	0.016
V	0.004(3)	-0.003(3)	-0.004(3)	-0.001(3)	0.016
R	0.006(2)	-0.004(2)	-0.001(2)	0.000(2)	0.014
I	0.005(2)	-0.002(2)	-0.000(2)	0.001(2)	0.013
LC 3-B	-0.013(8)	0.009(8)	0.014(8)	-0.021(8)	0.042
V	-0.019(5)	0.020(5)	-0.004(5)	0.005(5)	0.030
I	-0.017(5)	0.021(5)	-0.007(5)	-0.002(5)	0.031
LC 4-B	0.013(3)	-0.010(4)	0.005(4)	-0.003(3)	0.025
V	0.010(3)	-0.005(3)	-0.003(3)	-0.007(2)	0.020
I	0.003(3)	-0.003(3)	0.001(3)	-0.007(2)	0.020

Both the plots and the errors of the coefficients show that the sets LC 1 and LC 3 are too sparse and yield poor fits. LC 2 is a high quality light curve, and the resulting fits are better. LC 4 is the best of the three RAO light curves, and the resulting fits, particularly for the maxima and the whole light curve, prove it. Accordingly LC 2 will be chosen for modeling the system in a later chapter, while LC 4 will be used as an independent check.

The general shape of the light curve of two eclipsing stars may be represented by a function of the form  $a_2 \cos(2\theta)$  where  $a_2$  would be negative to account for the decrease in intensity at the primary minimum. This can be seen in Tables 2.7 and 2.8 as the value of  $a_2$  is more significant than those of any other term. But the shape of the light curve departs from that of a pure cosine. The term  $a_4$  introduces some of these distortions, as it affects the shape of the branches at each side of the minima. Table 2.6 shows how when fitting the minima  $a_4$  becomes dominant, with  $a_2$  second in order of importance.

Finally the odd cosine terms  $a_1$  and  $a_3$  represent the differences in shape and depth between the two minima with the reflection effect affecting  $a_1$  as well. Because of this, they are negligible in the fit to the maxima.

Due to its high quality, LC 2 is ideal to observe the proximity effect. The fit seen in Figure 2.12 closely follows the maxima and, as mentioned before, can be extended into the minima, where the smooth and continuous change can also be observed.

The coefficients in all three tables show the presence of changing asymmetries on the light curves, as the corresponding values vary significantly. Most of this change can be attributed to the change in O'Connell effect, which has already

been noted. The Fourier representation offers a way to quantify such change. We note also, that except for the  $a_0$  terms, the coefficients for the light curves LC 1 and 2 are not significantly different as is expected since they were observed at almost the same time, though by different instruments and observers. Another difference is the extent of time they cover. LC 2 was observed in three consecutive nights, while 20 days separate the first and last observations in LC 1.

The changing coefficients can be used to observe the changing O'Connell effect. In particular  $b_1$  is positive when  $max_I$  is brighter than  $max_{II}$ . In Table 2.7 we see it being negative in LC 3, and positive or close to zero for all the others.

The  $a_0$  coefficient is simply the average of all the points present in the light curve. Because of this, differences in  $a_0$  are mostly due to differences in coverage of the light curve. The RAO light curves have more points near the minima, while LC 2 is evenly spaced, resulting in significantly different averages.

Fourier series fitted to light curve data have been used in the past to remove some of the proximity effects, making it possible to solve the system with methods that apply to detached systems. We chose, however, not to modify the light curves. In Chapter 4 we discuss a model that attempts to deal with light curve anomalies such as those quantified here in a different way. We shall also use the  $a_2$  and  $a_4$  coefficient of the full light curve fit to test some of the results.

Next we examine the role of spectroscopic data in understanding the system.

## Chapter 3

### Spectroscopic Observations and Reduction

#### 3.1 Background

The radial velocity observations were obtained at the Dominion Astrophysical Observatory in Victoria by RAO observers during June 1985, August 1986 and April 1987. The observations were made with DAO's 1.82 m telescope and 21121 spectrograph. The latter provides a nominal reciprocal linear dispersion of 15 Å/mm. The sensing device is a reticon array that receives the light from the spectrograph after being amplified by an EMI single-stage image intensifier. The reticon can be "exposed" for an extended period of time to increase the photon count. Once the desired exposure time is reached, the image can be read into disk storage for later processing. Reference arc spectra from an Fe lamp are exposed before and after every star exposure. They are used later for wavelength calibration of the spectra.

Table 3.3 lists the spectra of TY Boo which were obtained at DAO. Typical exposure times for TY Boo were between 10 and 20 minutes depending on seeing and sky transparency. The exposure times cannot be greatly increased because the radial velocities of the components are changing during the exposure. The observations are thus phase-limited. This condition and the faintness of the system require the use of the image intensifier tube.

### 3.2 Spectral Type Determination

From the spectra obtained for radial velocity computation at DAO the spectral type could be determined by careful comparison with other reference spectra.

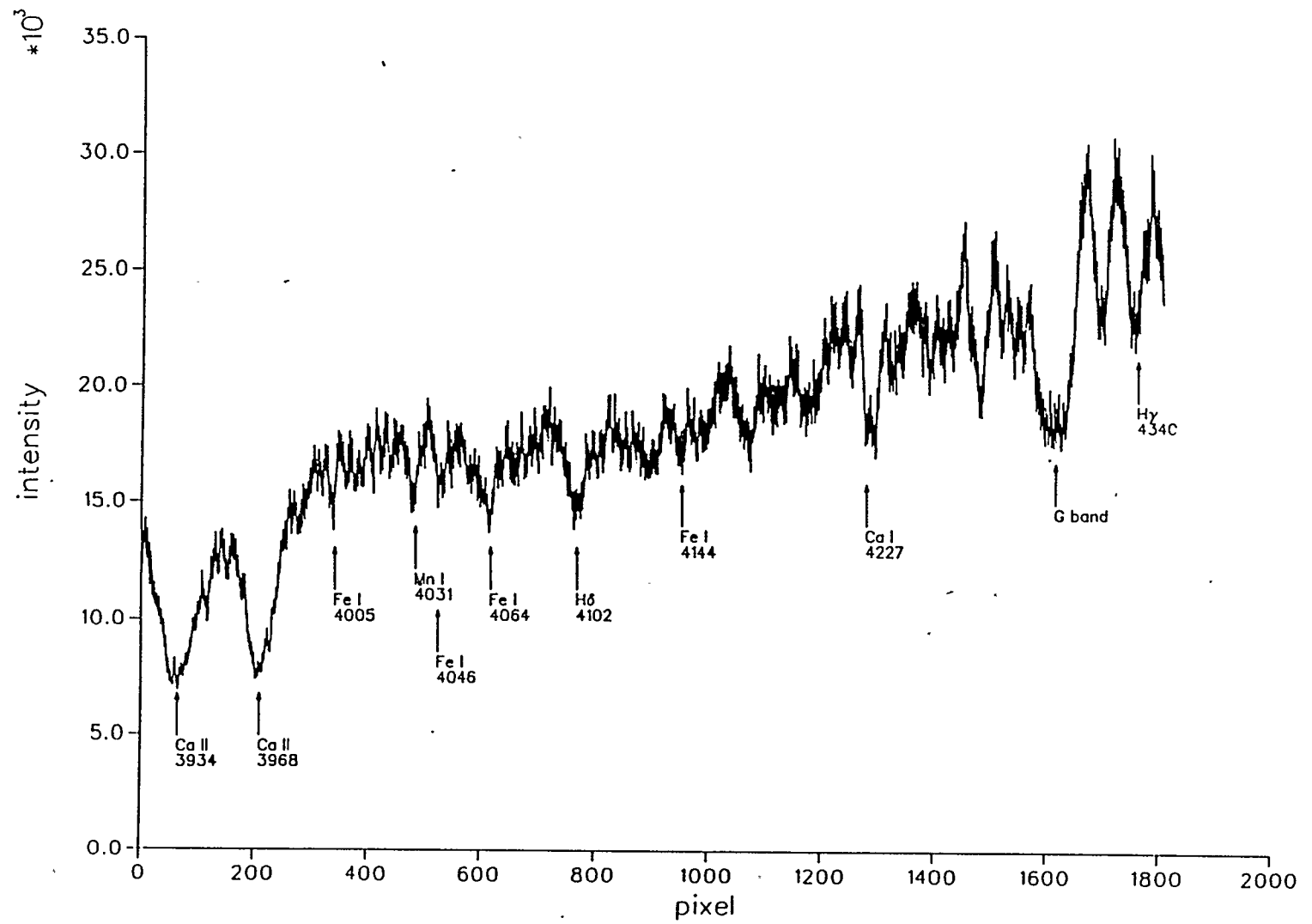
The most important features for classification purposes for early G spectra are indicated on the TY Boo spectrum in Figure 3.1 where the raw data have been plotted. The  $x$  axis represents the pixel number, with each pixel corresponding to a diode in the detector. The  $y$  axis is the intensity measured by each diode. Since the TY Boo spectrum is distorted, mostly by the use of the image tube, the lines cannot be identified by measuring their positions only, but rather by their relative positions compared to other lines in the spectrum. A determination can now be made by observing the most salient features of the spectrum.

The presence of the G band does confirm a spectral type near G. The principal source of standard star spectra which were used for comparison purposes was the Atlas of Representative Stellar Spectra (Yamasita et al. 1978). In the absence of anomalous effects, classification criteria for G systems involve the ratios of the depths of the line depths:

$$\text{Fe I } 4046 \text{ \AA}, 4144 \text{ \AA}, \text{Ca I } 4227 \text{ \AA} \quad \text{vs} \quad \text{H}\delta$$

However, when these criteria are applied to TY Boo, it is clear that the hydrogen lines are unreliable, probably due to emission infilling. This was noted to be the case also for RW Com (Milone, Wilson and Hrivnak 1987). According to Keenan and Mc Neil (1976) the following composition-independent criteria can be used to determine spectral types of G stars:

Figure 3.1: TY Boo Spectrum



Cr 4254 Å vs Fe 4250 Å

Cr 4254 Å vs Fe 4260 Å

Cr 4274 Å vs Fe 4272 Å

Spectra of TY Boo near primary and secondary minimum were then chosen. During primary minimum, star one would be partially eclipsed by star two, so that the spectrum of star two should dominate; the reverse situation should happen during secondary minimum. Previously published values for the spectra of the components of TY Boo were G3 and G7 (Carr 1972) so the stars HD 154417 (spectral type G3) and HD 144579 (spectral type G8) were chosen as comparisons.

Figure 3.2 shows portions of the spectrum of TY Boo near primary minimum. Following the above mentioned classification criteria we notice that the line of Cr 4254 Å has a depth equal to that of Fe 4250 Å and Fe 4260 Å. This is also seen in the spectrum of HD 144579 (G8) shown in Figure 3.3.

The spectrum of TY Boo near secondary minimum can be seen in Figure 3.4. In this spectrum the line of Cr 4254 Å is now fainter than the two neighboring Fe lines. This agrees with the spectrum of HD 154417 (G3) showed in Figure 3.5.

Blending of the lines Cr 4274 Å and 4272 Å in all of the spectra of TY Boo make it impossible to apply the last criterion, which might have helped to further confirm the classification. The determination of the system spectral type outside eclipse was similarly precluded by blending, particularly of the Fe 4260 Å line which lies next to a strong night sky emission feature. The blending made it impossible to determine the actual depth of the Fe line.

In conclusion star one in TY Boo seemed to be of spectral type G3 and star two

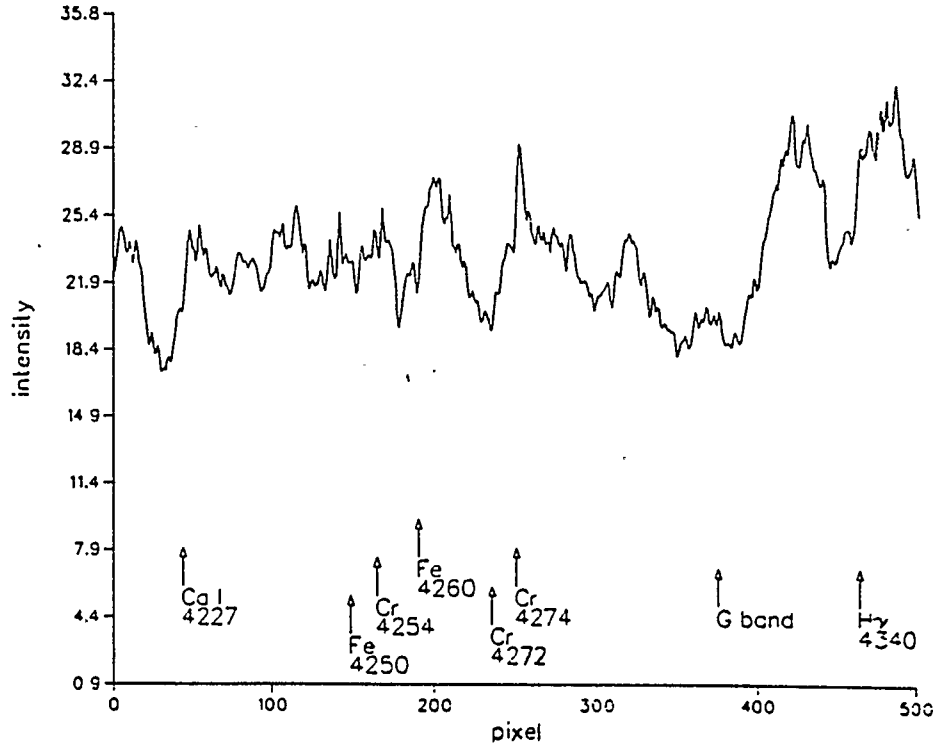


Figure 3.2: TY Boo spectrum, exposure No 0446, phase 0.06

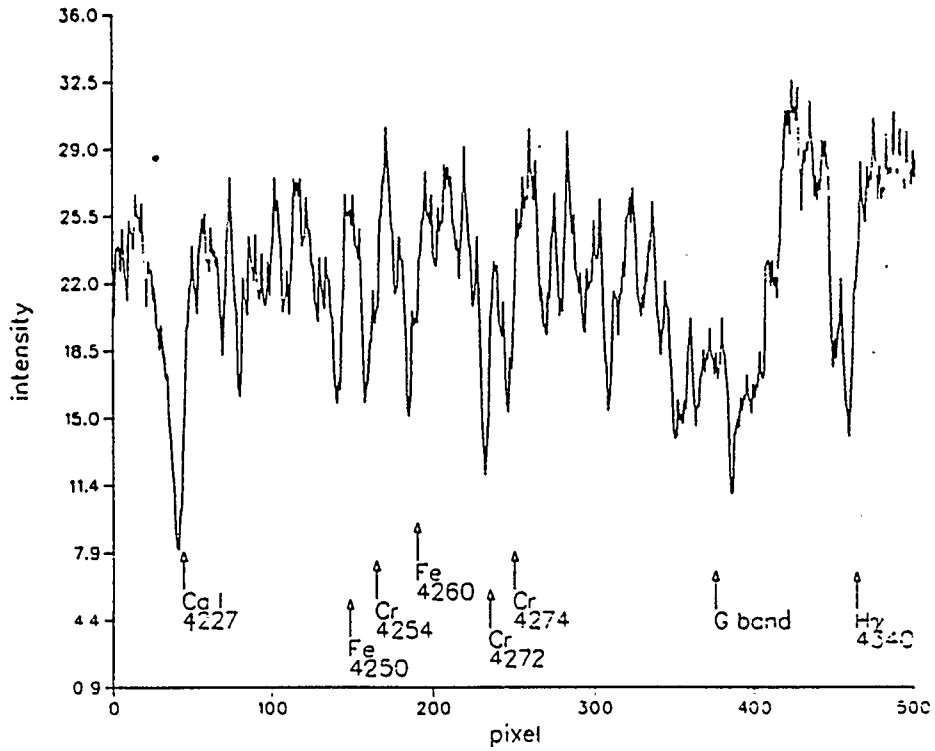


Figure 3.3: Comparison Spectrum HD144579 (G8)

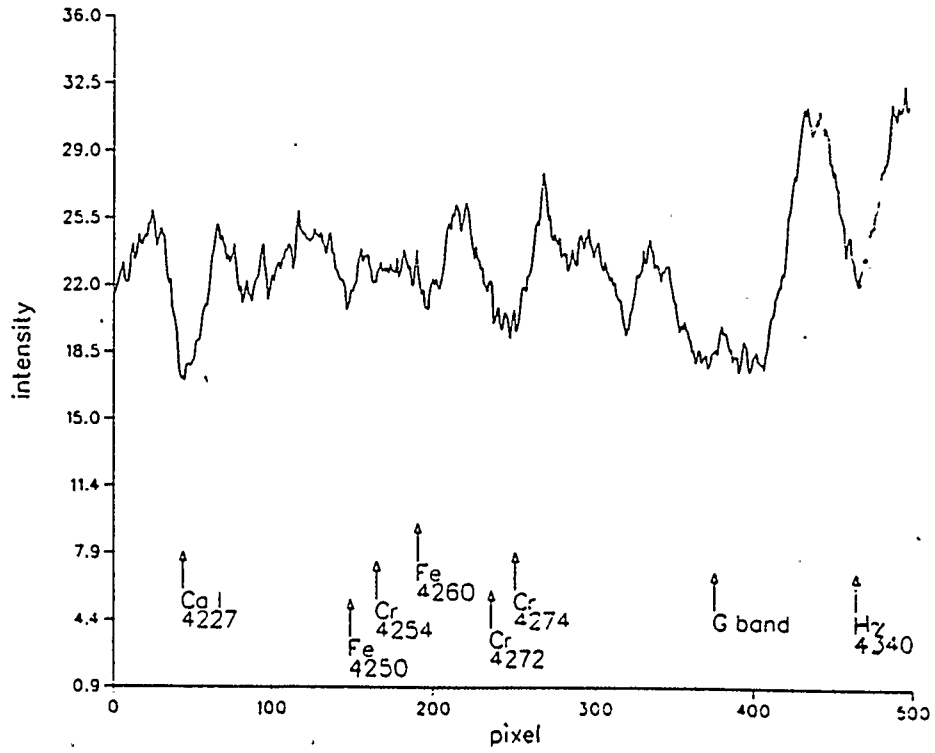


Figure 3.4: TY Boo spectrum, exposure No 0209, phase 0.49

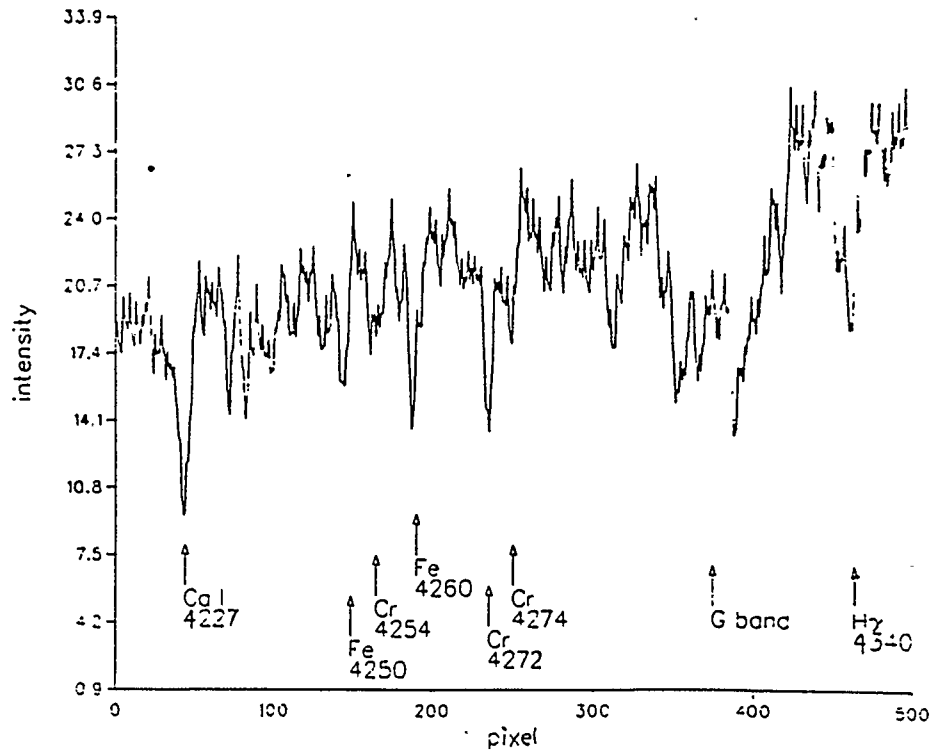


Figure 3.5: Comparison Spectrum HD154417 (G3)

of type G8, with an uncertainty of about 1/10 spectral type for each component.

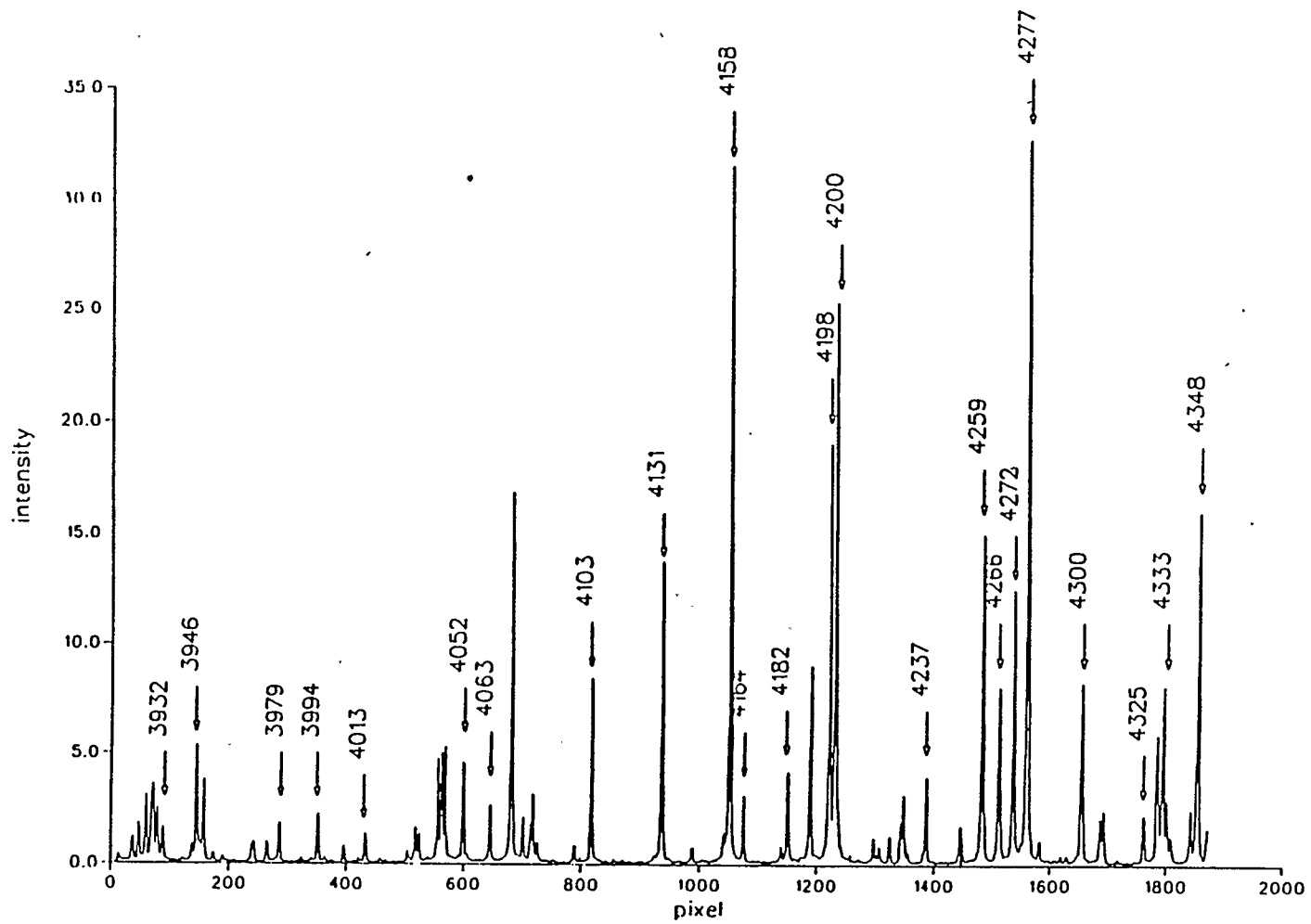
### 3.3 Data Reduction

The spectroscopic observations, in the form of digitized spectra, were reduced using DAO's REDUCTION and ANALYSE code (Hill 1982 and 1983) which cross-correlate the observed program star spectra with comparison star spectra in order to compute radial velocities. This technique will be discussed in more depth in Section 3.5.

The first package, REDUCTION, is used to calibrate the data through several steps. The first step involves reading in the arc files exposed before and after the image. The arc files are then scanned, and the positions of known lines are measured using cursor keys to move cross hairs on a graphics terminal. Figure 3.6 shows the most common lines used for calibration. These lines are usually singlets, a very desirable quality, since the program can run in an automatic mode in which it approximates the position of the line and then searches for it around this point. A multiplet would have several peaks in a small region of the spectra, making misidentification more likely.

The first line to be located is the fiducial line; usually the 4131 Å line of Fe. This line was identified and the corresponding reticon pixel number recorded during the observation run, since it lies near the center of the portion of the spectrum being observed. During reduction the user locates the lines, beginning with the fiducial line, and the program computes the centroid for each one of them. Figure 3.7 shows a sample screen in which both spectra are visible, in the region of the line

Figure 3.6: Fe arc Spectrum



being identified. The small arrow head above each spectrum indicates where the program estimates the position of the line.

Once a set of lines has been measured the program fits a polynomial function to the resulting wavelength vs position points, and computes the residuals. In this way wavelength nonlinearities in the star spectrum can be treated. Nonlinearity is expected mainly because the image intensifier produces an S-shaped distortion. The star file is then read in together with the coefficients from the  $O - C$  arc fit and linearized in wavelength.

The next step consists in measuring the continuum of the spectrum of the star, in order to normalize the spectrum. The normalization is necessary since the program will measure correlations between the features of the target spectrum and those of the comparison star, and any continuum fluctuations would be interpreted as very wide lines, contaminating the results. The continuum fluctuations are due to free-free and bound-free continuum opacities in the stars' atmospheres as well as varying effects of the earth atmosphere. The normalization is accomplished by placing the cross hairs on points along the spectrum. The program then reads in these points and fits a spline curve through them. The result is displayed on the screen and is shown in Figure 3.8. This function is then subtracted from the spectrum. The result is a more or less flat spectrum.

Finally the  $\lambda$  abscissa is converted to  $\ln \lambda$ , since the Doppler shift is linear in  $\ln \lambda$ , rather than  $\lambda$  itself. The file is then ready for cross correlation. The cross-correlation technique is the preferred one for treating W UMa systems because of the strongly blended lines in their spectra. The cross-correlation technique

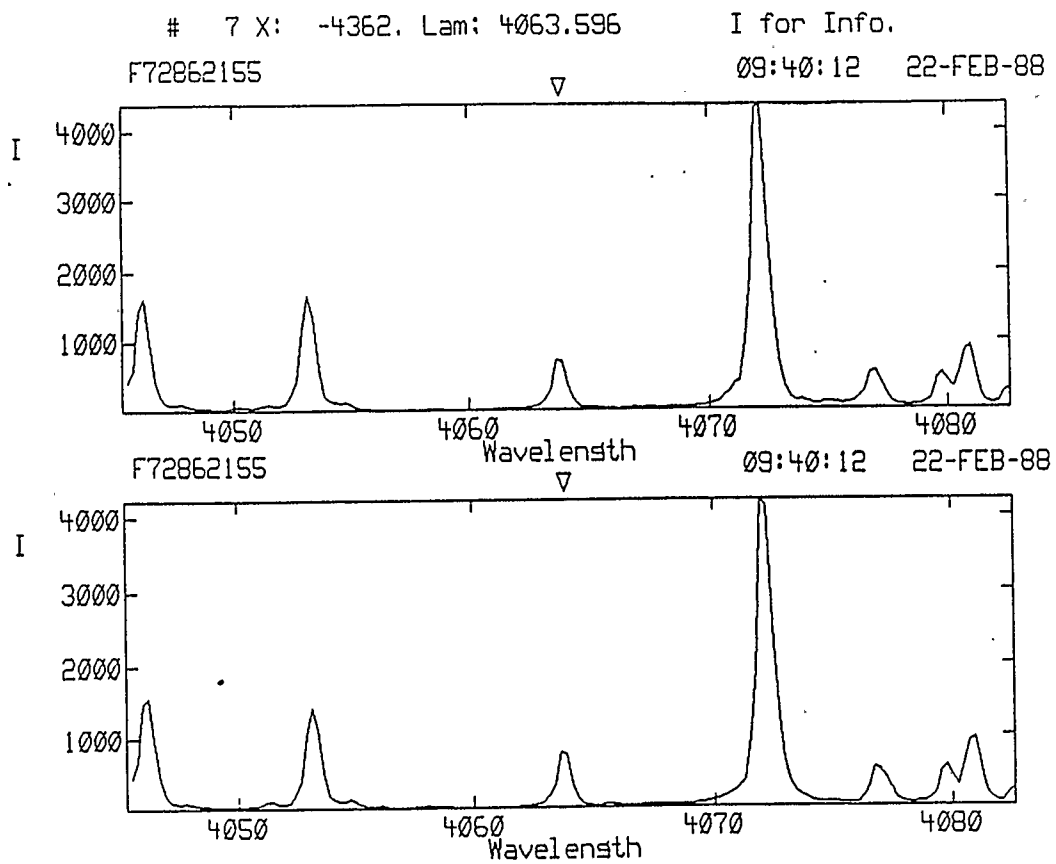


Figure 3.7: Arc line determination

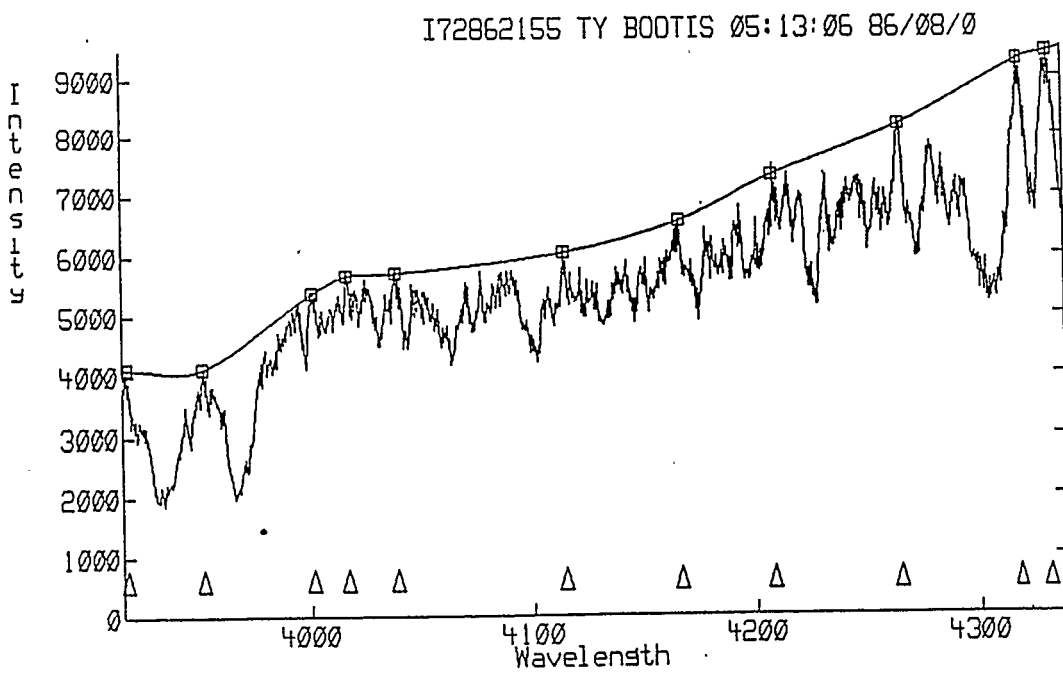


Figure 3.8: TY Boo spectrum with continuum fit

requires velocity standard stars, with which the program star is correlated. The main comparison stars for TY Boo were HD 144579, HD 181096 and HD 154417; the velocity standard HD 136202 was also used for a sub-set of the data. They were chosen from the list of radial velocity standards (Astronomical Almanac 1985) and are similar in spectral type to the variable star.

To cross correlate the data the program VCROSS (Hill 1983) was used. The program reads in both the program star and comparison star files. Selected spectral regions may be excluded from the cross-correlations. This yields a cleaner correlation, since only the sharper features are considered. Here the strong Ca II H and K lines, Balmer lines and the principle night sky lines have been excluded.

Once computed, the cross correlation is displayed on the screen, as seen in Figure 3.9.

The curve shows the two peaks corresponding to the Doppler shifted spectra of each star in TY Boo correlated with the comparison. The centroids of these peaks are taken as the radial velocities of each component with respect to the comparison.

The centroids can be found by having the program fit a Gaussian through each peak. The results, with corresponding errors, are reported directly in velocity units as can be seen on the top part of figure 3.9.

Since this is actually the velocity of each component with respect to the comparison star, the latter velocity must now be added.

Program \* U72862221 TY BOOTIS 05:17:57 86/08/0  
 Comp \* U72862151 HD144579 04:56:49 86/08/08 RV 0.00 k/s

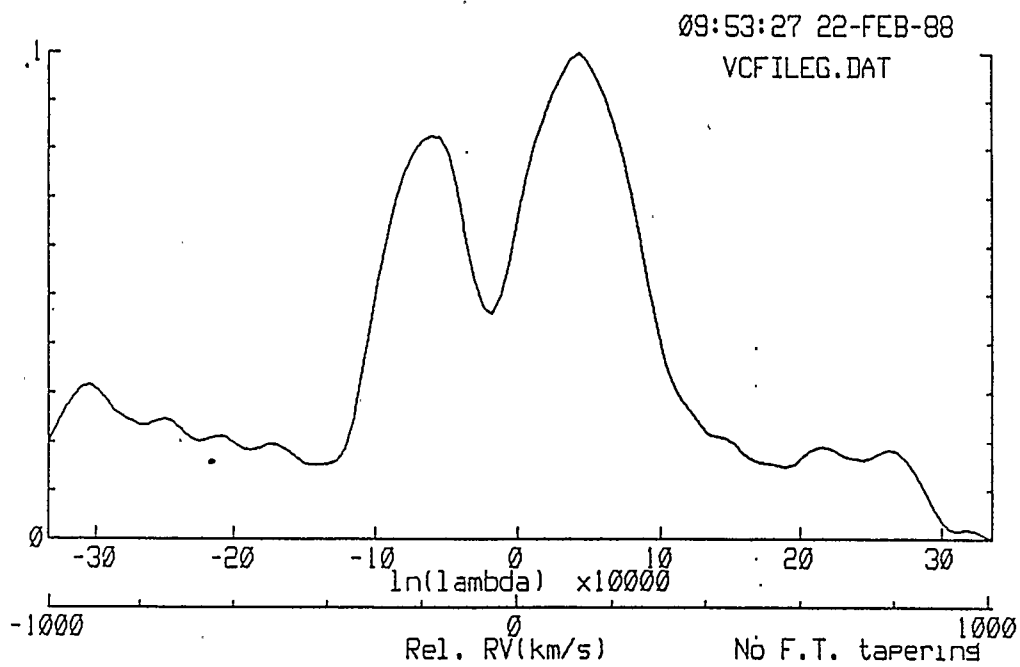


Figure 3.9: Cross-Correlation Curve

### 3.4 Radial Velocity of Comparison Stars

Unfortunately the published values for the radial velocities of each of the standards differ for various reasons. Table 3.1 lists the published values for the comparison star velocities.

To resolve the problem, cross-correlations were performed among these stars. Each resulting correlation curve had a single peak indicating that these were not binary stars, and placed at the difference between the velocities of the two correlated stars. When all possible combinations were computed there were three differences, corresponding to three independent equations, in which the three individual velocities could be taken as unknowns. Taking  $v_1$  as the velocity of HD 144579,  $v_2$  as that of HD 154417 and  $v_3$  as that of HD 181096 the equations are:

$$-v_1 + v_2 = 45.28 \text{ km/sec}$$

$$-v_1 + v_3 = 13.96 \text{ km/sec}$$

$$-v_2 + v_3 = -30.70 \text{ km/sec}$$

These equations, however, were not enough to solve for new values of the radial velocities. The situation is illustrated by Figure 3.10, where the radial velocities of the three stars are represented by three corresponding vectors. The results of the cross-correlations are the vector differences of the radial velocities of the cross-correlated stars, also illustrated in the same figure. It can be seen that these vectors have no information at all of the actual radial velocities being studied, but only of their differences; hence more data are needed.

Using the average of the published values as starting guesses new values were numerically computed. These values, when used in the above mentioned equations,

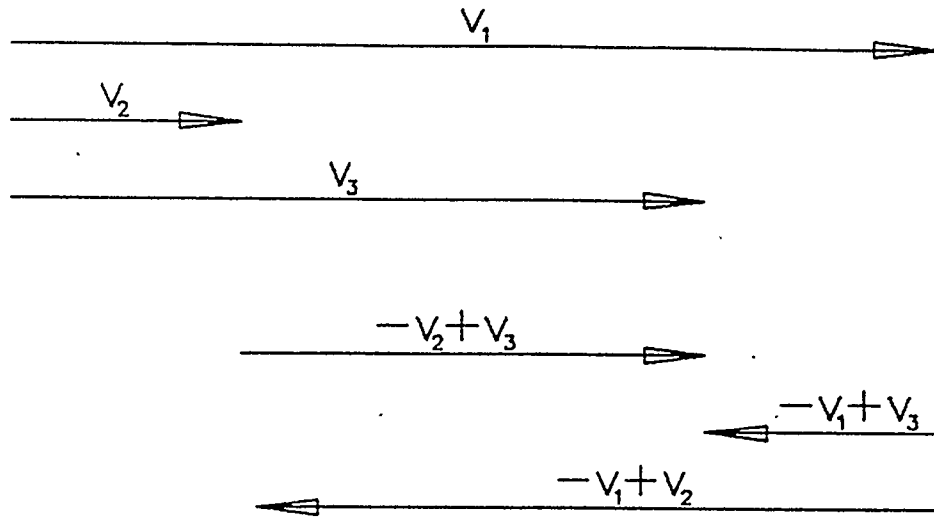


Figure 3.10: Vector diagram of cross-correlation results and their differences would yield the minimum possible differences with respect to the cross-correlation results, and would also minimize the differences with the published values themselves.

These were then the values used for the radial velocities of the comparison stars. The resulting radial velocities for TY Boo are listed in the appendix.

### 3.5 The Cross-Correlation Technique

Cross-correlation is a way of measuring Doppler shifts in digitized spectra. Simkin (1974) outlined this method and essentially introduced it to the astronomy community.

The cross correlation technique uses all available information on the recorded

Table 3.1: Comparison Stars Radial Velocities

HD	vel (km/sec)	obs	reference
144579	-60.0	3	Adams and Kohlschuter (1914)
	-59.6	3	Adams and Joy (1923)
	-60.8	2	Harper (1934)
	-59.2	11	Wilson and Joy (1950)
	-59.5	4	Boulon (1956)
	-55.1	8	Petrie et al. (1957)
	-56.9	6	Rebeiro (1965)
	-55.8	2	Ambert (1967)
	mean	-58.4 ± 2.1	
154417	-14.8	2	Harper and Ambert (1921)
	-18.6	7	Adams and Joy (1923)
	-18.0	3	Shajn and Albirtzky (1932)
	-20.1	3	Harper (1934)
	-17.3	1	Plaskett et al. (1948)
	-15.3	2	Evans (1963)
	-16.1	2	Evans (1963)
	-19.1	3	Ambert (1967)
mean	-17.4 ± 1.9		
181096	-45.0	6	Plaskett et al. (1921)
	-44.6	4	Adams et al. (1923)
mean	-44.8 ± 0.2		

Table 3.2: Computed Comparison Stars Radial Velocities

star	vel (km/sec)
HD 144579	-59.7 (2)
HD 154417	-14.7 (2)
HD 181096	-45.6 (2)

spectrum to measure the shift. It uses two spectra and compares both of them at different shifts, measuring at every point how “similar” the spectra are. This will give a peak when the shift matches the Doppler shift of the spectra.

We can then see that for a spectrum to be studied, it must have a fairly well determined spectral type, and one must be able to “generate” this spectrum from a known “prototype” spectrum by Doppler shifting it. The “prototype” is the undistorted star spectrum, while the observed one has been Doppler shifted.

If we call the relative velocity of the shifted spectrum to the prototype  $v$ , the resulting shift in lambda is not linear, but given by:

$$\lambda'/\lambda = \sqrt{\frac{1 + (v/c)}{1 - (v/c)}}$$

where  $(v/c)$  is the ratio of the relative velocity of the star to the speed of light,  $\lambda$  is the wavelength of a line in the unshifted spectrum and  $\lambda'$  the corresponding wavelength in the shifted spectrum. If we now define  $x = \ln(\lambda)$  then we can have the same difference expressed in the form

$$x' - x = \ln(\lambda'/\lambda) = \frac{1}{2} \ln \left( \frac{1 + (v/c)}{1 - (v/c)} \right)$$

Both spectra to be used in the cross-correlations must be in digital form, both must be calibrated in wavelength and be converted to normalized intensity. The spectra should ideally be of similar spectral type, be taken with the same instrument, and cover cover similar wavelength regions for the correlation to yield the sharpest results. Also any contamination from the sky, whether emission lines or continuum, must be masked out. All spectra must be stored in arrays which have

equal intervals in  $\ln \lambda$ , so that the  $\lambda$  corresponding to any cell in one array is equal to the corresponding  $\lambda$  in the other. This may require interpolating the original values.

We can now define the cross-correlation function as:

$$C(z) = a \int_{-\infty}^{+\infty} T(x)G(x+z)dx$$

Here  $T$  is the function describing the spectrum of the standard, and  $G$  that of the spectrum to be measured. This function will have a maximum at the shift  $z = z_0$ . In the case of stars,  $z_0$  is related to the Doppler shift of the spectrum  $G$  with respect to  $T$ . In this definition  $a$  is a scaling factor equal to the square root of the product of the mean square values of  $G$  and  $T$ , when the means of  $G$  and  $T$  have been set to zero by subtracting the average value of the spectral data from every data value.

For observational data, the continuous functions  $G(x)$  and  $T(x)$  become discrete points  $G(x_i)$  and  $T(x_i)$  in arrays of size  $N$  and  $K$  and sampled at equal intervals  $\Delta x$ . This is usually done by the detector, such as a Reticon array, or can be done afterwards by digitizing other type of data such as photographic plates on a densitometer. In the case of the Reticon the sampling is a function of both the spacing between diodes and the dispersion of the spectrograph. The length of the arrays is just the number of diodes in the array.

The cross correlation function  $C(z)$  becomes a set of unbiased cross correlation coefficients, also referred to as a c.c.f..

For a lag (or shift)  $z_L = \Delta x(L - 1)$  the coefficients are defined as

$$C_j(z_L) = \frac{a}{j} \sum_{i=1}^J T(x_i) G(x_i + z_L)$$

For small sets of data this equation can be readily evaluated by the computer. However when the data set is large (more than 1000 points when measuring shifts of about 2% of the data set) it is more efficient to calculate  $C_J(z_L)$  indirectly by using the Fast Fourier Transform (FFT) algorithm.

This introduces some complications, however, due to the fact that the spectral segments become periodic functions when they are expressed in terms of a finite Fourier series. For example a straightforward calculation of a continuous c.c.f. from the definition of  $C(z)$  by means of the Fourier transform gives

$$C(z) = a \int_{-\infty}^{+\infty} g(f) t(-f) e^{+2\pi i f z} df$$

where  $f$  is the transform variable,  $t$  and  $g$  are the Fourier transforms of  $T$  and  $G$ , and  $t(-f)$  is the conjugate transform of  $T(x)$ . Once again this can be expressed in terms of digitized data in the form

$$C(z_L) = a N^{-2} \sum_{j=1}^N g(f_j) t(-x_j) e^{+2\pi i f_j z_L}$$

where  $f_j = (j-1)/(N\Delta x)$ . However the coefficients from this expression are not the same as those from the non-periodic definition of  $C(z)$ , because now the entire periodic spectrum is included in the sum, and the last  $L$  terms of one spectrum will enter the cross correlation sum as products with the first  $L$  terms of the other. This is called aliasing and can introduce significant error into the measurement of  $z_0$  when it exceeds 10 or 20% of the array length.

The usual method for removing this overlap distortion is to set the mean of each data array to zero and then expand the arrays to twice their length by adding  $N$  terms of zero values. This however does not have to be done for small lag values. In this case it is sufficient to extend the array by the amount  $2z_0$  by adding enough zero terms.

To obtain the transformed arrays  $t$  and  $g$  one can use the FFT algorithm. There are lots of routines that can perform this fast transformation. The FFT takes advantage of the symmetries in the nested sums involved in the Fourier transform algorithm to save time.

Once the peak of the c.c.f. is found, the lag  $z_0$  can be transformed back into units of  $\lambda$  and hence velocity.

The implementation of the cross-correlation technique used in this study is that of Hill (1982) at the Dominion Astrophysical Observatory.

### 3.6 TY Boo Radial Velocities

The program VCROSS (Hill 1982) used to perform the cross-correlations between variable star and the comparison star spectra displays the c.c.f. on the graphics screen and allows the user to chose a region about the peak or peaks to be fitted. The fitting function can be either a simple parabola, a Gaussian or a Lorentzian. In the present work, Gaussian functions were selected because they appeared to fit the obtained c.c.f. best.

VCROSS reports the result of the fit in km/sec including the corresponding errors. The results for TY Boo are shown in Table 3.3 and graphed in Figure 3.11.

Table 3.3: Radial Velocities for TY Boo.

File	JD	Phase	Corr.	Comparison	$U$	$\sigma_u$	$V$	$\sigma_v$
name	+46000		to Sun	Star				
72862155	650.7203	0.1384	-18.34	HD 144579	37.7	1.4	-217.5	1.5
72862157	650.7321	0.1756	-18.35	HD 144579	62.0	2.6	-233.9	3.1
72862221	651.7223	0.2978	-18.25	HD 144579	68.9	5.8	-264.2	3.4
72862223	651.7320	0.3284	-18.26	HD 144579	65.1	1.3	-255.2	1.3
72862225	651.7411	0.3571	-18.26	HD 144579	59.5	2.7	-261.8	2.8
72862227	651.7515	0.3899	-18.27	HD 144579	43.6	1.4	-225.7	1.4
72862155	650.7203	0.1384	-18.34	HD 154417	49.9	1.5	-217.9	1.5
72862157	650.7321	0.1756	-18.35	HD 154417	73.4	4.3	-239.5	2.1
72862219	651.7119	0.2650	-18.24	HD 154417	67.8	4.1	-283.5	3.2
72862221	651.7223	0.2978	-18.25	HD 154417	70.2	4.9	-265.4	3.8
72862223	651.7320	0.3284	-18.26	HD 154417	63.5	2.4	-261.4	2.9
72862225	651.7411	0.3571	-18.26	HD 154417	61.4	3.5	-261.8	3.6
72862227	651.7515	0.3899	-18.27	HD 154417	47.8	2.1	-219.5	2.8
7287131	902.8316	0.0761	0.62	HD 144579	31.5	5.2	-175.6	6.0
7287137	902.9211	0.3583	0.45	HD 144579	54.9	3.3	-235.5	4.7
7287139	902.9454	0.4349	0.41	HD 144579	6.4	4.1	-194.5	4.0
7287131	902.8316	0.0761	0.62	HD 154417	55.2	11.4	-145.8	13.7
7287137	902.9211	0.3583	0.45	HD 154417	58.5	4.3	-238.2	6.2
7287139	902.9454	0.4349	0.41	HD 154417	21.8	4.8	-200.0	10.5
0209	232.8569	0.5642	-16.24	HD 136202	-113.4	8.8	43.9	5.8
0211	232.8743	0.6190	-16.26	HD 136202	-123.3	8.3	106.7	7.2
0213	232.8903	0.6695	-16.28	HD 136202	-117.1	4.5	156.5	4.8
0215	232.9042	0.7133	-16.29	HD 136202	-134.2	7.4	167.6	8.3
0217	232.9208	0.7657	-16.30	HD 136202	-137.5	5.8	186.4	5.2
0349	233.8979	0.8466	-16.46	HD 136202	-120.4	7.3	164.8	5.9
0352	233.9242	0.9295	-16.48	HD 136202	-53.6	14.1	106.9	8.5
0446	234.9172	0.0605	-16.64	HD 136202	20.4	13.5	-143.9	23.0
0448	234.9367	0.1220	-16.66	HD 136202	31.3	8.0	-185.1	15.8
0209	232.8569	0.5642	-16.24	HD 114762	-111.3	12.3	51.3	8.8
0211	232.8743	0.6190	-16.26	HD 114762	-121.6	6.5	117.5	6.8
0213	232.8903	0.6695	-16.28	HD 114762	-129.0	4.2	153.8	4.6
0215	232.9042	0.7133	-16.29	HD 114762	-140.7	4.6	185.3	5.0
0217	232.9208	0.7657	-16.30	HD 114762	-143.8	5.1	189.1	4.7
0349	233.8979	0.8466	-16.46	HD 114762	-135.6	6.7	170.3	6.2
0352	233.9242	0.9295	-16.48	HD 114762	-81.5	9.2	113.2	10.4
0446	234.9172	0.0605	-16.64	HD 114762	34.3	27.1	-120.3	46.0
0448	234.9367	0.1220	-16.66	HD 114762	32.3	9.7	-185.3	16.0

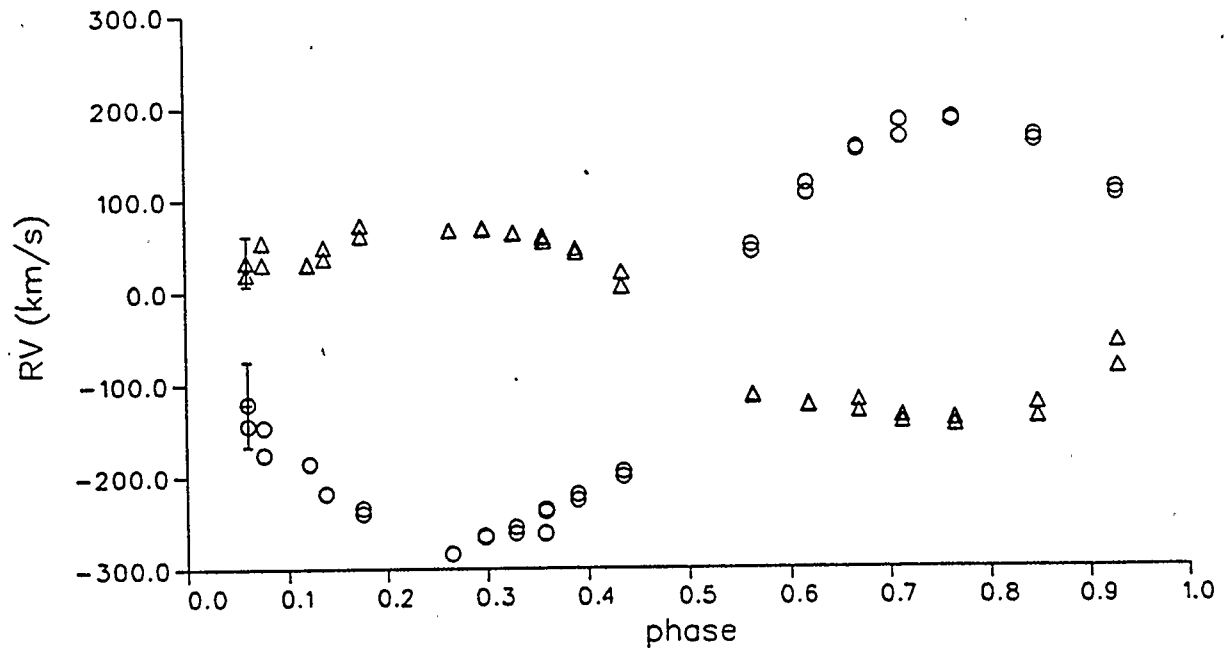


Figure 3.11: TY Boo Radial Velocity Curves

The radial velocity of a star in a circular orbit is given by the expression

$$V_r = \gamma + v_{or} \sin(\phi) \sin(i)$$

where  $v_{or}$  is the orbiting velocity,  $\gamma$  the radial velocity of the system's center of mass,  $\phi$  the angular phase and  $i$  the inclination of the orbital plane to the plane of the sky. We take  $\phi$  to be zero at primary minimum. Notice that for the secondary component the sign of  $V_r$  will be reversed, since it always moves in the opposite direction of the primary, receding after primary minimum, and approaching the observer after secondary minimum.

By using the transformation  $y = V_r$  and  $x = \sin(\phi)$  we reduce the expression to a linear relation in  $\sin(\phi)$  where the slope is given by  $v_{or} \sin(i)$  and the y-intercept by  $\gamma$ . Figure 3.12 shows the plot of the radial velocity of each component.

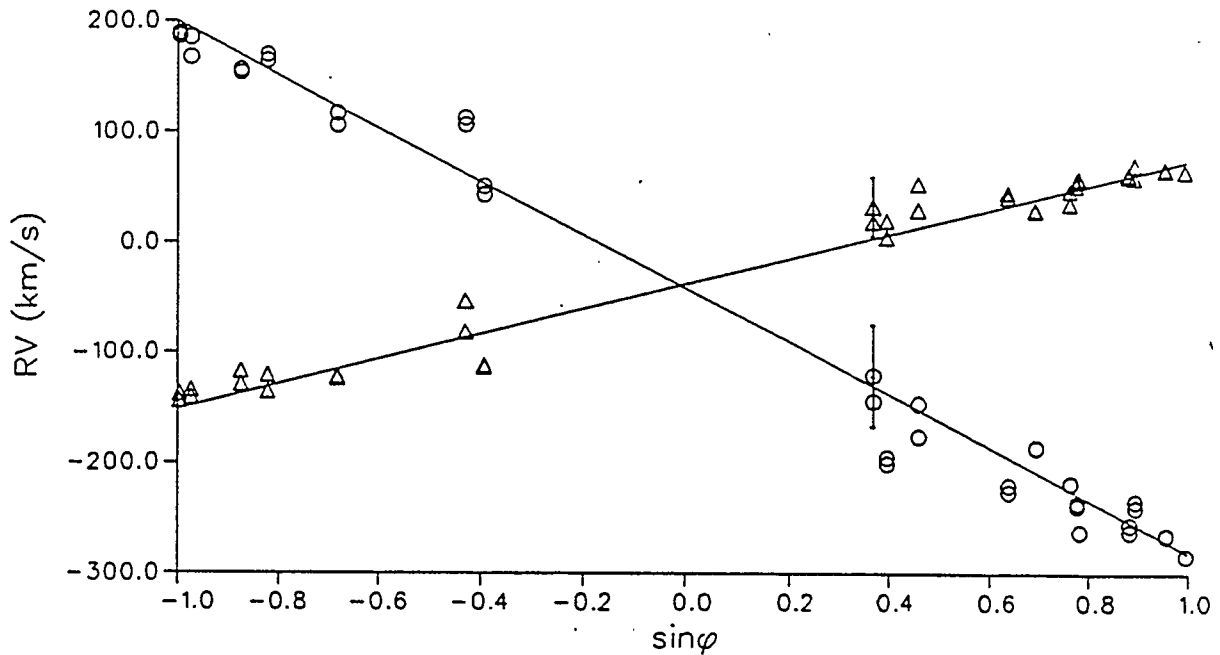


Figure 3.12:  $u$  and  $v$  vs  $\sin(\phi)$  and best fits.

The y-intercept is equal to the  $\gamma$  velocity of the system. Assuming a value for  $i$ , we compute the distances of the centers of the stars to the center of mass,  $r_1$  and  $r_2$  using

$$r_{1,2} = \frac{v_{or(1,2)}p}{2\pi}$$

where  $p$  is the period. This expression is valid only for a circular orbit, which is usually the case in W UMa systems. As for TY Boo, it was shown in Chapter 2 that the secondary minimum occurs at 0.5 in phase units and that the durations of both eclipses are approximately the same, supporting the case that the orbit of TY Boo is circular.

The mass ratio,  $q$ , and the velocity of the system,  $\gamma$ , were computed using the Wilson method (Wilson 1941). Following Wilson's notation we use  $u$  to denote

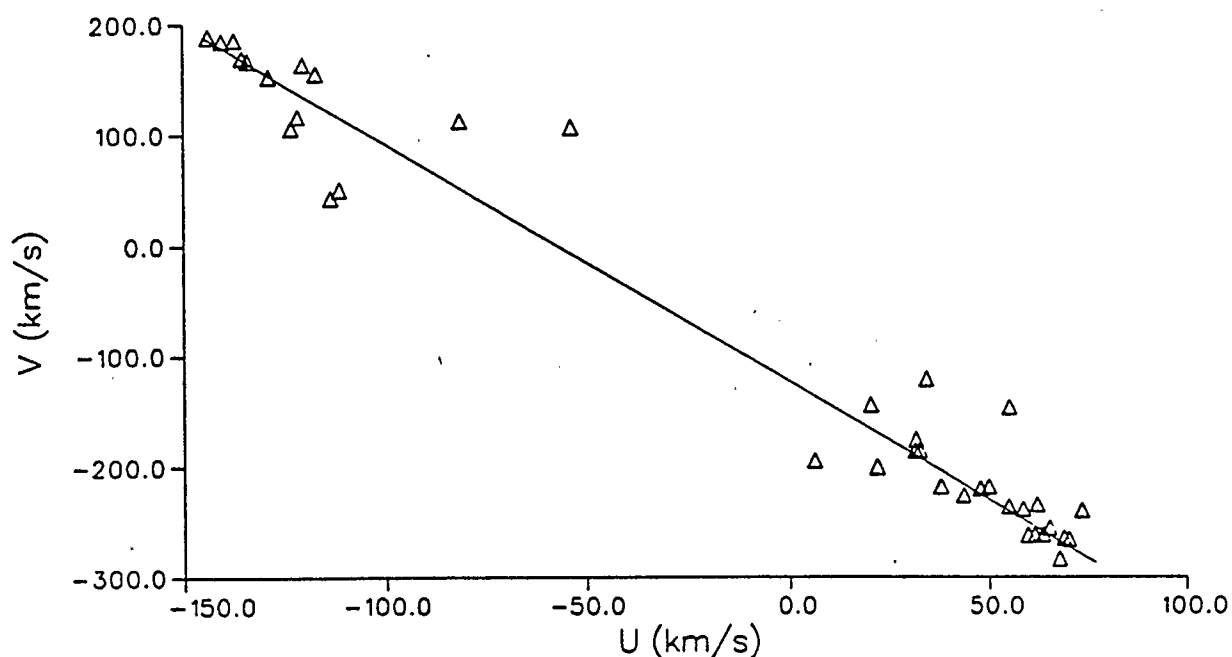


Figure 3.13:  $v$  vs  $u$  plot of TY Boo Radial Velocities

the radial velocity of the more massive star. Since this component is closer to the center of mass of the system, its velocity will have the smaller amplitude. The letter  $v$  is used for the less massive component. These two parameters are related by the expression

$$q = \frac{v - \gamma}{\gamma - u}$$

If  $v$  is plotted against  $u$  the resulting graph should be that of a straight line. Its slope would be the negative of the mass ratio  $q$ , defined as  $m_u/m_v$ , and the point where it intersects the  $x$  axis would be  $\gamma(1 + s)$  where  $s$  is the slope of the line.

Figure 3.13 shows the plot of  $v$  vs  $u$ , with the data points and the fit line. This line is found by performing a least squares fit on the  $n$  data points.

The resulting values are:

$$q = 2.08(7)$$

$$\gamma = -37(2) \text{ km/sec}$$

The quantities  $u$  and  $v$  can be computed from the product of the distance  $r$  and the angular velocity (given by the period). The mass ratio  $q$  is determined directly from  $m_u/m_v$ . The quantity  $a$  (the distance between the centers of the stars) is simply given by the sum  $r_u + r_v$ .

To estimate the goodness of the fit the linear correlation coefficient ( $R$ ) was also computed. The closer it is to 1, the better the fit. Table 3.4 shows the results of this method compared to those obtained by Wilson's method. The inclination was assumed to be  $75.0^\circ$  (Bradstreet private communication 1988). Even though this value would be improved upon later, a small change in  $i$  translates into an even smaller error in  $\sin(i)$  when  $i$  is close to  $90.0^\circ$ . The present method value for  $\gamma$  is an average of two separate values which agree within their standard errors. It can be seen that both  $\gamma$  and  $q$  agree between the two methods within errors. The present method produces additional results, in particular it provides  $a$  (or more generally  $a \sin(i)$ ), which is a needed parameter for the Wilson-Devinney program.

The radial velocity curves confirm TY Boo to be a W-type W UMa system. In these systems the cooler and more massive star is closer to the observer during primary minimum.

Table 3.4: Photometric elements.

	Wilson method	Present method
$U$	-	$117.2 \pm 2.0$ km/sec
$V$	-	$250.8 \pm 2.8$ km/sec
$\gamma$	$-37.0 \pm 2.0$ km/sec	$-37.5 \pm 5.1$ km/sec
$q$	$2.08 \pm 0.07$	$2.140 \pm 0.04$
$r_u$	-	$5.10 \times 10^5$ km
$R_u$	-	0.977
$r_v$	-	$1.10 \times 10^6$ km
$R_v$	-	0.926
$a$	-	$2.302 R_\odot$

## Chapter 4

### Light Curve and Radial Velocity Curve Analysis

With the availability of a set of initial values for the elements, modeling of the system could begin. The Wilson-Devinney code (Wilson and Devinney (1971)) would be used, running on the University of Calgary's Cyber 205 Super Computer. This program can operate in two basic modes: LC and DC. Operation of the program is also discussed at length by Leung (1977). LC stands for Light Curve, since in this mode the program computes synthetic light curves from the input parameters. DC stands for Differential Corrections, and here the program computes corrections to the desired parameters, for their adjustment.

#### 4.1 Light Curve Synthesis

The LC mode was used first. Here the values for the elements of the binary system are entered as input, and the program generates the corresponding synthetic light curve. The program uses the input parameters to create a model of the system. It then places a grid on the surfaces of the stars. Every cell in the grid is later scanned and, depending on the phase and position, it is found whether or not the cell is visible to the observer. If it is visible, the contribution to both the light and radial velocity curves is computed. All contributions from visible cells are added, to create the final output. By comparing the resulting light and/or velocity curves to the observed ones the elements can be fine tuned until a close match is

Table 4.1: Synthetic Light Curve Parameters.

Parameter	Description
$i$	inclination of the orbit
$L_1, L_2$	monochromatic luminosities of the two components
$x_1, x_2$	limb-darkening coefficients
$g_1, g_2$	gravity darkening exponents
$T_1, T_2$	surface temperatures
$q$	mass ratio defined as $m_2/m_1$
$\Omega_1, \Omega_2$	surface potentials

obtained. Preliminary values of the mass ratio, distance and orbit inclination had already been determined with relatively good accuracy, as described in the previous chapter. The initial temperatures were based on the spectral classifications done earlier. The scale of Popper (1980) was used. The LC mode allows adjustment of the potential of the surface of the stars ( $\Omega$ ), and this determines whether or not TY Boo is actually a contact system.

In order to study a binary system a set of parameters must be found to uniquely define such a system. The usual parameters are listed in Table 4.1.

For all these parameters the subscript “1” refers to the primary component, that is the star being eclipsed during the primary minimum. The orbital inclination is measured with respect to the plane of the sky. A system with an inclination of  $90.0^\circ$  lies in a plane which includes the line of sight of the observer. The luminosities are normalized so that their sum at maximum light equals one.

## 4.2 Roche Model

The geometry of the equipotential surface due to two corotating stars was studied by Kopal (1959) among others and is called the Roche potential, after the French mathematician Edouard Albert Roche. This model gives an analytical solution to the three dimensional shape of the equipotential surface by making certain assumptions about the system. First the two stars are taken to be in a circular orbit, secondly their rates of rotation are taken to be synchronous with the orbital motion, and, finally, the mass of the stars is assumed to be highly concentrated at the center. In practice, and when dealing with contact systems, these assumptions turn out to be very reasonable (Kopal 1978). In any type of contact system the interaction between the two stars usually makes the orbits circular, and the rotations synchronous.

If we now consider the two body system as a gravitational dipole, we can express the angular velocity of rotation  $\omega$  by using Kepler's laws for the circular case, where  $G$  is the gravitational constant.

$$\omega^2 = \frac{G(m_1 + m_2)}{R^3}$$

The potential at any point  $p$  can be found by first placing a coordinate system with the  $x$  axis on the line that joins the centers of the stars and origin on mass  $m_1$ . If  $R$  is the distance between the stars and  $x$  and  $y$  are the coordinates of point  $p$ , the potential is given by Kopal (1978)

$$\psi(p) = G\frac{m_1}{r_1} + G\frac{m_2}{r_2} + \frac{\omega^2}{2} \left\{ \left( x - \frac{m_2 R}{m_1 + m_2} \right)^2 + y^2 \right\}$$

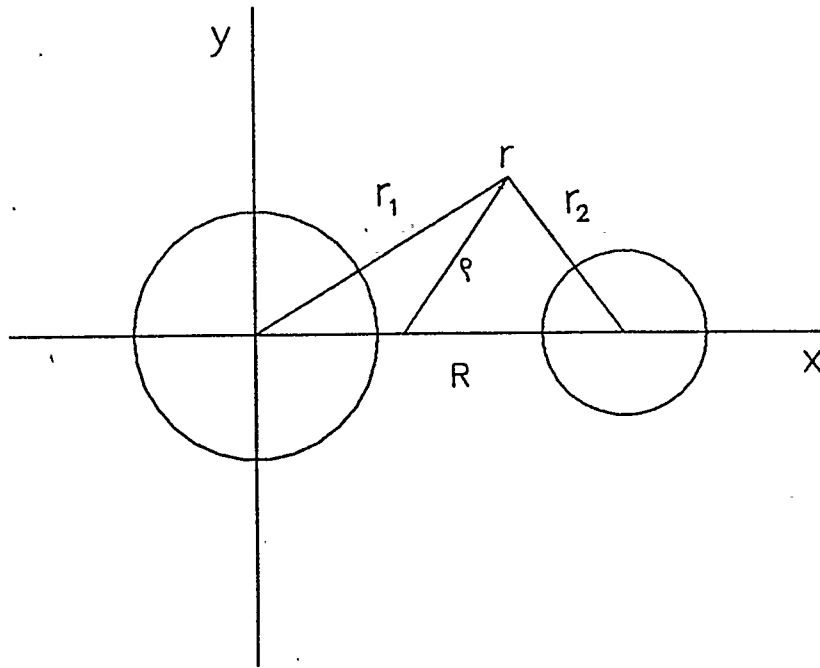


Figure 4.1: Coordinate system for Roche lobe computation

This expression can be rewritten in the form

$$\psi(r, q) = \frac{2}{(1+q)} \frac{1}{r_1} + \frac{2q}{(1+q)} \frac{1}{r_2} + \rho^2 = C$$

In these expressions  $q$  is the mass ratio,  $r_1$  and  $r_2$  are the distances of a point  $r$  to the centers of both stars, and  $\rho$  is the perpendicular distance from this point to the axis of rotation, as indicated in Figure 4.1. The unit of this potential is given by  $G(m_1 + m_2)/2R$  where  $R$  is the distance between the stars.

There are two useful ways of representing this type of potential, and both show the values on a plane that cuts the three dimensional potential. One consists in using a three dimensional surface plot, where  $x$  and  $y$  represent the actual coordinates in space, but  $z$  is the strength of the potential  $\psi(x, y)$ . Such representation is seen in Figure 4.2. The second method uses a contour plot to represent the

position of lines of equal potential on the chosen plane. This can be seen in Figure 4.3. Both these plots were made for a mass ratio of 2.08 from the results in Chapter 3. The value of the potential increases as the distance to the stars gets smaller. This means that if the value of the constant  $C$  were sufficiently large the resulting system would be detached.

It is also possible to have a system touching at just one point. This point is called  $L_1$  and the value of the potential of the corresponding surface is called the inner Lagrangian surface.

The initial values for the first LC run were provided by Bradstreet who also supplied the data set LC 2. The preliminary mass ratio  $q=3.4$  had been originally found by Milone, Fry and Grillmair (1987) from radial velocity data which were less well phase distributed than those used in the final analysis. With  $q=3.4$ , the first output agreed with Bradstreet's (private communication) output which also used this mass ratio.

Several runs were made with different values for the Roche potential. As previously mentioned a value too large would make the stars so small that the resulting system would be detached. On the other hand the adoption of too small values would result in a failure to predict the correct shape and amplitude of the light curve. The value of  $C = 5.30$  seemed to give a reasonable fit. The slightly improved parameters shown in Figure 4.4 were then input into the DC program.

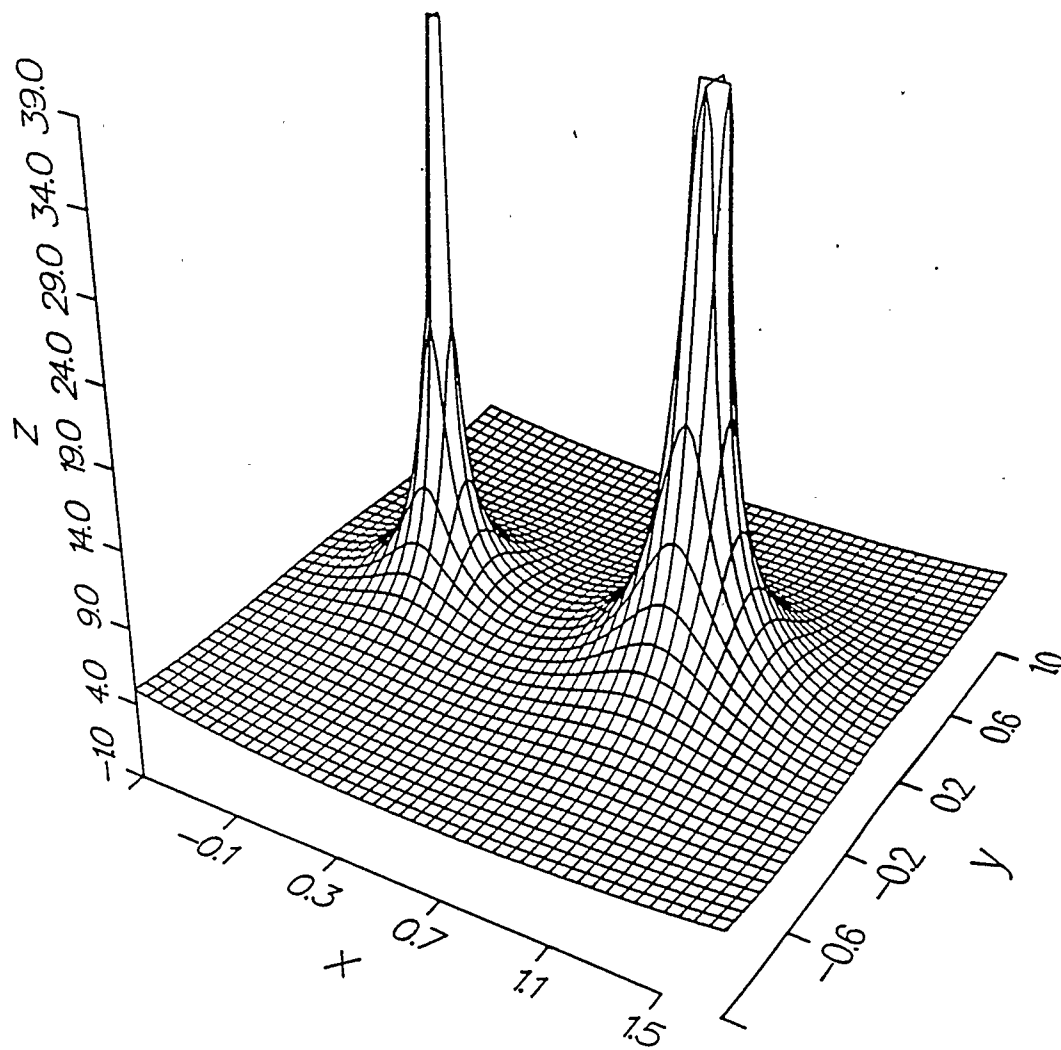


Figure 4.2: Roche Potential: Surface Plot

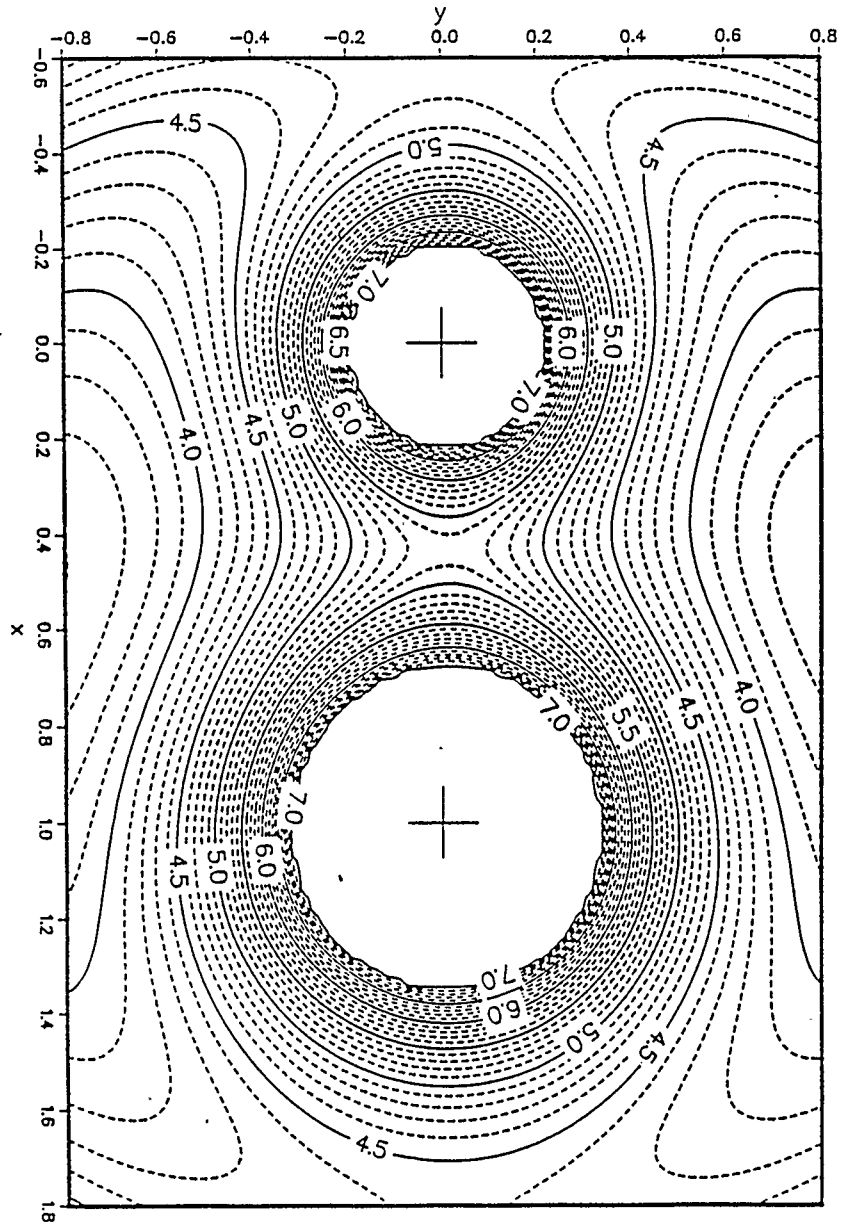


Figure 4.3: Roche Potential: Contour Plot

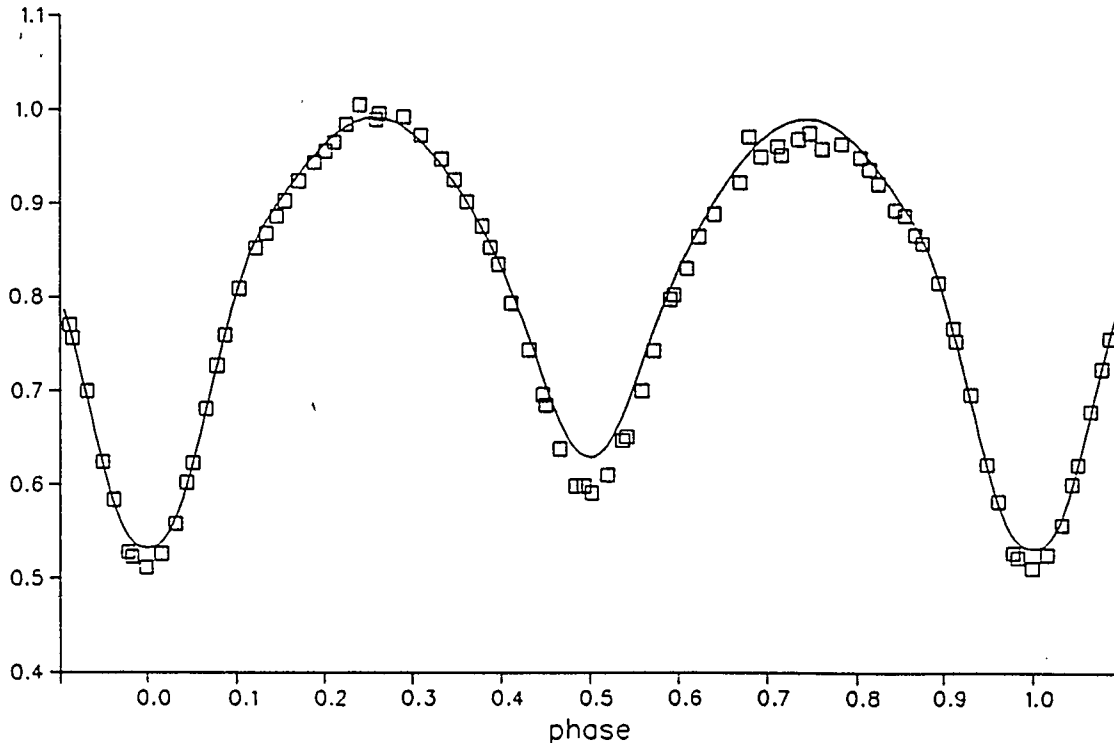


Figure 4.4: Data from Bradstreet compared to initial parameters.

### 4.3 Differential Corrections

In the DC mode the Wilson-Devinney program can compute differential corrections for the desired system parameters. The input includes the radial velocity and light curve data, together with the current system parameters. Through a list of 22 ones and zeroes the program can be instructed to vary some parameters, and compute differential corrections.

First a decision must be made as to the mode in which the program must be run. Of eight possible modes permitted by the Wilson-Devinney code, modes 3, 4 and 5 were used. In mode 3 the program assumes the system is in contact, so that  $y_2 = y_1$  and  $\Omega_2 = \Omega_1$ . The parameter  $T_2$  however is free, and it determines  $L_2$ , which can not be adjusted. Modes 4 and 5 are semi-detached modes: their uses

will be explained in a later section.

DC outputs a list of corrections for the parameters that were adjusted and their probable errors. If the correction is bigger than its error the user may then decide to apply it to the parameter. This adjusted value can then be run again, to compute new corrections. Eventually the iteration process will converge to a solution, as all the corrections become smaller than their errors. The program also outputs a sum of residuals between the data and the computed light and radial velocity curves. This quantity provides an estimate of the goodness of the fit.

The program also allows for subsets of parameters to be adjusted on the same run. Since the corresponding derivatives have already been calculated, a subset can then be computed much faster than in a new run. Because of this a large set of parameters were adjusted, and broken up into several subsets, one predominantly for the spectroscopic, and one for the light elements. The elements adjusted were  $a$ ,  $\gamma$ ,  $i$ ,  $T_2$ ,  $\Omega_1$  and  $L_1$ . Since  $L_1$  depends on wavelength four corrections were reported (one for each wavelength). Three subsets were created to avoid the problem of correlations among the parameters, as discussed by Wilson and Biermann (1976). Subset one included  $a$ ,  $i$ ,  $\gamma$  and  $\Omega_1$ ; subset two  $i$ ,  $T_2$  and  $L_1$  and subset three consisted of  $a$ ,  $\gamma$  and  $q$ . Adjustments were made to all parameters until the corrections became smaller than their probable errors.

#### 4.4 Spots

At this point the parameters were very close to the appropriate values, but asymmetries in the light curve became dominant and resulted in large residuals.

TY Boo had been chosen as an RAO programme system, and for further study in this thesis for its large O'Connell effect, among other reasons. Accordingly at this point it seemed reasonable to introduce one or more star spots to model the observed large asymmetries. The Wilson-Devinney program uses spots as a device to account for any large departures from a model light curve. Its invocation does not necessarily mean that an actual spot is thought to exist on the surface of the star, but merely that some mechanism is producing an effect on the light distribution. It has been shown, Milone, Wilson and Hrivnak (1987), that the parameter solutions are not strongly affected by this solution artifice as compared to a rectification process. It was decided to place a homogeneous cool spot on star 2.

Spots in the Wilson-Devinney program approximate circular regions on the surface of a star. A line in the input file lists the co-latitude ( $\phi$ ), longitude ( $\theta$ ), radius ( $\rho$ ) and a temperature factor ( $t_f$ ). The coordinate system used by the program consists in a latitude and longitude grid much like the one used for terrestrial coordinates. The co-latitude, however, runs from  $0^\circ$  at the north pole (which is inclined toward earth) to  $180^\circ$  at the south. Longitude is  $0^\circ$  at the meridian that includes the line of centers and  $360^\circ$  around the star, clockwise as seen from the north pole. The radius is in degrees as seen from the center of the star. The temperature factor, in units of the temperature of an unperturbed region at the same location, is larger than 1 for spots hotter than the surface, and less than 1 for cold spots.

Since the effect looked symmetric around secondary maximum, it was decided to place the spot so that it would face the observer at second quadrature. It was placed on star 2 at  $\phi = 90.0^\circ$  and  $\theta = 90.0^\circ$ . Values of  $\rho = 20.0^\circ$  and  $t_f = 0.95$

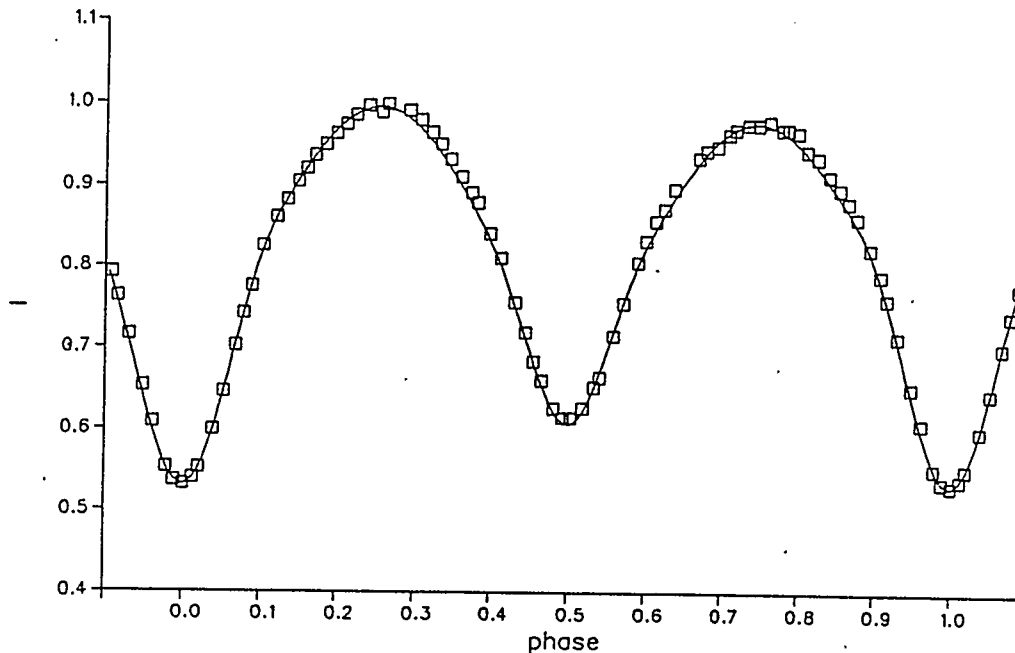


Figure 4.5: Spot 1, first attempt

were used. Figure 4.5 shows the resulting  $V$  light curve. It can be seen that the spot is too large, and maybe too cool.

Following the technique outlined by Milone, Wilson and Hrivnak (1987), several values for  $\rho$ , ranging from  $8.0^\circ$  to  $20.0^\circ$ , were run. As the value of  $\rho$  changed, so did the sum of the weighted residuals ( $\sum wr^2$ ) in the DC output. If these residuals are graphed versus  $\rho$  it can be seen that one value of  $\rho$  minimizes the residuals. Table 4.2 shows the values of  $\rho$  and the residuals. These values were fit by a polynomial of the form  $\sum wr^2 = a + b\rho + c\rho^2$ , where  $a$ ,  $b$  and  $c$  are constants. Figure 4.6 shows both the data and the best fit curve.

The  $\rho$  for the spot could now be calculated from  $\rho = -b/2c$ . Once the best value for  $\rho$  had been determined, the same procedure was used to adjust the temperature factor. Table 4.3 and Figure 4.7 illustrate this.

Table 4.2: Spot 1,  $\rho$  and  $\Sigma wr^2$ 

$\rho$	$\Sigma wr^2$
8.0	0.39233
10.0	0.38015
12.0	0.36832
14.0	0.36745
16.0	0.37504
18.0	0.39625
20.0	0.42805

a	0.5656	$\pm$	0.0029
b	-0.0309	$\pm$	0.0022
c	0.0012	$\pm$	0.0001

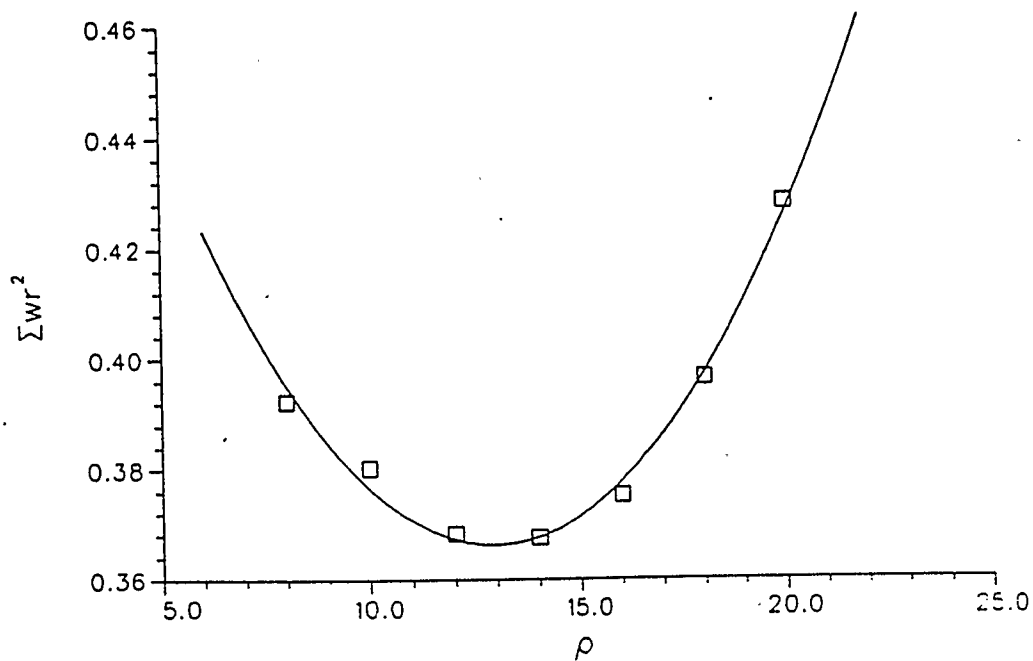
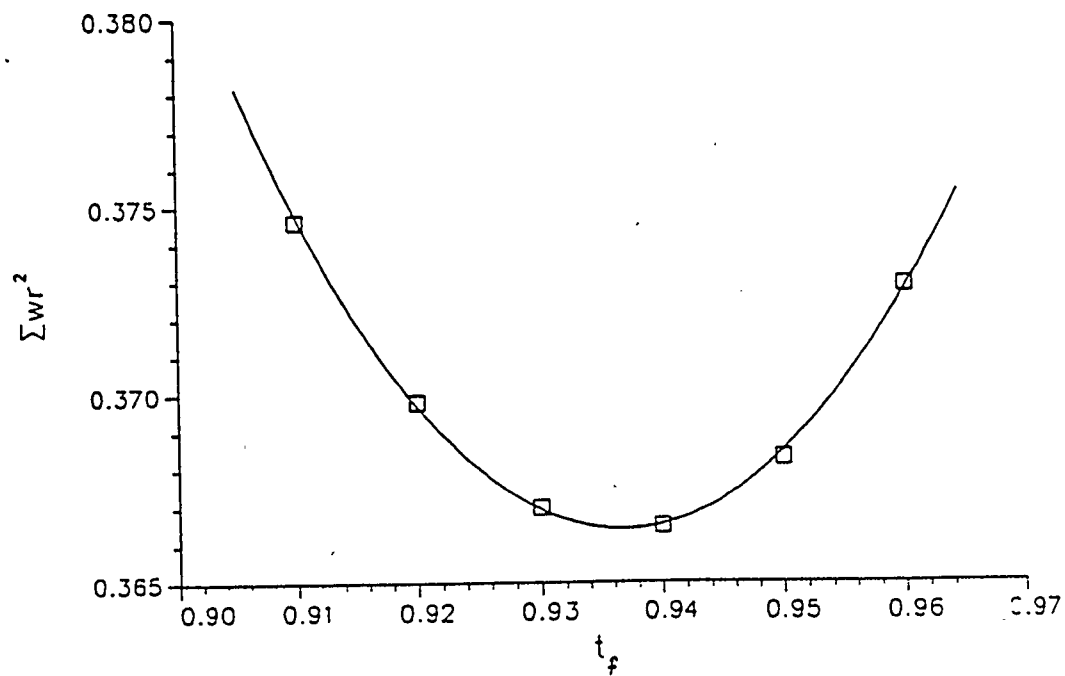
Figure 4.6: Spot 1,  $\Sigma wr^2$  for  $\rho$  determination

Table 4.3: Spot 1,  $t_f$  and  $\Sigma wr^2$ 

$t_f$	$\Sigma wr^2$
0.91	0.37464
0.92	0.36984
0.93	0.36704
0.94	0.36645
0.95	0.36832
0.96	0.37290

a	10.6412	$\pm$	0.0002
b	-21.9386	$\pm$	0.5665
c	11.7107	$\pm$	0.3029

Figure 4.7: Spot 1,  $\Sigma wr^2$  for  $t_f$  determination

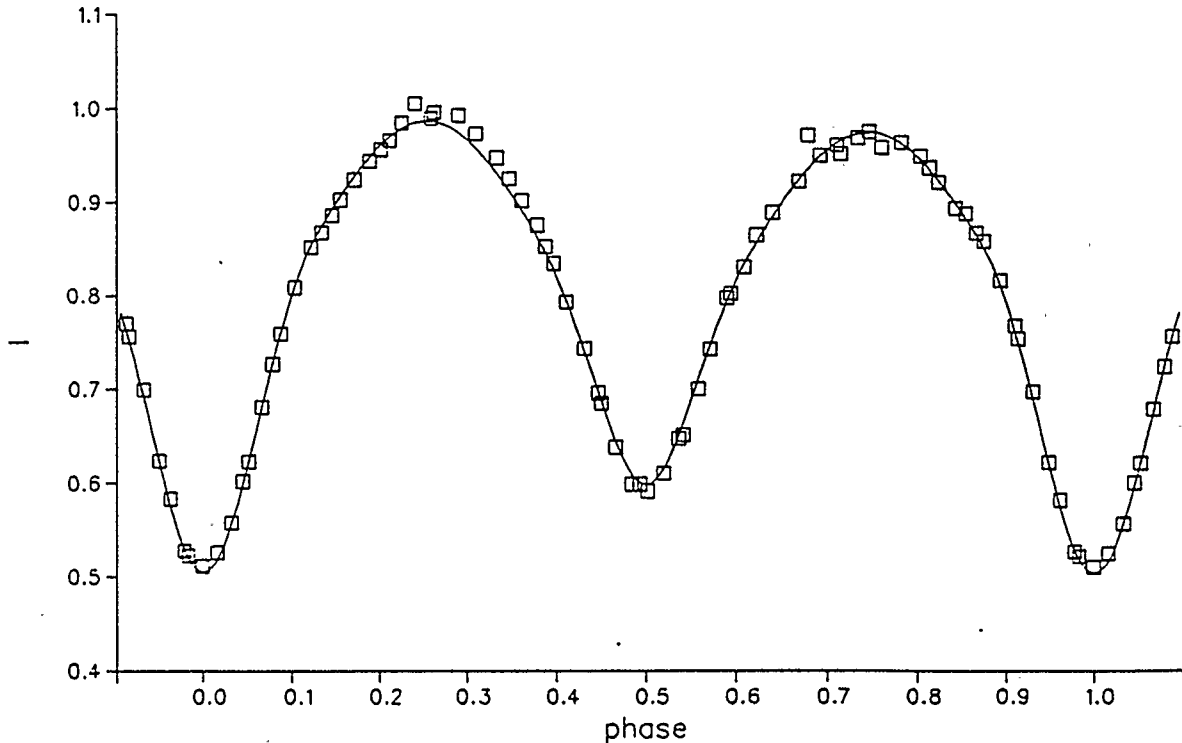


Figure 4.8: B light curve. 1 spot fit

The resulting values for the spot were found to be:

$$\rho: 12.91^\circ \pm 1.27^\circ$$

$$t_f: 0.94 \pm 0.03$$

When used in subsequent DC runs, a spot with these parameters reduced the values of the residuals considerably, and allowed further adjustment of the system parameters. Figures 4.8 through 4.11 show the resulting fits. At this point another asymmetry became dominant. As can be seen in the above mentioned figures, a bright spot appeared to be necessary around phase 0.3.

The same method was now used to adjust spot 2, only this time  $\theta$  had to be adjusted also, since it was not very clear what the optimum value should be. It was initially placed at  $\theta = 320.0^\circ$  on star 2, since in this way the sudden increase in

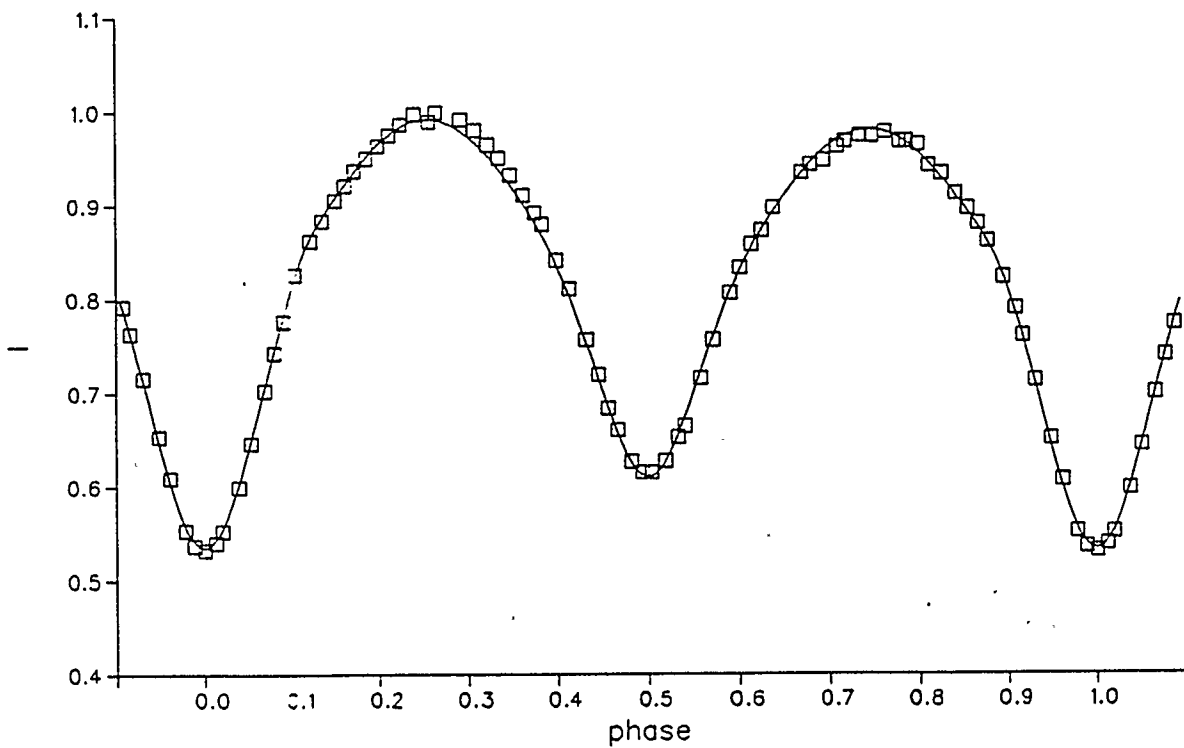


Figure 4.9: V light curve. 1 spot fit

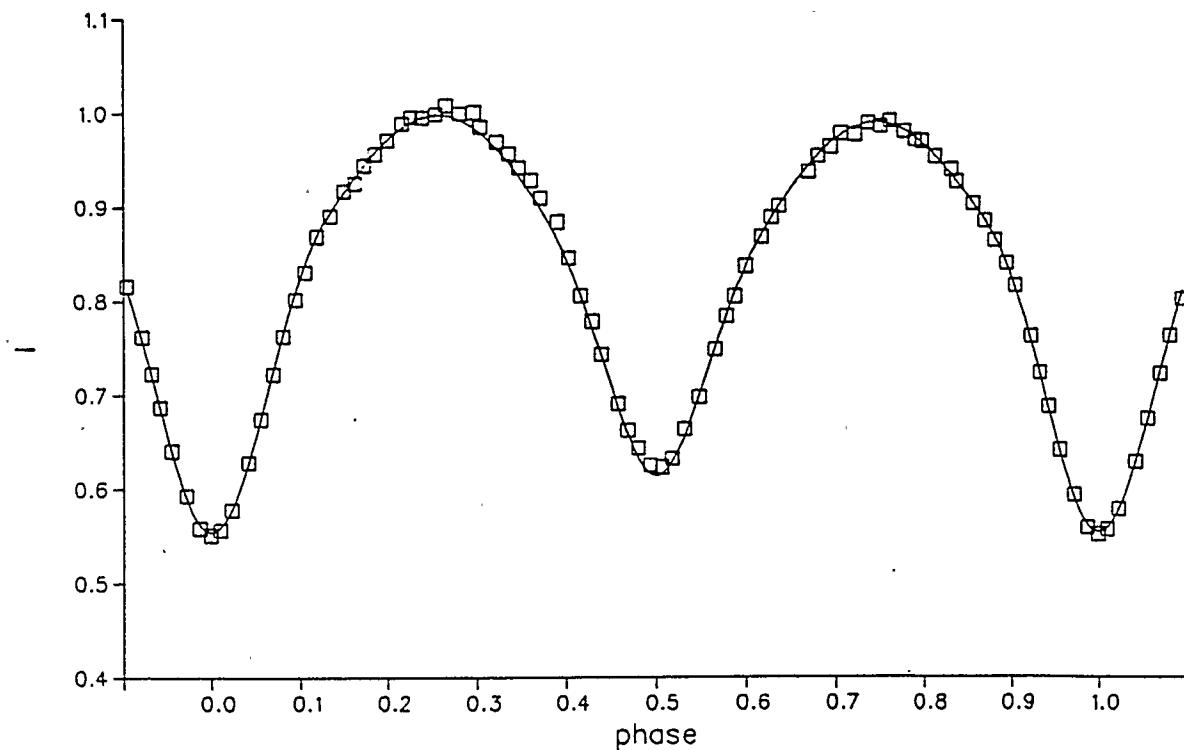


Figure 4.10: R light curve. 1 spot fit

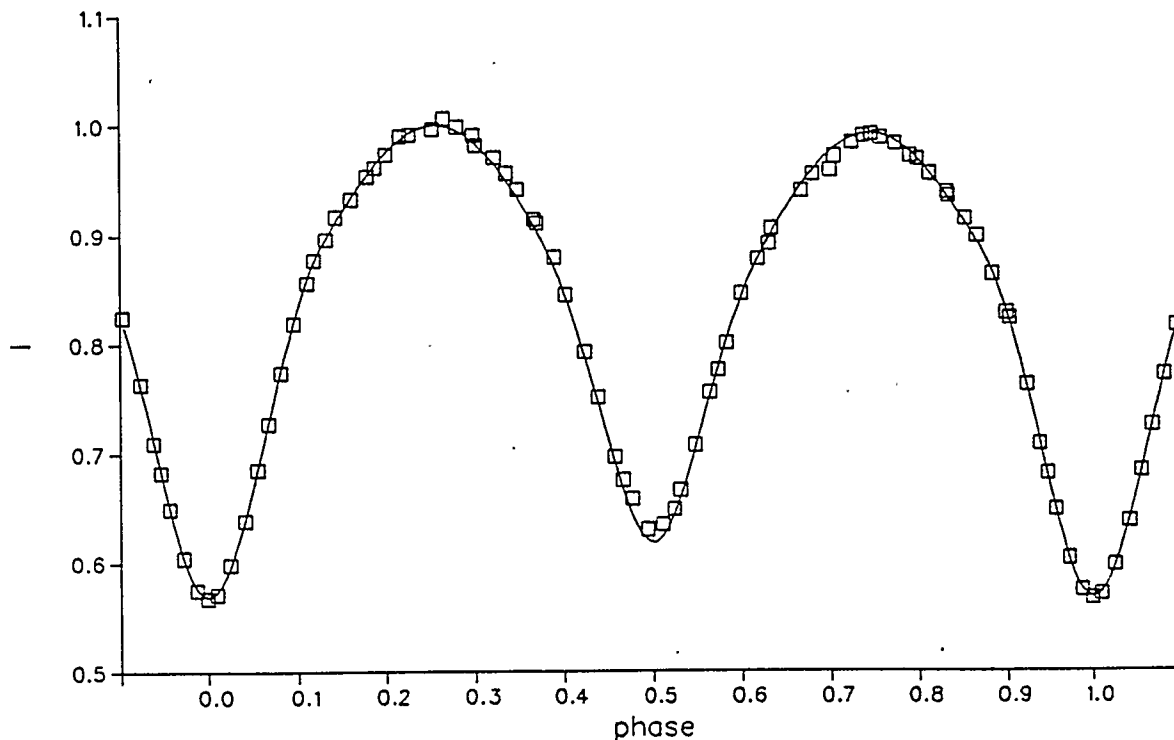


Figure 4.11: I light curve. 1 spot fit

luminosity right after quadrature would be explained as the spot came into view at second quadrature. The gradual drop could then be explained by the eclipse of the spot by star 1 right after second quadrature.

After adjusting the longitude, the size and the temperature factor in the same way as for spot 1, the best fit values for spot 2 were:

$$\theta: 323.1^\circ \pm 5.3^\circ$$

$$\rho: 9.9^\circ \pm 4.2^\circ$$

$$t_f: 1.07 \pm 0.05$$

Notice the large error in the size of the spot, probably due to the foreshortening at the point when it is visible, and the very sudden eclipse afterwards.

With both spots in place, to reduce any remaining residuals the final iterations

Table 4.4: Spot 2, longitude and  $\Sigma wr^2$ 

	longitude	$\Sigma wr^2$
	310.0	0.29562
	320.0	0.29344
	330.0	0.29423
	340.0	0.29685
a	1.5465	$\pm 0.0003$
b	-0.0078	$\pm 0.0008$
c	0.0000	$\pm 0.0000$

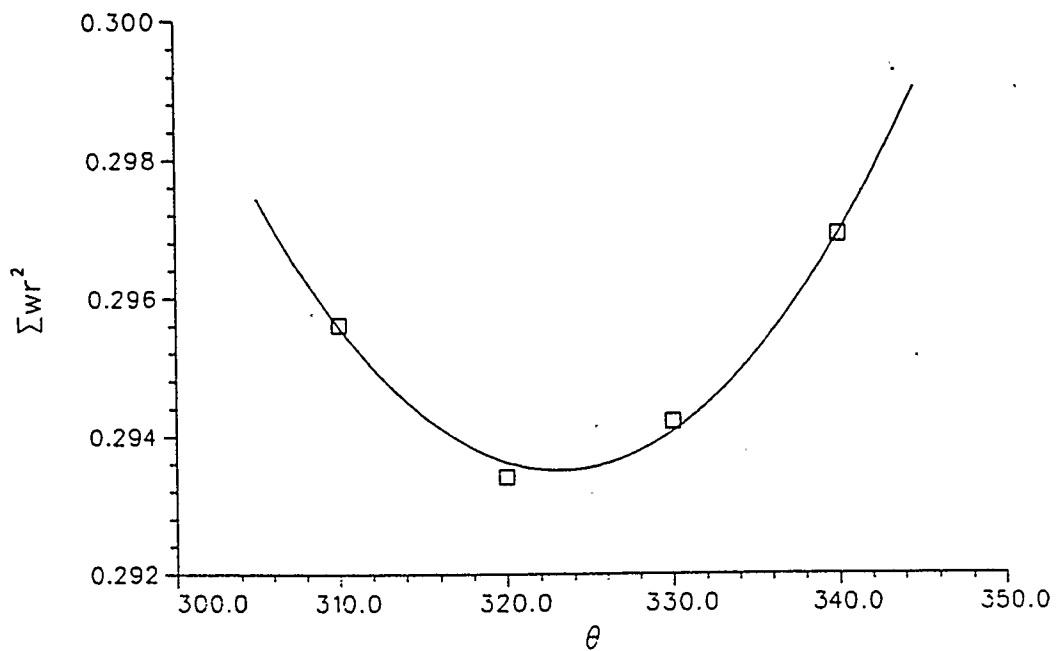
Figure 4.12: Spot 2.  $\Sigma wr^2$  for longitude determination

Table 4.5: Spot 2,  $\rho$  and  $\Sigma wr^2$ 

$\rho$	$\Sigma wr^2$
8.0	0.29654
10.0	0.29377
12.0	0.29644
14.0	0.32357

a	0.4733	$\pm$	0.0043
b	-0.0369	$\pm$	0.0117
c	0.0019	$\pm$	0.0005

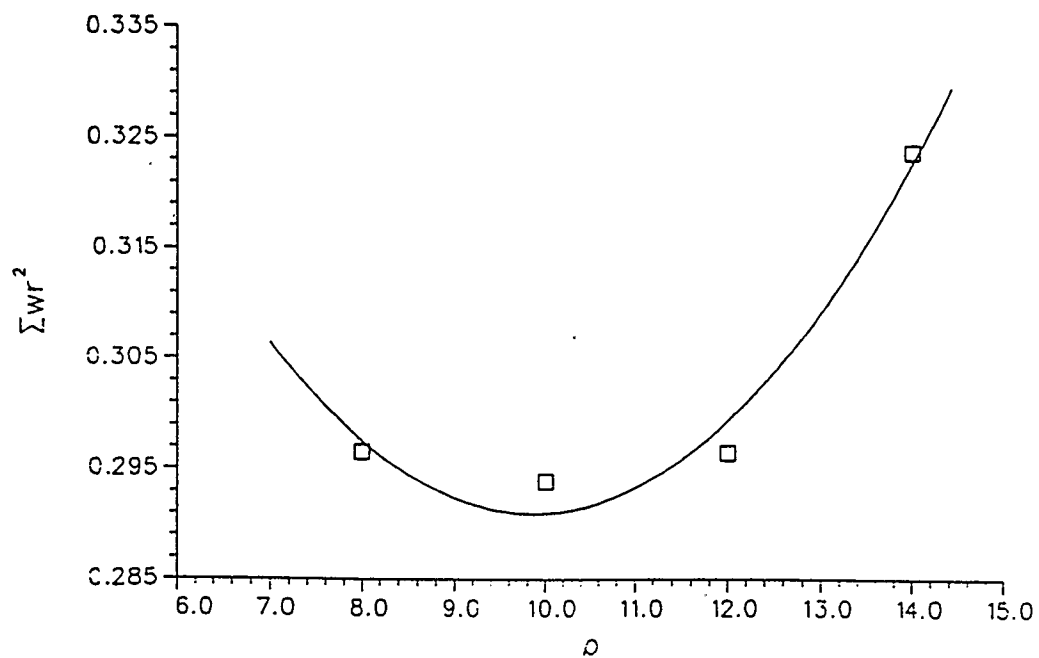
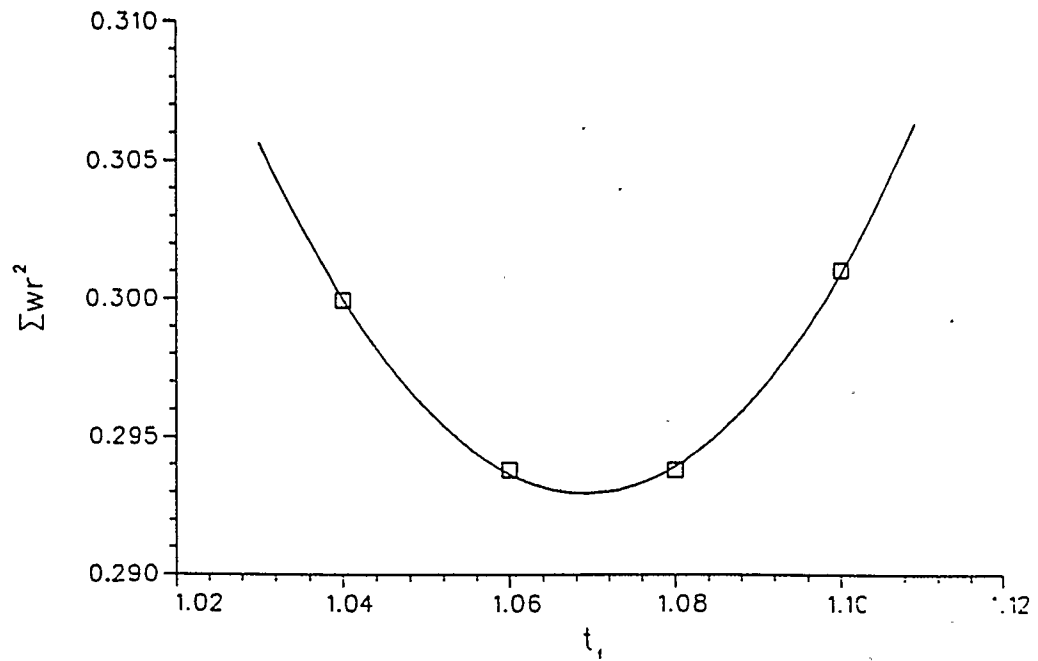
Figure 4.13: Spot 2,  $\Sigma wr^2$  for  $\rho$  determination

Table 4.6: Spot 2,  $t_f$  and  $\Sigma wr^2$ 

	$t_f$	$\Sigma wr^2$
	1.04	0.29990
	1.06	0.29377
	1.08	0.29378
	1.10	0.30094
a	9.7860	$\pm 0.0002$
b	-17.7597	$\pm 0.6042$
c	8.3062	$\pm 0.2823$

Figure 4.14: Spot 2,  $\Sigma wr^2$  for  $t_f$  determination

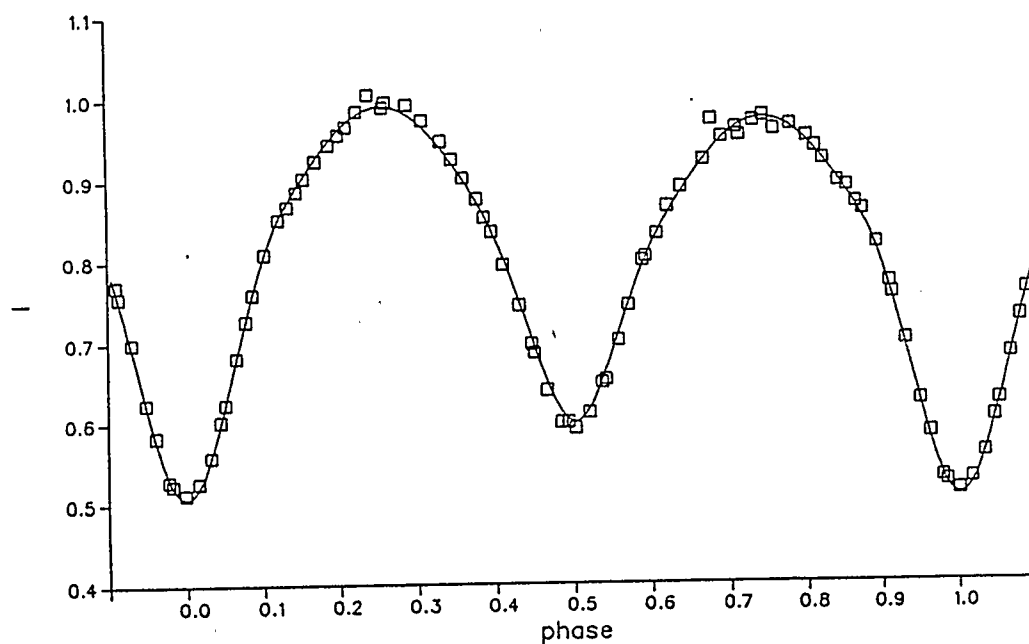


Figure 4.15: B light curve, 2 spot fit

with DC were performed. The fits to the light curves can be seen in Figures 4.15 through 4.18.

## 4.5 Graphical Representation of the Model

Modern computers and specially written software allowed the modeler to obtain a graphical representation of the physical appearance of the system. This is equivalent to graphing the equipotential surface determined by the Roche potential.

A program was developed which was able to draw a three dimensional view of the star system, given its mass ratio, Roche potential and phase. Drawings for several phases appear in Figures 4.5 through 4.5. This program is capable of hidden line removal and is a useful aid for visualizing the eclipse mechanism and

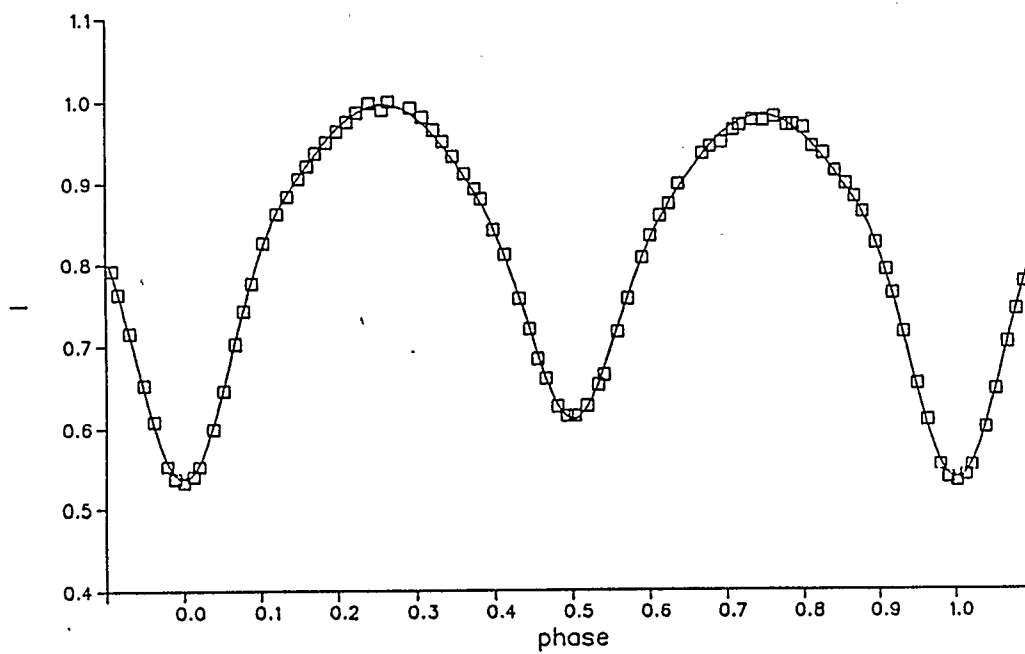


Figure 4.16: V light curve, 2 spot fit

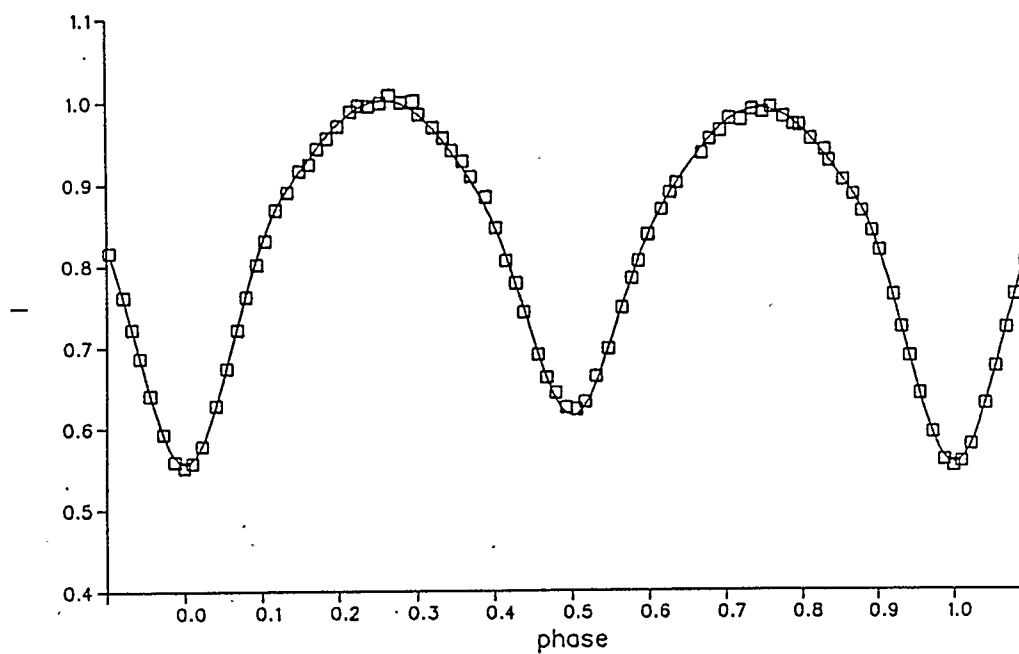


Figure 4.17: R light curve, 2 spot fit

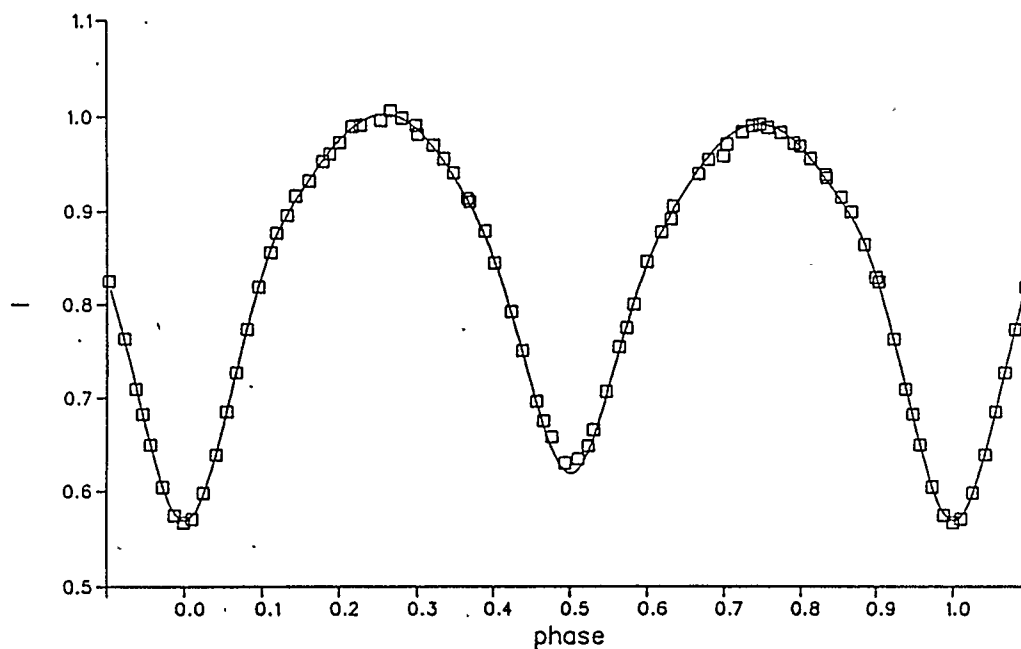


Figure 4.18: I light curve, 2 spot fit

spots. In order to graph the Roche lobes the potential function has to be solved at a grid of points in three dimensional space, and the hidden line removal algorithm is then used to decide whether to plot this point or not.

First the plotting coordinate system is set up. The  $x$  axis is chosen along the line that joins the centers of the stars, the  $y$  axis is on the axis of rotation of the system and the  $z$  axis is perpendicular to both. This is the common usage in graphics programming and differs from the type of coordinate axis normally used in the Roche geometry.

The system is rotated to match the orbital inclination, and then rotated in the plane of the orbit to match the corresponding phase. This determines the position of the observer with respect to the system. The Roche potential equation is then solved by the Newton-Raphson method first along lines running from the outer

limb of one star, through the connecting bridge to the limb of the opposite star. This gives the  $x$ ,  $y$  and  $z$  coordinate of all the points that represent the surface of the binary system.

To determine whether or not the point must be plotted, it is necessary to know if it is being eclipsed by other parts of the star. To do this a line starting at the given point and pointing towards the observer is computed. An imaginary point is then moved along this line, and the potential computed at every step. If the potential at any point becomes larger than the surface potential this means the line intersects the equipotential surface, and hence the point is being eclipsed by this part of the surface. If this doesn't happen the point is plotted.

The program is very useful when visualizing the eclipse mechanism. It can show the eclipses being total, or partial, by showing how much of each star is visible at any given phase. Another advantage of the program is its ability to show the location of cold or hot spots on the surface of the star, and to observe how they are eclipsed.

## 4.6 Tests of the Model

To check the validity of the fitting results, the Wilson-Devinney program was also run in modes 4 and 5. When run in mode 3 the program assumes that the stars are indeed in contact so that  $\Omega_1 = \Omega_2$ . In order to test this assumption for TY Boo the program was set to run in semi-detached modes. If the system was truly in contact, the solutions should converge to the contact case. Such a test was run on RW Com by Milone, Wilson and Hrivnak (1987). Schiller and Milone (1988)

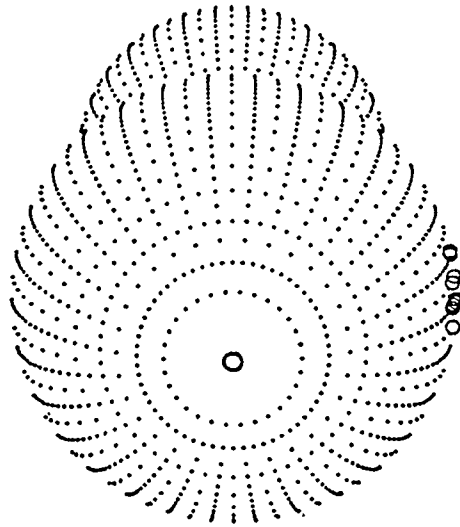


Figure 4.19: Model of TY Boo facing earth at phase 0.0

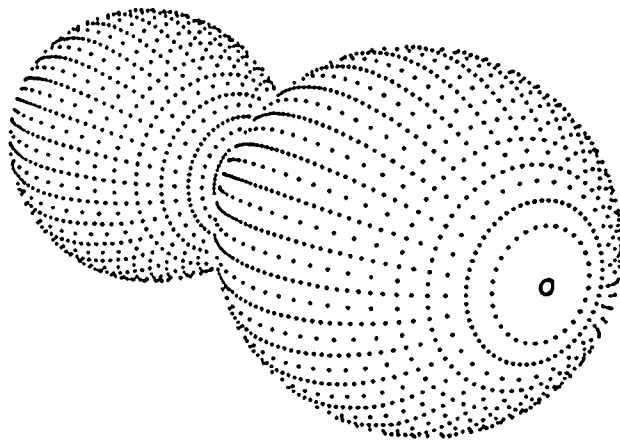


Figure 4.20: Model of TY Boo facing earth at phase 0.1

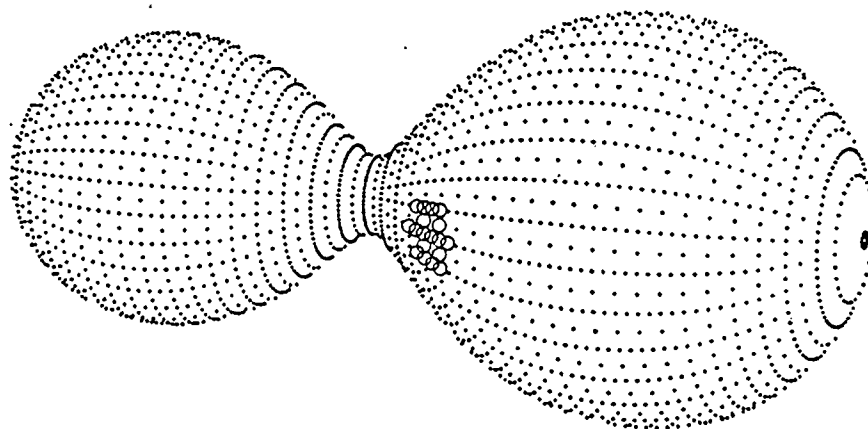


Figure 4.21: Model of TY Boo facing earth at phase 0.2

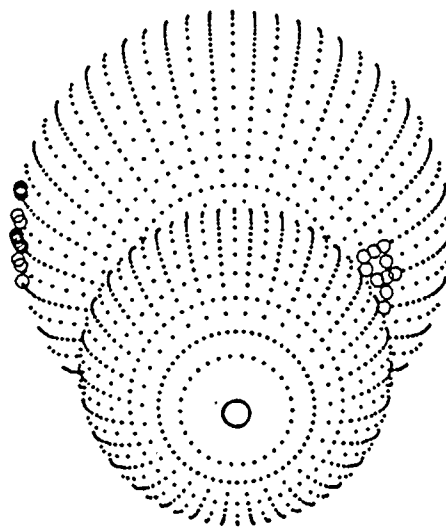


Figure 4.22: Model of TY Boo facing earth at phase 0.5

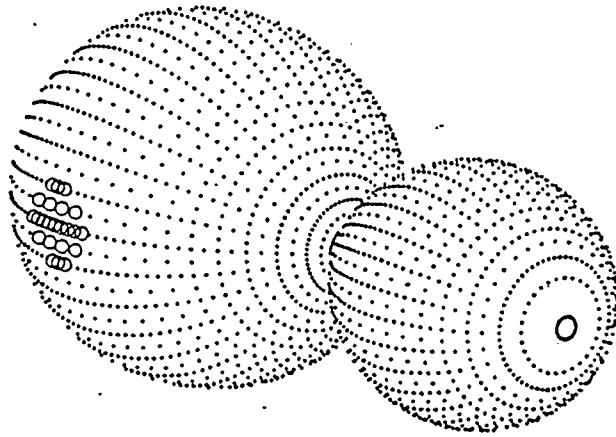


Figure 4.23: Model of TY Boo facing earth at phase 0.6

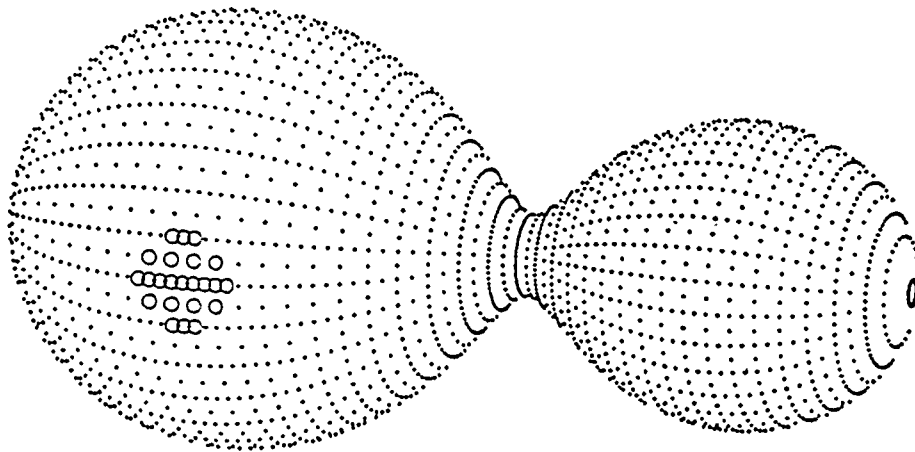


Figure 4.24: Model of TY Boo facing earth at phase 0.7

applied a similar technique on DS And, only in this case a detached system was suspected. The tests were done by starting with values that meant contact, and observing them converge to detached.

In mode 4 the primary is set to fill its Roche lobe, regardless of the input value, because of this,  $\Omega_1$  can not be adjusted. Mode 5 is the equivalent mode where the secondary fills its Roche lobe and  $\Omega_2$  can not be adjusted.

From the tables of Plavec and Kratochvil (1964) it was found that for a system with a mass ratio of 2.085 the value of  $\Omega_{inner}$  was 5.372. This means that a value larger than this for either of the two stars would yield a semi-detached system.

As the iterations were performed, each of the modes gave slightly different results for  $L$  and  $i$ , because in each mode the potential of one of the stars was being held at the critical value, and hence the size was smaller than in mode 3. The values of the potential of the star being adjusted, were found to converge to values smaller than the critical value, confirming the contact system solution. These results are also shown in Table 4.7.

A second test of the solution elements was to use as input the RAO light curves mentioned in Chapter 2 (LC 1, LC 3 and LC 4), and run them in DC mode. The 1985 and 1986 data were relatively sparse, so only the 1987 BVI curves were used (LC 4). After they were converted to units of luminosity and normalized to the first maximum, a new Wilson-Devinney input file was created. It was decided to normalize the light curves to a value of 1 at the brightest maximum for consistency, since this approach had already been followed by Bradstreet with LC 2. However, as discussed by Milone, Wilson and Hrivnak (1987), the choice of either maximum, or even the average of the two, does not change the results much.

The parameters for this run were set to the previously found values. After only two iterations all corrections fell within errors. The results are listed in Table 4.7, where  $\ell$  is the monochromatic luminosity normalized so that the sum of the contributions from both components add up to 1.

The data set LC 4 was run without any spots, which helps to explain the larger  $\Sigma wr^2$  for this data set. The presence of spots in LC 2 helped reduce the residuals, and hence the uncertainty of the results but the resulting parameters were virtually identical since the previously found results were used as input.

A second run with data set LC 4 was done where the input values were those previously found, but perturbed by  $\pm 10\%$ . Once again the results converged to those values previously found.

#### 4.7 Contact Parameter and Fill-Out Factor

From the tables of Plavec and Kratochvil (1964) the value of  $\Omega_{outer}$  was also found. It was now possible to find the contact parameter  $f$ , defined as

$$f = \frac{\Omega_{inner} - \Omega}{\Omega_{inner} - \Omega_{outer}}$$

This factor gives an indication of the degree of filling of the contact envelope. It was found to be equal to 0.087. This is a small value showing that the system is barely in contact, the semi-detached mode solutions, however, confirm the contact condition.

To test the results we resort to the values obtained by the Fourier fit to the light curves. Ruciński (1973) suggests a relation between the terms  $a_2$  and  $a_4$  versus the

Table 4.7: TY Boo, Solutions to Radial Velocity and Light Curves

	LC 2	LC 4 unperturbed	LC 4 perturbed	
$a$	2.33(1)	2.33(2)	2.34(2)	$R_{\odot}$
$\gamma$	-39(7)	-39(10)	-39(10)	$km/sec$
$i$	75.90(7)	75.58(18)	75.66(19)	$degrees$
$T_1^*$	5623(100)	5623(100)	5623(100)	$K$
$T_1 - T_2$	395(5)	395(12)	403(11)	$K$
$\Omega_1 = \Omega_2$	5.320(3)	5.324(8)	5.348(7)	
$q$	2.084(3)	2.084(3)	2.084(3)	
$g_1 = g_2^*$	0.32	0.32	0.32	
$A_1 = A_2^*$	0.5	0.5	0.5	
$A_1 = A_2^*$	0.5	0.5	0.5	
$x_{1B}^*$	0.97	0.97	0.97	
$x_{1V}^*$	0.87	0.87	0.87	
$x_{1R}^*$	0.84	0.84	0.84	
$x_{1I}^*$	0.80	0.80	0.80	
$x_{2B}^*$	0.97	0.97	0.97	
$x_{2V}^*$	0.87	0.87	0.87	
$x_{2R}^*$	0.84	0.84	0.84	
$x_{2I}^*$	0.80	0.80	0.80	
$l_3^*$	0.0	0.0	0.0	
$l_{1B}$	0.439(1)	0.439(4)	0.440(4)	
$l_{1V}$	0.419(1)	0.418(4)	0.420(4)	
$l_{1R}$	0.404(1)	-	-	
$l_{1I}$	0.393(1)	0.393(4)	0.394(4)	
$l_{2B}$	0.561(1)	0.561(4)	0.560(4)	
$l_{2V}$	0.581(1)	0.582(4)	0.580(4)	
$l_{2R}$	0.596(1)	-	-	
$l_{2I}$	0.607(1)	0.607(4)	0.606(6)	
$r_{1pole}$	0.301(6)	0.305(5)	0.298(5)	$a$
$r_{1side}$	0.315(7)	0.314(6)	0.312(6)	$a$
$r_{1back}$	0.350(13)	0.349(12)	0.345(11)	$a$
$r_{2pole}$	0.422(3)	0.422(3)	0.419(3)	$a$
$r_{2side}$	0.450(4)	0.449(5)	0.446(4)	$a$
$r_{2back}$	0.479(6)	0.478(7)	0.475(7)	$a$
$\Sigma wr^2$	0.2678	0.6244	0.5699	

\* assumed and unadjusted

mass ratio  $q$  and the contact parameter  $f$ . In this paper the fill-out parameter is defined in a way similar to that of the contact parameter already computed. His definition, which we will now designate  $f'$  is

$$f' = \frac{\Omega - \Omega_{outer}}{\Omega_{inner} - \Omega_{outer}}$$

This fill-out parameter has a value of one for systems that touch at only one point, and zero for those in full contact. Notice that this means that  $f = 1 - f'$ . Another difference is in the definition of the mass ratio, which we now designate  $q'$ . Ruciński defines it as

$$q' = m_2/m_1 \leq 1$$

The subscripts are defined in terms of mass ( $m_1$  being the more massive star) and not in term of surface brightness.

To be consistent with this notation we recompute  $f'$  and  $q'$  for TY Boo and arrive at these values:

$$q' = 0.48$$

$$f' = 0.91$$

$$a_2 = -0.191$$

$$a_4 = -0.043$$

Figure 4.25 reproduces Ruciński's (1973) graph. Filled dots correspond to  $f' = 1$ , open circles to  $f' = 0$  and half-filled circles to  $f' = 1/2$ . These points were computed for two values of the inclination. The set that extends further towards the upper right hand corner was computed with  $i = 90.0^\circ$ , the other with  $i = 75.0^\circ$ .

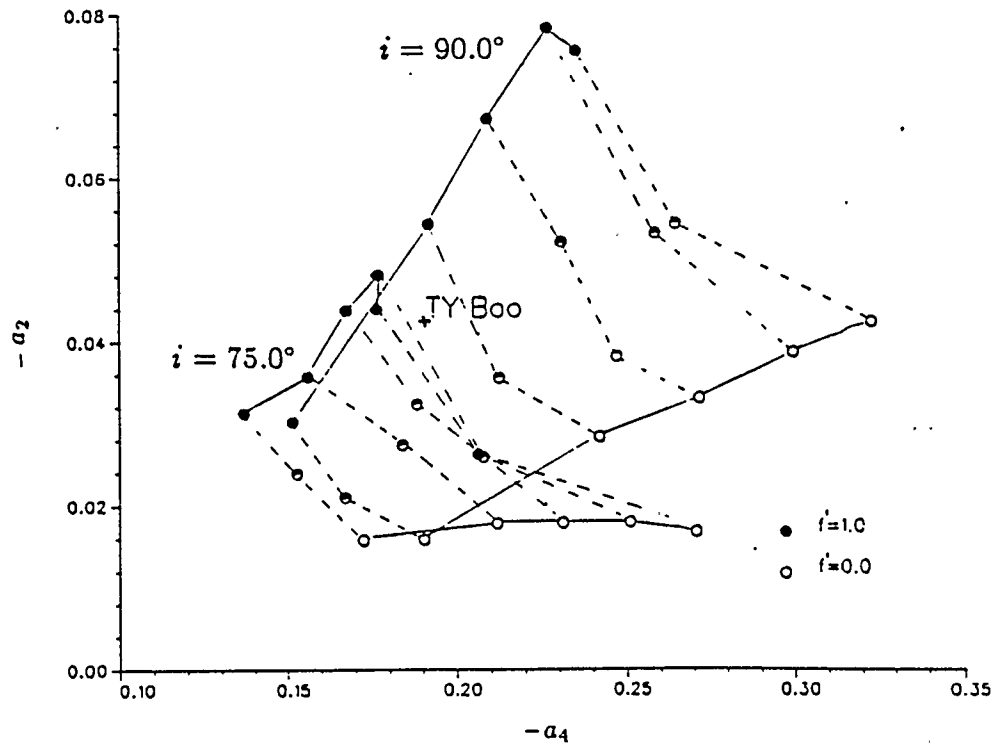
The position of the values of  $a_4$  and  $a_2$  for TY Boo in Figure 4.25 indicate that  $f'$  must be between 0.5 and 1. We also see that it is very close to the  $i = 75^\circ$  region, as expected.

Ruciński also plotted known stars on the same type of plot. In Figure 4.26 we find that the placement of TY Boo among these stars, showing it to be by no means unique. In this plot, the lines of  $f' = 0.0, 0.5$  and  $1.0$  for  $i = 90.0^\circ$  have been indicated for convenience.

The stars UX Eri ( $f'=0.9$ ) and AC Boo ( $f'=0.8$ ) fall very close to TY Boo. Both of these systems have been observed in the past. Schieven et al.(1983) observed AC Boo and Binnendijk (1967) UX Eri. In both cases asymmetries in the light curves and changes in period, both long and short term, were found. This makes these two binaries prime targets for future work.

The way in which the contact condition affects the two stars can be seen by plotting them in a mass-luminosity graph. Figure 4.27 shows the data studied by Griffiths, Hicks and Milone (1988), in which the logarithm of mass and luminosity of main sequence stars, normalized to solar values, has been plotted. It can be seen that component 2, the more luminous star, lies below the normal stars. Star 1, however, lies above the population. This could be explained by the transfer of energy from star 2 to 1. Since star 2 is also the more massive one the equilibrium will be closer to its original energy, explaining why it is the closest one to the normal trend.

In his model for W UMa stars Lucy (1968) indicates that entropy must be transferred from one star to the other through the "throat" of the common convective envelope. As Mochnacki (1971) mentions, some of these systems are in very

Figure 4.25:  $f'$  determination

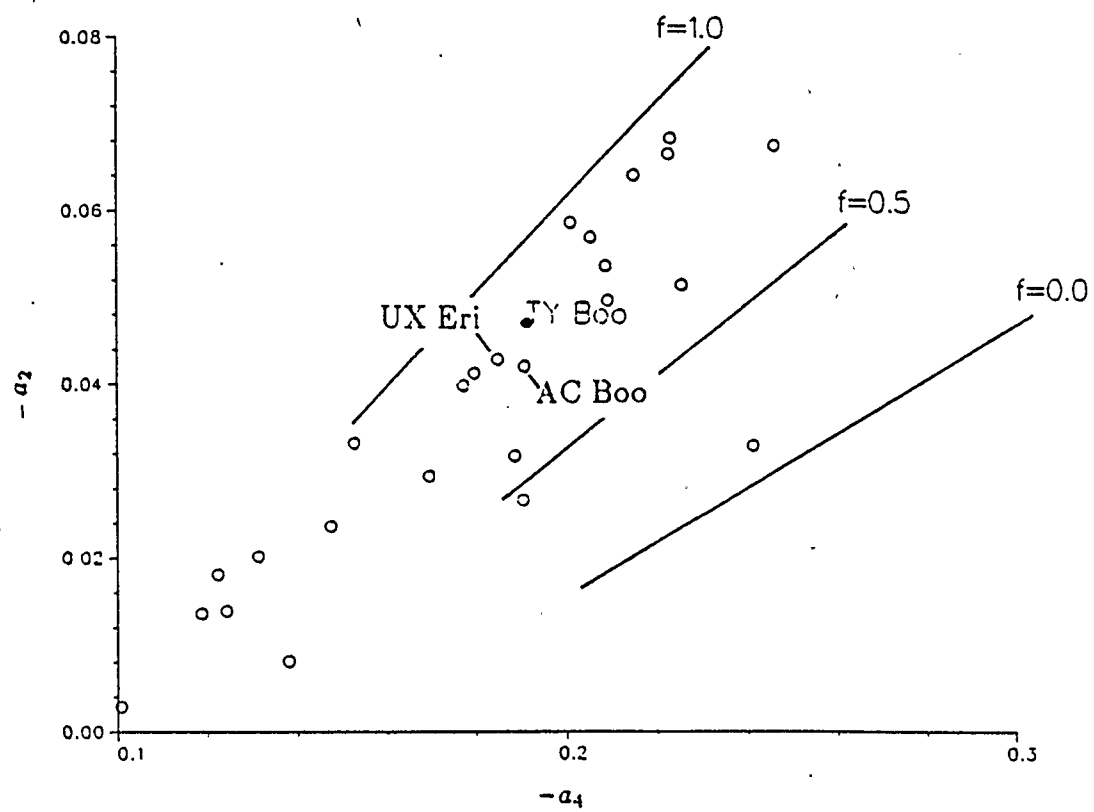


Figure 4.26: Comparison of TY Boo with other stars

shallow contact, and any activity near the contact point may impede the normal energy flow. This “choking”, as he calls it, may disappear in a sudden way causing flare activity. This is not uncommon in W UMa type stars, and has been observed in TY Boo as well. During an observing run at DAO in June 1985 Milone, Fry and Grillmair (1987) observed a flare develop in the spectrum of TY Boo. Four such spectra are reproduced in Figure 4.28. Notice that the sharp Ca II emission features at 3933 and 3968 Å increase in intensity as time progresses.

## 4.8 Conclusions

In this thesis it has been established that TY Boo is a W type system on the basis of its radial velocity curve. It is useful to compare the results obtained here with the general characteristics of these systems as presented by Ruciński (1973).

**Spectral Type:** W UMa stars tend to be in the F–G region, with the W-type systems being the “later”. We found the components of TY Boo to be G3 and G7.

**Activity:** W-type systems tend to have “strong or very strong changes of light curve, asymmetries of maxima”. This thesis demonstrates the change in the O’Connell effect and other changes in the light curve of TY Boo from year to year.

**Mass-ratio:** W-type systems have “larger ratios, 0.33-0.88” this corresponds to Ruciński’s notation. The value for TY Boo in the same notation is 0.48, in agreement with the characterization.

**Degree of contact:** W-type systems have “shallow envelopes”. At  $f' = 0.91$  TY Boo fills the contact envelope by less than 10%.

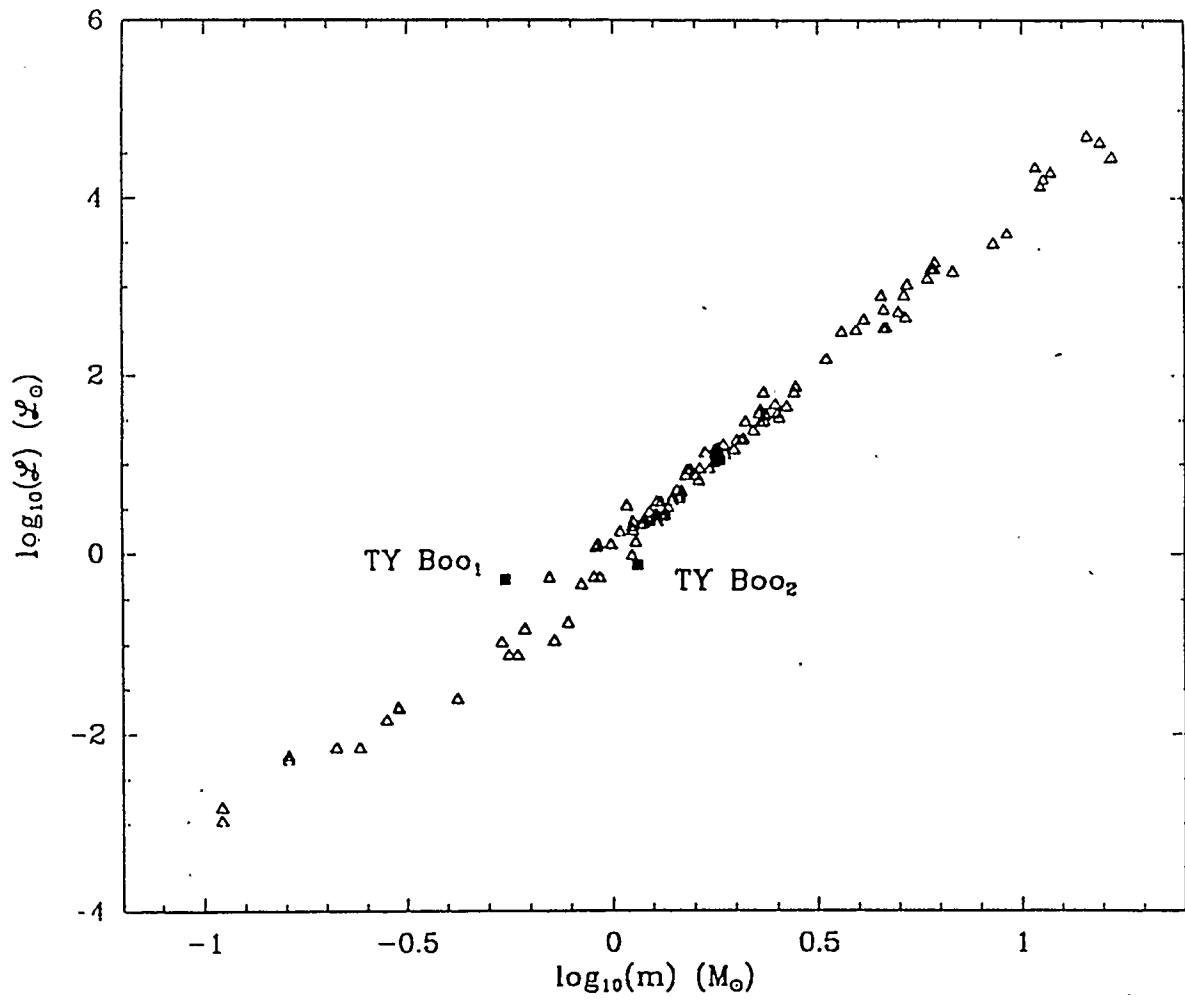


Figure 4.27: Mass-luminosity plot. Main-sequence stars, and TY Boo-1 and 2

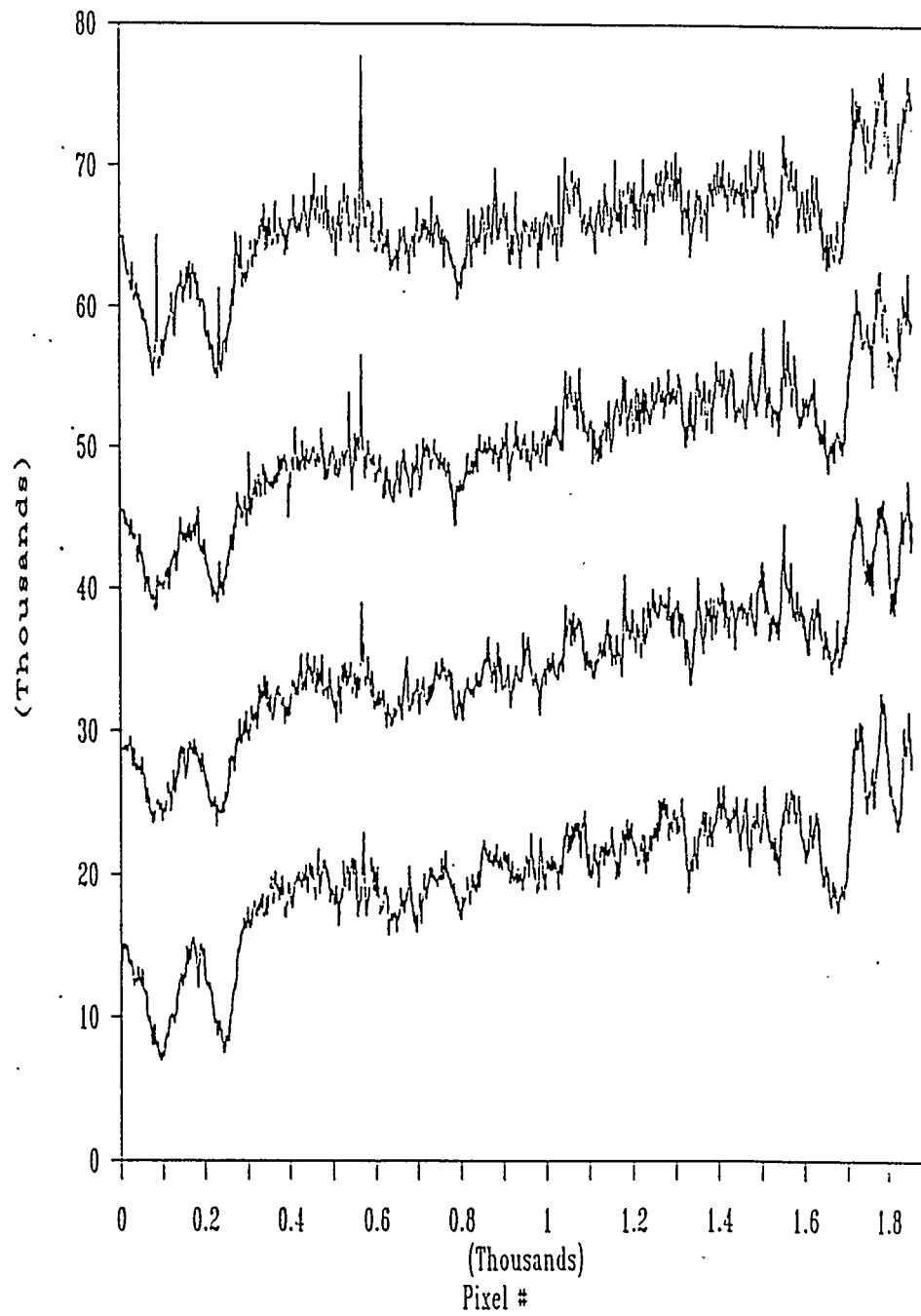


Figure 4.28: Flare observed in the spectrum of TY Boo. June 1985

Table 4.8: TY Boo, Absolute Parameters

	Bradstreet light curve	RAO 87 light curve	
$a$	2.33(1)	2.33(2)	$R_{\odot}$
$\gamma$	-39(7)	-39(10)	Km/Sec
$f$	0.087(7)	0.087(7)	
$\bar{R}_1$	0.739(13)	0.748(11)	$R_{\odot}$
$\bar{R}_2$	1.048(7)	1.046(7)	$R_{\odot}$
$T_1$	5623(100)	5623(100)	$K$
$T_2$	5228(66)	5228(159)	$K$
$m_1$	$1.090(6) \times 10^{33}$	$1.09(1) \times 10^{33}$	$gr$
$m_2$	$2.27(2) \times 10^{33}$	$2.27(4) \times 10^{33}$	$gr$
$\bar{\rho}_1$	1.90(1)	1.84(8)	$gr/cm^3$
$\bar{\rho}_2$	1.40(3)	1.41(4)	$gr/cm^3$
1	0.51(2)	0.50(2)	$\odot$
2	0.73(1)	0.74(2)	$\odot$
Distance	326(16)	326(36)	$Pcs$

**Other characteristics:** Another characteristic of W UMa systems is a reddening of the light curve during both minima. This is due to differences in the surface temperature of the stars, which are lower towards the tidally elongated ends. During eclipses the light from one of the ends becomes dominant, shifting the colour index towards the red, as can be seen in Figure 4.29. Here the difference of the  $B$  and  $V$  light curves from LC 2 have been plotted in magnitudes. In this unit, larger values of the difference  $B - V$  indicate redder colour.

In conclusion, the parameters of TY Boo appear consistent with a typical W-type W UMa system. Its short period, mass ratio far from unity and asymmetries in the light curve confirm this. Table 4.8 lists the absolute parameters of TY Boo, obtained from the photometric and spectroscopic solutions.

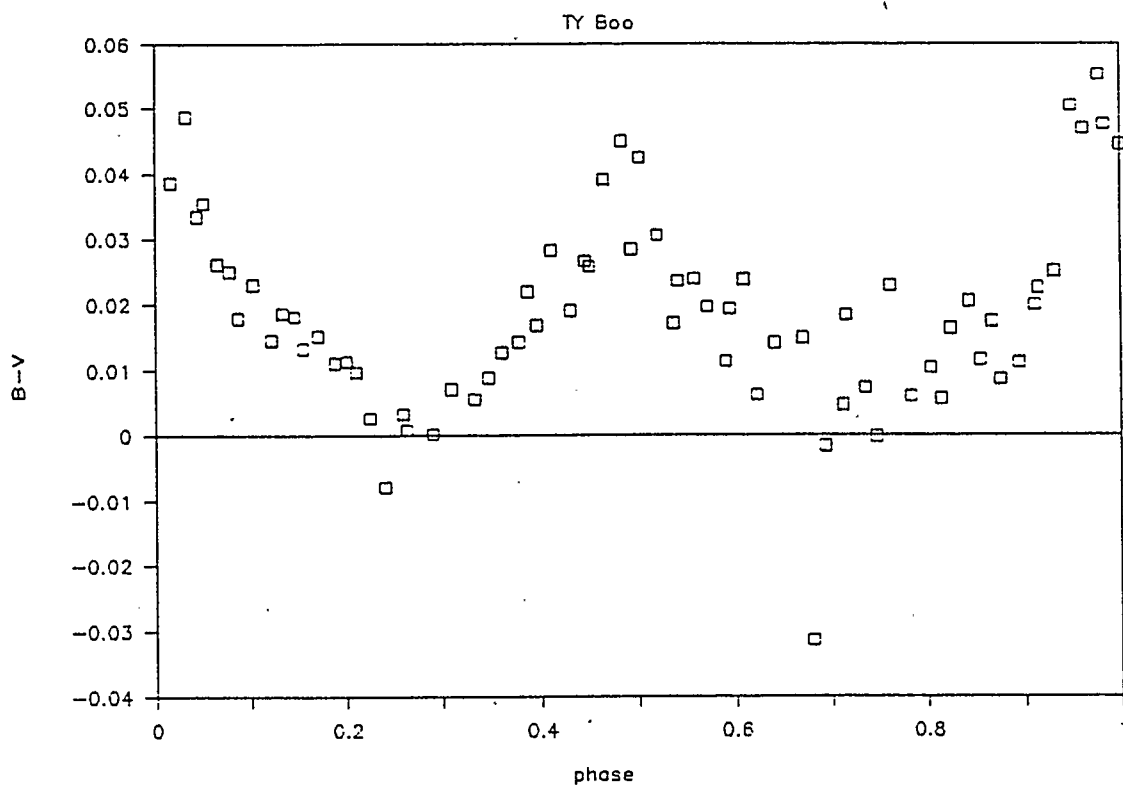


Figure 4.29: Plot of  $B - V$  from LC 2

We found new elements of this binary system by collecting all available data, and also including some new observations.

We succeeded in fitting the light and radial velocity curves of TY Boo, a W-type W UMa system, which displays O'Connell effect. The close agreement between the spotted and unspotted model fitting shows that spots are a practical way of dealing with asymmetries in the light curves. They reduce the uncertainty in the results, and at the same time the system elements are not strongly affected by their use.

We have also found TY Boo to be, like RW Com, a shallow contact binary. This condition was tested and confirmed by the Wilson-Devinney program run in semi-detached mode, and the  $a_2$  and  $a_4$  Fourier coefficients.

Further work on TY Boo should include analysis of other light curves taken at other times and in other band passes. This would provide clues to the origin of the asymmetries in the system. The expansion of the Wilson Devinney code taking place at this time at the University of Calgary could allow the inclusion of observations in other band passes.

Work could also be extended to other W UMa systems, in particular those that exhibit marked thermal discontinuity. We have already pointed out UX Eri and AC Boo as two likely candidates.

The type of study which has been conducted on TY Boo, with the analytical tools employed here, could be extended to other similar binary stars. Results so obtained should help us to better understand W UMa systems.

## Bibliography

- Adams, W.S. and Kohlschuter, A. 1914, *Ap. J.*, **39**, 341.
- Adams, W.S. and Joy, A.H. 1923, *Ap. J.*, **57**, 149.
- Al-Naimiy, H.M. 1977 , *Astrophys. Space Sci.*, **53**, 181.
- Ambert, M. 1967, *Pub. Obs. Haute-Provence*, **9**, N17.
- Bendat, J.S., Piersol, A.G. 1971, *Random Data: Analysis and Measurement Procedures*, Wiley-Interscience, New York
- Binnendijk, L. 1967, *A. J.*, **72**, 82.
- Boulon, J. 1956, *Pub. Obs. Haute-Provence*, **3**, 58.
- Carr, R.B. 1972 , *A.J* , **77**, 155.
- Davige, T.J., The O'Connell effect in eclipsing binaries. 1981, University of Calgary Master Thesis.
- Davide, T.J., Milone, E.F. 1984, *Ap. J. Suppl.*, **55**, 571.
- Diethelm, R. 1972, *BBSAG Bull.* 1972, **3**.
- Diethelm, R. 1976a, *BBSAG Bull.* 1976, **27**.
- Diethelm, R. 1976b, *BBSAG Bull.* 1976, **28**.
- Diethelm, R. 1977, *BBSAG Bull.* 1977, **34**.

- Diethelm, R. 1980, *BBSAG Bull.* 1980, **47**.
- Evans, D.S. 1963, *ROB*, **77**, 5.
- Griffiths, S.C., Hicks, R.B. and Milone, E.F. 1988, *J. Royal Astr. Soc. of Can.*, **82**, No. 1, 1.
- Groisman G., Milone E.F. 1987, *Bull. Am. Astron. Soc.*, **19**, 955.
- Guthnick, Von P., Prager, R. 1926, *Astr. Nachr.*, **228**, 99.
- Götz, Von W., Wenzel W. 1967, *Mitteilungen über Veränderliche Sterne*, **4**, 67.
- Harper, W.E. 1934, *Pub. Dominion Ast. Obs.*, **6**, 151.
- Harper, W.E. and Ambert, M. 1921, *Pub. Dominion Ast. Obs.*, **2**, 199.
- Hill, G. 1982, *Pub. Dom. Ap. Obs.*, **16**, 59.
- Irwin, J.B. 1973, *Ap. J.*, **179**, 241.
- Jordan, F.C 1931, *Publ. A.A.S.*, **7**, 52.
- Keenan, P.C., Mc Neil, R.C., 1976, *An Atlas of Spectra of the Cooler Stars*, The Ohio State University Press. Ohio.
- Koch, R.H. 1974, *A.J.*, **79**, 34.
- Kopal, Z. 1978, *Dynamics of close binary systems*, D Reidel Publishing Company, Holland.
- Kwee K.K., and Van Woerden H., 1956, *Bull. Ast. Inst. Netherlands*, **12**, 327.

- Leung, K, Wilson, R.E. 1977, *Ap. J.*, **211**, 853.
- Lucy, L.B. 1968 , *Ap. J.*, **151**, 1123.
- Lucy, L.B. 1968 , *Ap. J.*, **153**, 877.
- Mihalas and Binney, *Galactic Astronomy. Structure and Kinematics*, 1981, pg 80.
- Milone E.F., Fry D.J.I., Grillmair C.J. 1987, *Bull. Am. Astron. Soc.*, **19**, 643.
- Milone E.F., Wilson R.E., Hrivnak B.J. 1987, *Ap. J.*, **319**, 325.
- Mochnecki, S. W. 1971, M.Sc. thesis, University of Canterbury.
- Niarchos, P.G. 1978 , *Astrophys. Space Sci.*, **58**, 301.
- O'Connell, D.J.K. 1951 , *Riverview Pub.*, **2**, 85.
- Petrie, R.M. et al. 1957, *Pub. Dominion Ast. Obs.*, **10**, 415.
- Plaskett, J.S. et al. 1921, *Pub. Dominion Ast. Obs.*, **2**, 1.
- Plaskett, J.S. et al. 1948, *Pub. Dominion Ast. Obs.*, **2**, 103.
- Rebeiro, E. 1965, *Pub. Obs. Haute-Provence*, **8**, N6.
- Ruciński, S.M. 1973 , *Acta Astr.*, **23**, 79.
- Russell, H.N., and Merrill, J.E. 1952, Princeton Univ. Obs.Contr. No.26.
- Samec, R.G. and Bookmeyer B.B. 1987, *Publ. A.S.P.*, **99**, 824.
- Schieven. G., Morton, J.C., McLean. B.J., and Hughes, V.A. 1983, *Astron. & Astrophys. Supp.*, **52**, 463.

Schiller, S.J. and Milone, E.F. 1988, *A. J.*, **95**, 1466.

Shajn, G. and Albirtzky, V. 1932, *MN*, **92**, 771.

Simkin, S.M. 1974, *Astron. & Astrophys.*, **31**, 129.

Szafraniec, R. 1948, *Acta Astr.*, **4**, 81.

Szafraniec, R. 1949, *Acta Astr.*, **4**, 85.

Szafraniec, R. 1950, *Acta Astr.*, **4**, 113.

Szafraniec, R. 1951, *Acta Astr.*, **5**, 5.

Szafraniec, R. 1953, *Acta Astr.*, **5**, 52.

Szafraniec, R. 1955, *Acta Astr.*, **5**, 189.

Szafraniec, R. 1956, *Acta Astr.*, **6**, 141.

Szafraniec, R. 1957, *Acta Astr.*, **7**, 188.

Szafraniec, R. 1958, *Acta Astr.*, **8**, 189.

Szafraniec, R. 1959, *Acta Astr.*, **9**, 48.

Szafraniec, R. 1960, *Acta Astr.*, **10**, 69.

Szafraniec, R. 1963, *Acta Astr.*, **13**, 79.

Szafraniec, R. 1966, *Acta Astr.*, **16**, 157.

Szafraniec, R. 1952. *Acta Astr.*, **2**, 86.

Schembor, Ö. 1930, *Astronomische Nachrichten* , **238**, 215.

Wells, D.C., Greisen, E.W., Harten, R.H. 1981 , *Astron. Astrophys. Suppl. Ser.*,  
**44** , 363.

Wilson, O.C. 1941 , *Ap. J.*, **93**, 29.

Wilson, R.E., Biermann, P. 1976, *Astr. Ap.*, **48**, 349.

Wilson, R.E., Devinney, E.J. 1971, *Ap. J.*, **166**, 605.

Wilson, R.E., Devinney, E.J. 1973, *Ap. J.*, **182**, 539.

Wilson, R.E. 1979, *Ap. J.*, **234**, 1054.

Wilson, R.E. and Joy, A.H. 1950, *Ap. J.*, **11**, 221.

Wood, D.V., Forbes J.E. 1963, *A.J.*, **68**, 257.

## Appendix A

### Spectroscopic and photometric data

The present appendix lists the radial velocity and light curve data employed in the present work. Table A.1 lists the radial velocity data. The first column indicates the Julian Date of the observation, the second the corresponding phase. The comparison star used in the cross-correlation is listed in column three. The last four columns indicate the radial velocity of the more massive component (V) and the less massive component (U) with their errors, all in *km/sec*.

Tables A.3 through A.8 lists the normal points from the 1986 and 1987 light curves obtained at the Rothney Astrophysical Observatory in 1987. For every bandpass (B, V and I) the phase is indicated together with a weight (W), this weight is inversely proportional to the uncertainty of the luminosity of the point.

Tables A.9 through A.12 list the normal points of the light curves obtained by Bradstreet (private communication). They list the phase, the number of data points (N) averaged, the monochromatic luminosity and the corresponding error ( $\sigma$ ).

Table A.1: Cross-correlation results (all velocities in km/sec)

JD	comp.	U	$\sigma_U$	V	$\sigma_V$
+46000	phase star				
650.7203	0.1384 HD 144579	37.72	1.36	-217.53	1.53
650.7321	0.1756 HD 144579	61.96	2.62	-233.89	3.14
651.7223	0.2978 HD 144579	68.89	5.78	-264.22	3.36
651.7320	0.3284 HD 144579	65.07	1.27	-255.15	1.33
651.7411	0.3571 HD 144579	59.54	2.67	-261.77	2.83
651.7515	0.3899 HD 144579	43.57	1.36	-225.69	1.41
650.7203	0.1384 HD 154417	49.88	1.54	-217.86	1.51
650.7321	0.1756 HD 154417	73.44	4.30	-239.53	2.14
651.7119	0.2650 HD 154417	67.77	4.14	-283.51	3.20
651.7223	0.2978 HD 154417	70.22	4.94	-265.41	3.76
651.7320	0.3284 HD 154417	63.45	2.37	-261.42	2.87
651.7411	0.3571 HD 154417	61.35	3.46	-261.77	3.57
651.7515	0.3899 HD 154417	47.84	2.12	-219.51	2.80
902.8316	0.0761 HD 144579	31.48	5.18	-175.57	5.97
902.9211	0.3583 HD 144579	54.87	3.29	-235.52	4.70
902.9454	0.4349 HD 144579	6.41	4.06	-194.48	4.00
902.8316	0.0761 HD 154417	55.21	11.40	-145.75	13.72
902.9211	0.3583 HD 154417	58.47	4.29	-238.15	6.17
902.9454	0.4349 HD 154417	21.77	4.75	-200.04	10.47
232.8569	0.5642 HD 136202	-113.44	8.83	43.87	5.80
232.8743	0.6190 HD 136202	-123.33	8.31	106.66	7.17
232.8903	0.6695 HD 136202	-117.08	4.52	156.46	4.80
232.9042	0.7133 HD 136202	-134.22	7.35	167.59	8.25
232.9208	0.7657 HD 136202	-137.53	5.84	186.41	5.20
233.8979	0.8466 HD 136202	-120.41	7.31	164.82	5.89
233.9242	0.9295 HD 136202	-53.61	14.09	106.91	8.46
234.9172	0.0605 HD 136202	20.36	13.51	-143.85	23.00
234.9367	0.1220 HD 136202	31.26	7.96	-185.14	15.75
232.8569	0.5642 HD 114762	-111.33	12.25	51.26	8.83
232.8743	0.6190 HD 114762	-121.62	6.53	117.47	6.75
232.8903	0.6695 HD 114762	-129.02	4.15	153.76	4.62
232.9042	0.7133 HD 114762	-140.67	4.63	185.27	4.96
232.9208	0.7657 HD 114762	-143.84	5.08	189.12	4.73
233.8979	0.8466 HD 114762	-135.63	6.67	170.26	6.20
233.9242	0.9295 HD 114762	-81.48	9.18	113.20	10.41
234.9172	0.0605 HD 114762	34.25	27.11	-120.30	46.04
234.9367	0.1220 HD 114762	32.33	9.71	-185.32	15.98

Table A.2: RAO 1985 light curves.

Phase	DV	DB	DI	Phase	DV	DB	DI
0.0413	4.123	3.941	4.231	0.5413	3.975	3.808	4.115
0.0784	3.916	3.688	4.053	0.7019	3.592	3.382	3.735
0.1419	3.707	3.508	3.870	0.7510	3.579	3.342	3.734
0.2115	3.541	3.304	3.711	0.7982	3.624	3.371	3.761
0.2554	3.574	3.394	3.732	0.8418	3.676	3.401	3.804
0.1736	3.620	3.491	3.776	0.8861	3.732	3.541	3.889
0.2091	3.561	3.339	3.792	0.9333	3.891	3.725	3.982
0.2382	3.600	3.391	3.757	0.9819	4.064	4.008	4.236
0.1622	3.661	3.417	3.789	0.7660	3.575	3.403	3.730
0.2009	3.615	3.358	3.744	0.8071	3.628	-	3.739
0.2429	3.567	3.351	3.724	0.8164	3.625	-	3.781
0.3232	3.603	3.352	3.764	0.8282	3.624	3.413	3.765
0.3657	3.672	3.446	3.823	0.8399	3.629	-	3.764
0.4052	3.758	3.543	3.904	0.8651	3.699	-	3.828
0.4443	3.908	3.680	4.036	0.8744	3.705	-	3.823
0.4846	4.057	3.867	4.188	0.8861	3.751	3.572	3.856
0.5219	4.043	3.858	4.172	0.8979	3.742	-	3.907
0.5826	3.847	3.642	3.981	0.9193	3.897	-	4.002
0.6224	3.726	3.507	3.865	0.9286	3.916	-	4.052
0.6628	3.634	3.435	3.794	0.9404	3.995	3.798	4.116
-	-	-	-	0.9521	4.042	-	4.162

Table A.3: RAO 1986 V light curve. Normal points.

Phase	L(V)	W	Phase	L(V)	W
0.0130	0.6002	1.4	0.5583	0.6625	1.0
0.0334	0.6199	0.8	0.5850	0.8604	1.0
0.0511	0.6851	1.7	0.6035	0.8882	1.0
0.0685	0.7413	0.2	0.6283	0.9470	1.0
0.0929	0.8326	0.6	0.6460	0.9462	1.0
0.1182	0.8591	1.6	0.6658	1.0042	1.4
0.1447	0.8994	1.0	0.6940	0.9906	0.9
0.1655	0.9687	1.0	0.7147	1.0213	0.7
0.2013	0.9463	1.0	0.7346	1.0220	0.8
0.2238	0.9838	0.8	0.7517	1.0011	0.9
0.2512	0.9800	0.8	0.7714	1.0248	1.7
0.2771	0.9680	1.0	0.7850	0.9793	0.4
0.3003	0.9822	1.4	0.8049	0.9813	0.8
0.3285	0.9509	0.6	0.8282	0.9457	0.7
0.3569	0.8889	1.4	0.8408	0.9603	1.4
0.3711	0.8518	1.0	0.8599	0.8909	0.7
0.3867	0.8118	1.0	0.8860	0.8484	0.6
0.4175	0.7363	1.0	0.9153	0.7901	0.5
0.4409	0.6776	1.0	0.9358	0.7282	0.5
0.4634	0.6094	1.0	0.9487	0.7117	1.0
0.4868	0.5812	1.0	0.9719	0.5913	0.5
0.5117	0.5721	1.0	0.9928	0.5634	1.0
0.5356	0.6145	1.0			

Table A.4: RAO 1986 B light curve. Normal points.

Phase	L(B)	W	Phase	L(B)	W
0.0130	0.5718	1.4	0.5356	0.5691	1.0
0.0334	0.5972	0.7	0.5583	0.4572	1.0
0.0525	0.6732	1.4	0.6283	0.9424	0.6
0.0685	0.7317	0.4	0.6460	0.9546	1.0
0.0929	0.8378	0.5	0.6658	1.0016	1.4
0.1182	0.8533	1.2	0.6943	1.0140	1.0
0.1431	0.9455	0.7	0.7178	1.0467	1.0
0.1655	0.9565	1.0	0.7463	1.0214	1.7
0.2013	0.9252	1.0	0.7605	1.0149	0.7
0.2238	0.9857	1.4	0.7773	0.9952	0.7
0.2512	0.9906	0.8	0.7926	1.0345	1.4
0.2771	0.9422	1.0	0.8111	0.9790	0.9
0.2991	0.9983	1.0	0.8362	0.9313	0.9
0.3306	0.9163	1.0	0.8599	0.9078	0.7
0.3599	0.8603	1.0	0.8860	0.8193	0.4
0.3867	0.8341	1.0	0.9153	0.7912	0.6
0.4175	0.7073	1.0	0.9358	0.7264	1.4
0.4409	0.6905	1.0	0.9487	0.6947	1.0
0.4634	0.5880	1.0	0.9719	0.5790	0.6
0.4868	0.5508	1.0	0.9928	0.5327	0.9
0.5117	0.5751	1.0	-	-	-

Table A.5: RAO 1986 I light curve. Normal points.

Phase	L(I)	W	Phase	L(I)	W
0.0130	0.6123	0.6	0.5583	0.6605	1.0
0.0334	0.6569	0.7	0.5850	0.8511	1.0
0.0511	0.7096	1.7	0.6035	0.9067	1.0
0.0685	0.7632	0.3	0.6283	0.9431	1.3
0.0929	0.8506	0.4	0.6460	0.9470	1.0
0.1182	0.8752	0.6	0.6658	0.9752	1.4
0.1447	0.9102	0.8	0.6940	1.0066	1.7
0.1655	0.9614	1.0	0.7147	1.0168	0.7
0.2013	1.0145	1.0	0.7346	1.0127	0.6
0.2238	0.9919	1.4	0.7517	1.0010	0.6
0.2512	0.9777	0.5	0.7714	1.0052	1.0
0.2771	0.9745	1.0	0.7850	0.9833	0.6
0.3003	0.9816	1.1	0.8049	0.9820	0.9
0.3285	0.9631	0.4	0.8282	0.9582	0.8
0.3569	0.8847	1.4	0.8408	0.9621	1.4
0.3711	0.8471	1.0	0.8599	0.9031	0.8
0.3867	0.7996	1.0	0.8860	0.8626	0.8
0.4175	0.7528	1.0	0.9153	0.8022	0.5
0.4409	0.6931	1.0	0.9358	0.7585	0.5
0.4634	0.6193	1.0	0.9487	0.7407	1.0
0.4868	0.5840	1.0	0.9719	0.6334	0.8
0.5117	0.6013	1.0	0.9928	0.5931	1.9
0.5356	0.6238	1.0	-	-	-

Table A.6: RAO 1987 V light curve. Normal points.

Phase	L(V)	W	Phase	L(V)	W
0.0034	0.5558	1.0	0.5313	0.6695	0.9
0.0200	0.5676	0.7	0.5537	0.7180	1.0
0.0366	0.6126	0.4	0.5713	0.7691	1.0
0.0571	0.6827	0.4	0.5876	0.8239	0.5
0.0740	0.7342	0.5	0.6033	0.8484	1.2
0.0889	0.8169	1.0	0.6230	0.8740	0.7
0.1172	0.8967	1.0	0.6387	0.9104	0.8
0.1284	0.9078	1.0	0.6580	0.9292	1.3
0.1606	0.9442	1.4	0.6738	0.9446	1.4
0.1772	0.9649	0.8	0.6934	0.9709	1.4
0.1982	0.9924	1.1	0.7097	0.9925	0.6
0.2151	1.0092	1.4	0.7285	0.9856	1.4
0.2349	1.0269	1.4	0.7422	1.0117	1.0
0.2507	1.0352	1.0	0.7622	0.9823	1.7
0.2964	0.9928	1.4	0.7743	1.0056	1.7
0.3076	0.9866	1.0	0.7837	0.9877	1.4
0.3278	0.9580	1.5	0.7979	0.9687	1.1
0.3389	0.9641	1.4	0.8088	0.9509	0.8
0.3516	0.9553	1.6	0.8198	0.9490	1.6
0.3699	0.9239	1.3	0.8414	0.9144	0.7
0.3884	0.8930	1.4	0.8610	0.9256	1.4
0.4086	0.8396	0.8	0.8826	0.8807	1.2
0.4182	0.7995	1.0	0.8945	0.8424	1.2
0.4324	0.7732	1.1	0.9077	0.8127	1.1
0.4450	0.7278	0.9	0.9219	0.7999	0.4
0.4583	0.7004	1.7	0.9338	0.7320	1.4
0.4724	0.6642	0.5	0.9455	0.6781	0.6
0.4875	0.6466	0.6	0.9624	0.6356	1.1
0.5000	0.6423	1.0	0.9827	0.5487	1.0
0.5149	0.6227	1.4	-	-	-

Table A.7: RAO 1987 B light curve. Normal points.

Phase	L(B)	W	Phase	L(B)	W
0.0034	0.5107	1.0	0.5537	0.7108	1.0
0.0200	0.5696	0.7	0.5713	0.7561	1.0
0.0366	0.5767	1.4	0.5830	0.7794	1.0
0.0571	0.6705	0.7	0.6033	0.8261	0.5
0.0740	0.7283	1.4	0.6230	0.8833	1.2
0.1284	0.8921	1.0	0.6387	0.8777	0.5
0.1606	0.9592	0.8	0.6580	0.9291	0.8
0.1772	0.9630	1.4	0.6738	0.9481	1.4
0.1982	0.9944	1.4	0.6934	0.9696	0.7
0.2151	0.9868	1.1	0.7097	0.9837	1.4
0.2349	1.0238	1.4	0.7285	0.9831	1.0
0.2507	1.0310	1.4	0.7422	1.0068	1.0
0.2964	1.0115	1.4	0.7622	1.0155	1.0
0.3278	1.0001	1.4	0.7732	0.9626	0.2
0.3389	0.9758	0.4	0.7837	0.9869	1.4
0.3513	0.9533	0.8	0.7979	0.9957	0.7
0.3699	0.9161	2.0	0.8088	0.9602	0.8
0.3884	0.8839	1.4	0.8198	0.9448	1.7
0.4086	0.8492	1.3	0.8414	0.9270	0.6
0.4182	0.8349	0.9	0.8610	0.9070	0.4
0.4324	0.7707	1.4	0.8826	0.8807	0.6
0.4450	0.7420	1.4	0.8945	0.8317	1.4
0.4583	0.7126	0.3	0.9077	0.8172	0.3
0.4724	0.6701	1.4	0.9219	0.6775	0.3
0.4875	0.6265	1.4	0.9338	0.6987	0.7
0.5000	0.6201	1.0	0.9455	0.6512	0.8
0.5149	0.6114	0.7	0.9624	0.5942	1.4
0.5313	0.6588	1.2	0.9827	0.5446	1.4

Table A.8: RAO 1987 I light curve. Normal points.

Phase	L(I)	W	Phase	L(I)	W
0.0034	0.5752	1.0	0.5149	0.6383	0.4
0.0200	0.6105	0.9	0.5313	0.6657	0.6
0.0366	0.6499	0.4	0.5537	0.7129	1.0
0.0571	0.7037	0.4	0.5713	0.8046	1.0
0.0740	0.7646	0.6	0.5876	0.8129	0.4
0.0889	0.8141	1.0	0.6033	0.8729	0.5
0.1172	0.8879	1.0	0.6230	0.8952	0.7
0.1284	0.9022	1.0	0.6387	0.9195	0.5
0.1606	0.9586	1.4	0.6580	0.9533	1.4
0.1772	0.9794	1.4	0.6738	0.9709	1.4
0.1982	0.9893	1.4	0.6934	0.9837	1.4
0.2151	0.9988	1.0	0.7097	0.9935	1.4
0.2349	1.0105	1.4	0.7285	1.0119	1.4
0.2471	1.0108	1.0	0.7422	1.0066	1.0
0.2964	0.9943	1.4	0.7622	0.9892	0.7
0.3076	1.0032	1.0	0.7743	0.9973	1.0
0.3278	0.9788	1.7	0.7905	1.0023	0.5
0.3389	0.9635	0.6	0.8016	0.9872	0.7
0.3516	0.9479	0.7	0.8140	0.9670	0.9
0.3699	0.9175	2.0	0.8247	0.9502	1.0
0.3884	0.9224	1.4	0.8414	0.9461	1.0
0.4076	0.8445	0.6	0.8610	0.9235	1.7
0.4182	0.8163	0.7	0.8826	0.8801	1.3
0.4324	0.7785	1.1	0.8945	0.8584	1.4
0.4450	0.7426	0.5	0.9077	0.8227	1.7
0.4600	0.7000	0.5	0.9219	0.7923	1.7
0.4724	0.6834	0.6	0.9338	0.7523	1.4
0.4875	0.6574	0.8	0.9455	0.7080	0.4
0.5000	0.6501	1.0	0.9624	0.6476	0.3
-	-	-	0.9827	0.5842	0.5

Table A.9: Bradstreet Normal points. B bandpass.

Phase	L(B)	$\sigma$	Phase	L(B)	$\sigma$
0.0162	0.5260	0.0026	0.5021	0.5916	0.0005
0.0325	0.5580	0.0028	0.5200	0.6107	0.0032
0.0448	0.6023	0.0019	0.5369	0.6479	0.0031
0.0514	0.6234	0.0057	0.5415	0.6519	0.0003
0.0660	0.6813	0.0069	0.5584	0.7010	0.0039
0.0786	0.7271	0.0049	0.5717	0.7439	0.0026
0.0874	0.7593	0.0000	0.5902	0.7989	0.0011
0.1035	0.8089	0.0037	0.5944	0.8035	0.0011
0.1218	0.8521	0.0018	0.6090	0.8318	0.0046
0.1340	0.8676	0.0062	0.6227	0.8662	0.0016
0.1461	0.8859	0.0028	0.6402	0.8900	0.0029
0.1551	0.9028	0.0042	0.6693	0.9237	0.0048
0.1709	0.9241	0.0010	0.6795	0.9731	0.0038
0.1884	0.9441	0.0028	0.6927	0.9515	0.0045
0.2013	0.9563	0.0022	0.7116	0.9629	0.0010
0.2113	0.9662	0.0026	0.7151	0.9532	0.0000
0.2250	0.9849	0.0055	0.7341	0.9707	0.0017
0.2403	1.0055	0.0016	0.7465	0.9771	0.0040
0.2592	0.9899	0.0073	0.7606	0.9606	0.0100
0.2626	0.9963	0.0000	0.7825	0.9661	0.0036
0.2902	0.9931	0.0014	0.8035	0.9513	0.0019
0.3092	0.9734	0.0007	0.8140	0.9393	0.0052
0.3328	0.9481	0.0029	0.8244	0.9237	0.0017
0.3468	0.9258	0.0036	0.8432	0.8960	0.0027
0.3606	0.9025	0.0017	0.8546	0.8904	0.0016
0.3778	0.8763	0.0038	0.8665	0.8695	0.0018
0.3868	0.8531	0.0145	0.8754	0.8610	0.0004
0.3962	0.8353	0.0011	0.8941	0.8188	0.0012
0.4111	0.7943	0.0035	0.9105	0.7702	0.0004
0.4312	0.7444	0.0040	0.9139	0.7561	0.0010
0.4466	0.6969	0.0000	0.9305	0.6997	0.0024
0.4502	0.6859	0.0049	0.9484	0.6240	0.0069
0.4659	0.6388	0.0028	0.9613	0.5836	0.0054
0.4840	0.5992	0.0055	0.9778	0.5279	0.0023
0.4932	0.5992	0.0014	0.9827	0.5229	0.0032
-	-	-	0.9993	0.5112	0.0007

Table A.10: Bradstreet Normal points. V bandpass.

Phase	L(V)	$\sigma$	Phase	L(V)	$\sigma$
0.0007	0.5320	0.0010	0.4933	0.6150	0.0003
0.0129	0.5396	0.0033	0.5043	0.6152	0.0014
0.0205	0.5521	0.0000	0.5197	0.6276	0.0025
0.0386	0.5996	0.0144	0.5340	0.6533	0.0061
0.0522	0.6469	0.0079	0.5412	0.6653	0.0046
0.0674	0.7031	0.0058	0.5584	0.7166	0.0086
0.0784	0.7434	0.0042	0.5717	0.7574	0.0062
0.0889	0.7766	0.0004	0.5902	0.8072	0.0030
0.1035	0.8262	0.0043	0.6010	0.8346	0.0054
0.1210	0.8623	0.0033	0.6137	0.8594	0.0028
0.1347	0.8837	0.0024	0.6251	0.8742	0.0032
0.1494	0.9057	0.0015	0.6378	0.8987	0.0017
0.1603	0.9213	0.0024	0.6694	0.9365	0.0024
0.1711	0.9374	0.0015	0.6796	0.9454	0.0009
0.1853	0.9506	0.0019	0.6938	0.9504	0.0044
0.1989	0.9642	0.0011	0.7093	0.9654	0.0028
0.2119	0.9753	0.0027	0.7175	0.9710	0.0036
0.2242	0.9867	0.0020	0.7341	0.9772	0.0015
0.2403	0.9982	0.0014	0.7470	0.9769	0.0052
0.2569	0.9899	0.0036	0.7617	0.9813	0.0005
0.2649	1.0000	0.0028	0.7783	0.9714	0.0004
0.2925	0.9927	0.0027	0.7865	0.9714	0.0004
0.3077	0.9814	0.0006	0.7994	0.9678	0.0004
0.3219	0.9656	0.0036	0.8117	0.9455	0.0023
0.3339	0.9516	0.0021	0.8259	0.9367	0.0036
0.3468	0.9333	0.0029	0.8417	0.9148	0.0040
0.3613	0.9120	0.0022	0.8554	0.8989	0.0041
0.3745	0.8929	0.0008	0.8670	0.8828	0.0021
0.3825	0.8806	0.0016	0.8776	0.8638	0.0016
0.3987	0.8424	0.0067	0.8949	0.8254	0.0030
0.4128	0.8115	0.0063	0.9083	0.7925	0.0026
0.4312	0.7575	0.0034	0.9163	0.7631	0.0025
0.4447	0.7204	0.0020	0.9305	0.7160	0.0031
0.4557	0.6844	0.0092	0.9484	0.6536	0.0081
0.4664	0.6611	0.0046	0.9614	0.6090	0.0075
0.4816	0.6269	0.0000	0.9786	0.5528	0.0034
-	-	-	0.9889	0.5365	0.0039

Table A.11: Bradstreet Normal points. R bandpass.

Phase	L(R)	$\sigma$	Phase	L(R)	$\sigma$
0.0096	0.5569	0.0012	0.5067	0.6232	0.0003
0.0224	0.5781	0.0027	0.5182	0.6323	0.0013
0.0411	0.6286	0.0078	0.5318	0.6639	0.0039
0.0549	0.6744	0.0065	0.5477	0.6978	0.0062
0.0688	0.7225	0.0036	0.5652	0.7480	0.0006
0.0801	0.7624	0.0034	0.5780	0.7831	0.0040
0.0939	0.8019	0.0110	0.5861	0.8046	0.0015
0.1050	0.8305	0.0056	0.5988	0.8366	0.0042
0.1188	0.8688	0.0061	0.6161	0.8678	0.0024
0.1337	0.8906	0.0033	0.6273	0.8884	0.0004
0.1494	0.9169	0.0011	0.6356	0.9003	0.0008
0.1618	0.9251	0.0031	0.6686	0.9369	0.0022
0.1722	0.9438	0.0023	0.6796	0.9541	0.0022
0.1853	0.9563	0.0028	0.6929	0.9638	0.0031
0.1994	0.9709	0.0015	0.7050	0.9783	0.0016
0.2157	0.9888	0.0020	0.7197	0.9768	0.0013
0.2257	0.9956	0.0027	0.7346	0.9894	0.0038
0.2381	0.9948	0.0019	0.7482	0.9861	0.0009
0.2534	0.9989	0.0023	0.7594	0.9917	0.0009
0.2652	1.0083	0.0038	0.7761	0.9804	0.0005
0.2800	0.9995	0.0106	0.7889	0.9719	0.0009
0.2957	1.0009	0.0060	0.7972	0.9701	0.0009
0.3029	0.9849	0.0023	0.8124	0.9537	0.0011
0.3209	0.9690	0.0021	0.8307	0.9402	0.0000
0.3341	0.9565	0.0024	0.8368	0.9273	0.0026
0.3455	0.9414	0.0017	0.8554	0.9036	0.0023
0.3594	0.9283	0.0023	0.8687	0.8853	0.0025
0.3699	0.9095	0.0021	0.8800	0.8646	0.0024
0.3888	0.8839	0.0051	0.8930	0.8400	0.0062
0.4016	0.8457	0.0035	0.9034	0.8162	0.0049
0.4152	0.8056	0.0142	0.9211	0.7621	0.0088
0.4280	0.7780	0.0004	0.9318	0.7227	0.0079
0.4385	0.7432	0.0061	0.9421	0.6868	0.0019
0.4570	0.6906	0.0013	0.9550	0.6408	0.0034
0.4677	0.6625	0.0052	0.9717	0.5932	0.0061
0.4794	0.6433	0.0036	0.9868	0.5588	0.0028
0.4932	0.6255	0.0006	0.9992	0.5513	0.0009

Table A.12: Bradstreet Normal points. R bandpass.

Phase	L(I)	$\sigma$	Phase	L(I)	$\sigma$
0.0096	0.5713	0.0013	0.5238	0.6483	0.0027
0.0246	0.5981	0.0033	0.5310	0.6658	0.0050
0.0411	0.6387	0.0034	0.5477	0.7075	0.0026
0.0546	0.6855	0.0049	0.5643	0.7556	0.0040
0.0670	0.7277	0.0062	0.5736	0.7762	0.0157
0.0809	0.7741	0.0046	0.5829	0.8009	0.0056
0.0954	0.8187	0.0034	0.5995	0.8467	0.0031
0.1110	0.8561	0.0033	0.6183	0.8790	0.0024
0.1186	0.8774	0.0074	0.6307	0.8929	0.0087
0.1324	0.8960	0.0021	0.6337	0.9070	0.0000
0.1431	0.9169	0.0025	0.6668	0.9413	0.0040
0.1608	0.9330	0.0028	0.6803	0.9565	0.0017
0.1788	0.9537	0.0013	0.6995	0.9603	0.0000
0.1877	0.9618	0.0013	0.7038	0.9730	0.0033
0.2006	0.9740	0.0017	0.7238	0.9858	0.0012
0.2163	0.9903	0.0041	0.7364	0.9917	0.0027
0.2268	0.9923	0.0010	0.7462	0.9934	0.0018
0.2529	0.9972	0.0022	0.7562	0.9902	0.0044
0.2653	1.0065	0.0063	0.7737	0.9845	0.0018
0.2800	0.9993	0.0037	0.7912	0.9736	0.0009
0.2980	0.9917	0.0037	0.7988	0.9707	0.0036
0.3006	0.9822	0.0032	0.8127	0.9573	0.0021
0.3210	0.9710	0.0019	0.8326	0.9402	0.0000
0.3345	0.9568	0.0049	0.8343	0.9373	0.0016
0.3470	0.9419	0.0009	0.8536	0.9160	0.0017
0.3660	0.9145	0.0000	0.8663	0.9005	0.0035
0.3693	0.9110	0.0020	0.8840	0.8650	0.0019
0.3888	0.8796	0.0012	0.8996	0.8295	0.0000
0.4017	0.8451	0.0023	0.9030	0.8249	0.0024
0.4236	0.7930	0.0018	0.9227	0.7637	0.0032
0.4384	0.7513	0.0031	0.9374	0.7101	0.0019
0.4570	0.6969	0.0026	0.9463	0.6827	0.0179
0.4658	0.6755	0.0057	0.9559	0.6494	0.0057
0.4759	0.6581	0.0025	0.9717	0.6044	0.0033
0.4933	0.6297	0.0003	0.9872	0.5749	0.0019
0.5107	0.6342	0.0022	0.9992	0.5675	0.0007

## Appendix B

### Hardware and software

#### B.1 The RADS System

The rapid alternate detection system has been on line at the University of Calgary since 1981. It was designed to allow high quality photometry even under less than desirable sky conditions.

The system was described in detail by Milone, Robb, Babott and Hansen (1982). It is installed on the 41 cm reflecting telescope of the Rothney Astrophysical Observatory.

The heart of the system is an oscillating Cassegrain secondary mirror which can be driven to any of four different positions.

The secondary mirror is directly driven by an electrodynamic vibrator. A transducer is mounted opposite the driver, and allows measuring the position of the mirror. This whole unit can be rotated 360° about the optical axis of the mirror, permitting a selection of a comparison star at any position angle.

The driver is controlled by a wave form generator. The amplitude of the signal determines the position of the mirror, and its length determines the time it will stay at that position. The amplitude can be varied across about 4.5 minutes of arc.

A data acquisition system receives this signal and keeps four individual counts, one for each position of the mirror. Independent counts of the integration times,

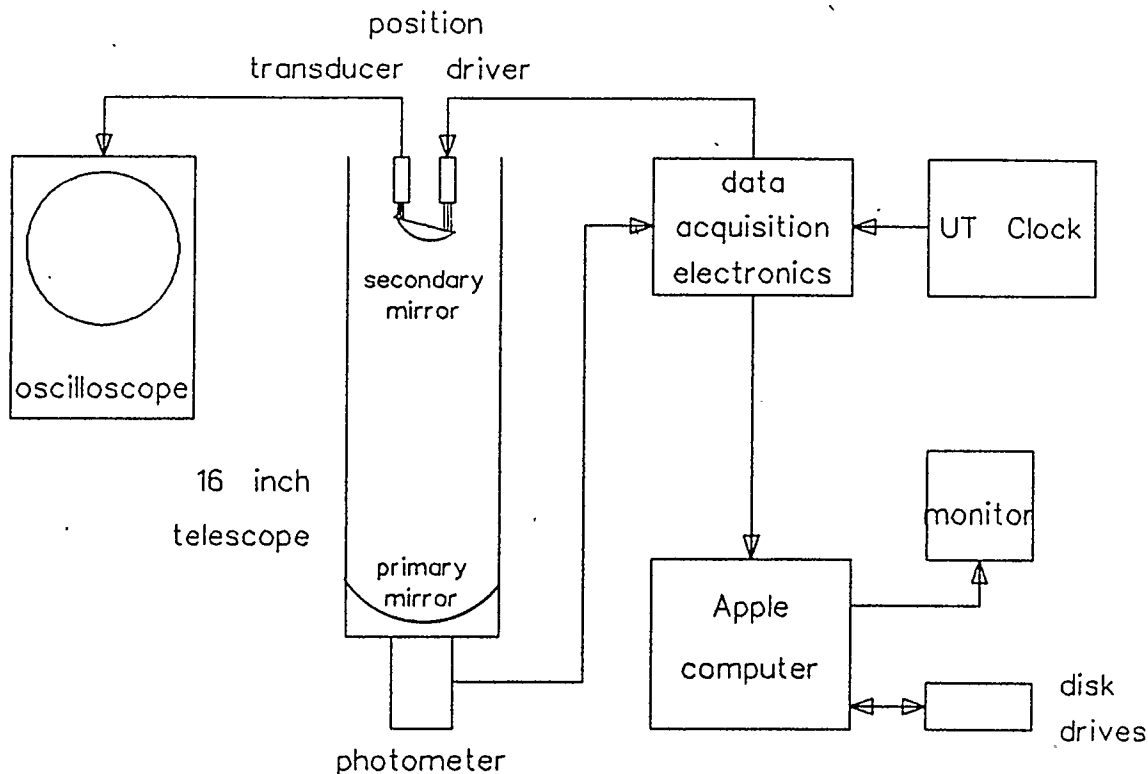


Figure B.1: RADS system

accurate to  $\pm 1\mu s$  are also obtained. The Universal Time is also read from a digital clock. When the desired integration time is reached the counts are normalized according to the integration time for each channel. All data are then stored by an Apple IIe microcomputer on 5-1/4 inch floppy disks, and also printed out. Figure B.1 shows a diagram of the RADS system, adapted from Milone et al. (1982).

To reduce noise, the photomultiplier tube is dry-ice cooled, operating at a

temperature of about  $-70^{\circ}\text{C}$ . This reduces the dark counts to a minimum.

The fact that all four channels are obtained with the same photomultiplier tube eliminates the possible sensitivity differences of a multi tube system. The speed of the chopping allows for rapid consecutive measurements of the variable, the comparison and the sky, removing much of the transparency variations due to clouds and sky brightness variations.

## B.2 Data Reduction

The RAO data was gathered on an Apple IIe microcomputer. A similar machine was used to reduce it; software developed and tested at University of Calgary over several years was used for the reduction. At the present time the reduction programs are in the process of being transported to PC type computers. The faster execution speed and the more powerful versions of BASIC available on these machines will translate into more productivity for the user.

Though the radial velocity data were reduced on the Dominion Observatory VAX computer from the University of Calgary, a Tektronix emulation program on a Zenith Z-150 equipped with a modem allowed the remote use of this software from Calgary via Datapac. The program was flexible enough to allow the storage of the cross correlation graphs on disk for later printing, and reproduced all the characteristics of the mentioned terminal.

The data obtained were then entered into a spreadsheet on the same personal computer. The appropriate corrections were entered in separate columns and the heliocentric radial velocities were then computed. The formulas for computing

mass ratio and gamma velocity according to Wilson were also entered on the same spreadsheet, and these numbers also computed. Finally the graphics capability of the PC was used to realize the radial velocity curves.

A program was also developed for computing normal points. The results were then graphed on the screen, and an output file written in the input format of the Wilson-Devinney code. This file was later transferred via modem to the Cyber 205 supercomputer at the University of Calgary.

Once again the graphic capabilities of the spreadsheet were used to visualize the output of the Wilson-Devinney program in LC mode, as compared to the observed light curves. Once a value of the potential was found, a program for solving equations by differential corrections was used on the PC to obtain a rough estimate of the cross section of the star. This program took as input the Roche potential formula, the mass ratio and the positions of the centers of the stars. It then computed, by iterations, the Y values of points along the edge of the system for X running from one end to the other.

### **B.3 Use of Mainframe Computers**

The heart of the project was the modeling carried out with the Wilson-Devinney program (Wilson and Devinney, 1971), which computed both the synthetic light curves and the differential corrections to the system parameters. It was run on the Cyber 205 supercomputer at the University of Calgary. The computer operates only in "batch" mode, and the programs must be submitted from a front end computer. During the length of the project the front end was changed from a

Cyber 175 to a Cyber 860, this change was transparent to our program. There was, however, also a change in the operating system on the Cyber 205. This brought out some incompatibilities with the code, which were corrected.

The power of the supercomputer is essential when executing a program like that of Wilson. The process of computing both the differential corrections and the light curves requires a lot of iterative work. The sheer speed of the computer shortens the length of each run to no more than twenty minutes of real time. In this way a day of work can mean several runs, and hence much faster results.

The Multics system was used for its flexibility and ease of use. Almost all the graphs were generated by FORTRAN programs written on Multics, and using the graphics subroutine library DISSPLA. When only medium quality output were required, a screen dump into a dot matrix printer was usually enough. For high quality output both the Calcomp plotter and the QMS laser printer were employed.

Data could easily be transferred between the mainframes and the personal computers by the use of modems. In the case of the Apple and the PC a serial connection was made and the data transferred. The transfer between the Cyber 860 and Multics was possible by using a special line called the HASP link. In this way the output from the Wilson-Devinney code could be moved over to Multics for graphing. The plotted fittings are indispensable tools, and the ultimate test of the success of the modeling.

The graphing program could then read the output without any editing needed. It could also read a file with radial velocity data, and another one with light curve data. If desired, all sets could be plotted, and the output parameters listed for faster reference. A sample output can be seen in Figure B.2.

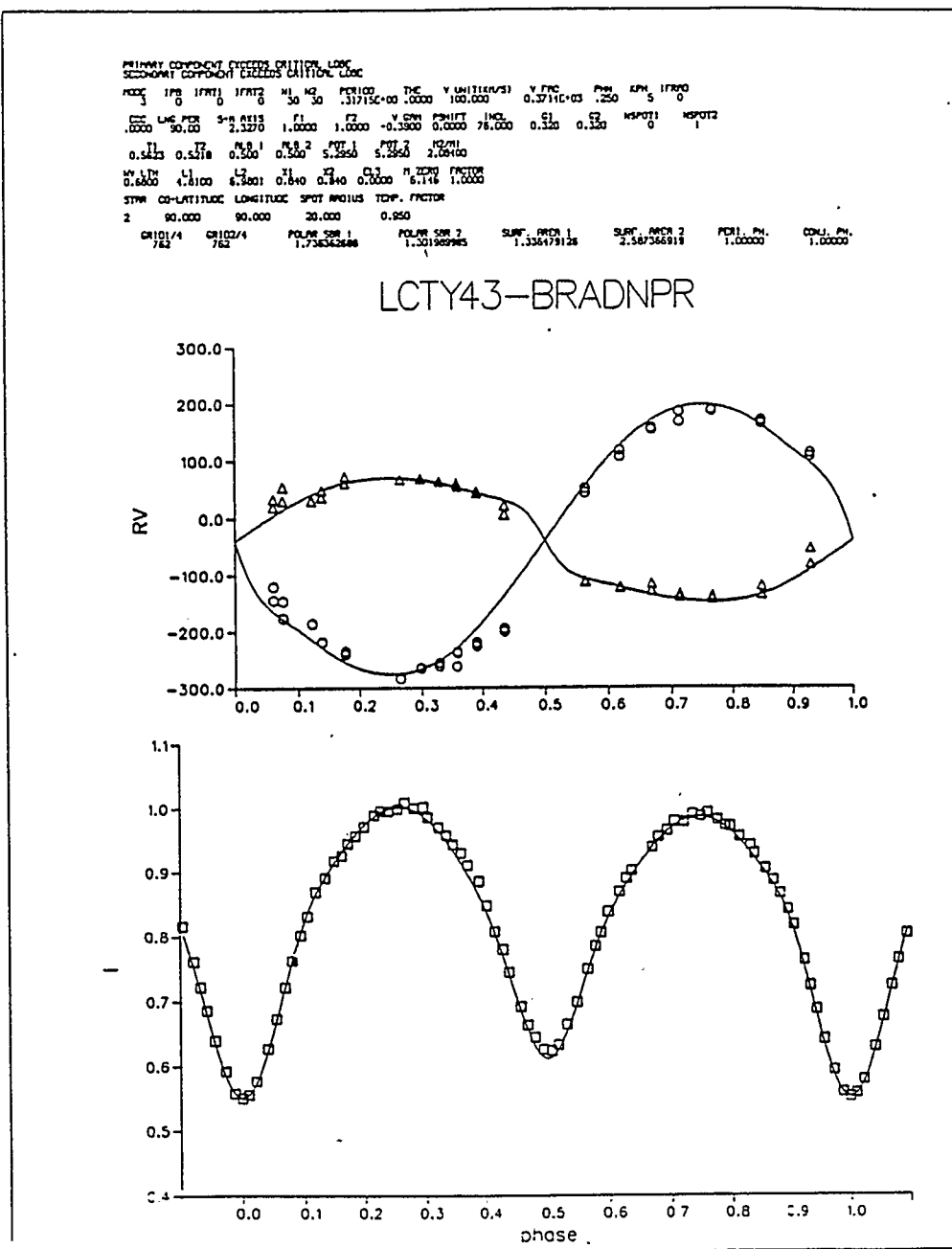


Figure B.2: Sample graph from the LC mode output

Finally the text of this thesis itself was written on the Multics system, and typeset using the program TeX. Graphs were printed on the laser printer and later pasted into the manuscript.